GEOCHEMISTRY OF THE BIMODAL QUATERNARY VOLCANISM IN THE MEDICINE LAKE HIGHLAND, NORTHERN CALIFORNIA

A Thesis

Presented to

the Faculty of the Department of Geology

New Mexico Institute of Mining and Technology

In Partial Fulfillment

of the Requirements for the Degree

Master of Science

in Geochemistry

by

David L. Hayslip

April 1973

TABLE OF CONTENTS

LIST OF ILLUSTRATIONS

ABSTRACT

Determinations of major and trace element chemistry of the Quaternary bimodal volcanic assemblage in the medicine Lake Highland of northern California suggest that the Modoc basalts were derived by partial melting of an upper mantle plagioclase peridotite parent. Two main periods of magma generation occurred each having a complex near surface history before eruption.

The silicic lavas also appear to have undergone a complex near surface history. No genetic relationship was delineated between the siliceous flows and either the Modoc basalts or the older Highland andesites.

Possibly more geochemical data has or is in the process of being gathered in the Highland area than has ever been determined for any other single volcanic complex. The provincal location, time of volcanicity, and wide variation in chemical composition of the assemblage necessitate a voluminous amount of data before the true geologic history of the Highland can be explained.

INTRODUCTION

Purpose

The purpose of this study is to determine and evaluate the major and trace element chemistry of the bimodal Quaternary volcanism in the Medicine Lake Highland of northern California. Particular emphasis is given to the genesis of the magmas and their relationship in time and space with Cascade, Modoc Plateau, and Great Basin volcanism. A complementary geochemical study of previous volcanism in the area has been undertaken by C. Barsky (Washington University, Saint Louis), and is now (1973) nearing completion. Also in progress is a strontium isotope study by P. A. Mueller (University of North Carolina).

Methods of Investigation

Field work in the area was primarily devoted to sampling of the volcanics for geochemical analysis. Minor amounts of mapping were also performed to supplement existing geologic maps.

Laboratory investigations included a cursory examination of thin sections in addition to major and trace element analysis of the samples. Determination of Si, Ti, Al, Fe, Mg, Ca, Na, K, Rb, Sr, Cu, Ni, Co, Zr, and Ba concentrations were made using non-destructive X-ray fluorescence and neutron activation analytical methods.

Acknowledgements

The author expresses his sincere thanks to Dr. Jacques R. Renault who served as his advisor and made many valuable contributions to the investigation. Dr. Kent C. Condie is thanked for suggesting the study and directing it in the preliminary phases. Deeply appreciated is the assistance and encouragement given by Dr. Gale K. Billings and Dr. Charles E. Chapin, members of the thesis committee. Very special thanks go to Dr. Charles W. Walker, State Mineralogist, New Mexico State Bureau of Mines and Mineral Resources, for his assistance and advise concerning the X-ray fluorescence analytical work. The Sandia Corporation and their reactor staff is thanked for their time and cooperation; without which, the neutron activation work would not have been possible. Also thanked is Miss Rosie Trujillo, whose typing expertise is reflected in the quality of this manuscript.

This study was financed in part by the National Science Foundation (Grant number GA-26390) and the Geoscience Department, New Mexico Institute of Mining and Technology.

GEOGRAPHICAL AND GEOLOGICAL SETTING

Location

The area studied encompasses 500 square miles in northeastern Siskiyou and northwestern Modoc Counties, California (Fig. 1), and includes Lava Beds National Monument. The Medicine Lake Highland lies in the center of this area, 35 miles northeast of Mount Shasta and immediately south of Lava Beds National Monument. The town of Tulelake, California lies about 10 miles north of the thesis area. State route 139 runs along the eastern side of the area and numerous secondary and logging roads provide ample access.

The geologic setting of the Highland is of major importance, for the area lies on the eastern boundary of the Cascade Range adjacent to the Modoc Plateau, and about 70 miles west of the boundary of the Great Basin province. Higgins (1973) has recently defined a high-alumina shield volcano belt (Fig. 2) which he considers a sub-province of Waters' high-alumina plateau basalt petrologic province. The Medicine Lake Highland and Newberry Volcano of central Oregon are located in this sub-province, both volcanic centers being very analogous to one another, especially with regard to their youngest periods of volcanicity. This comparison will be developed in more detail later in this paper.

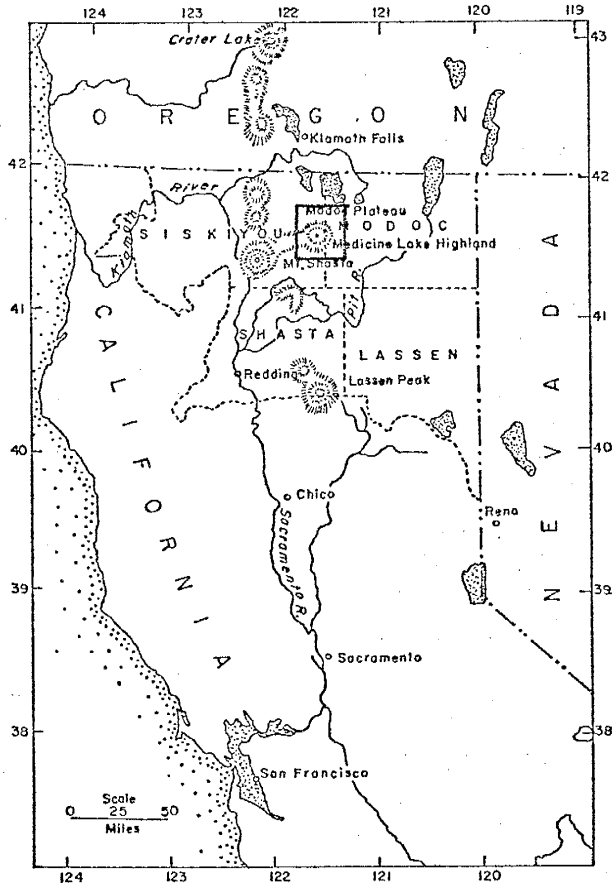

Figure 1. Map of northern California, showing the thesis area location.

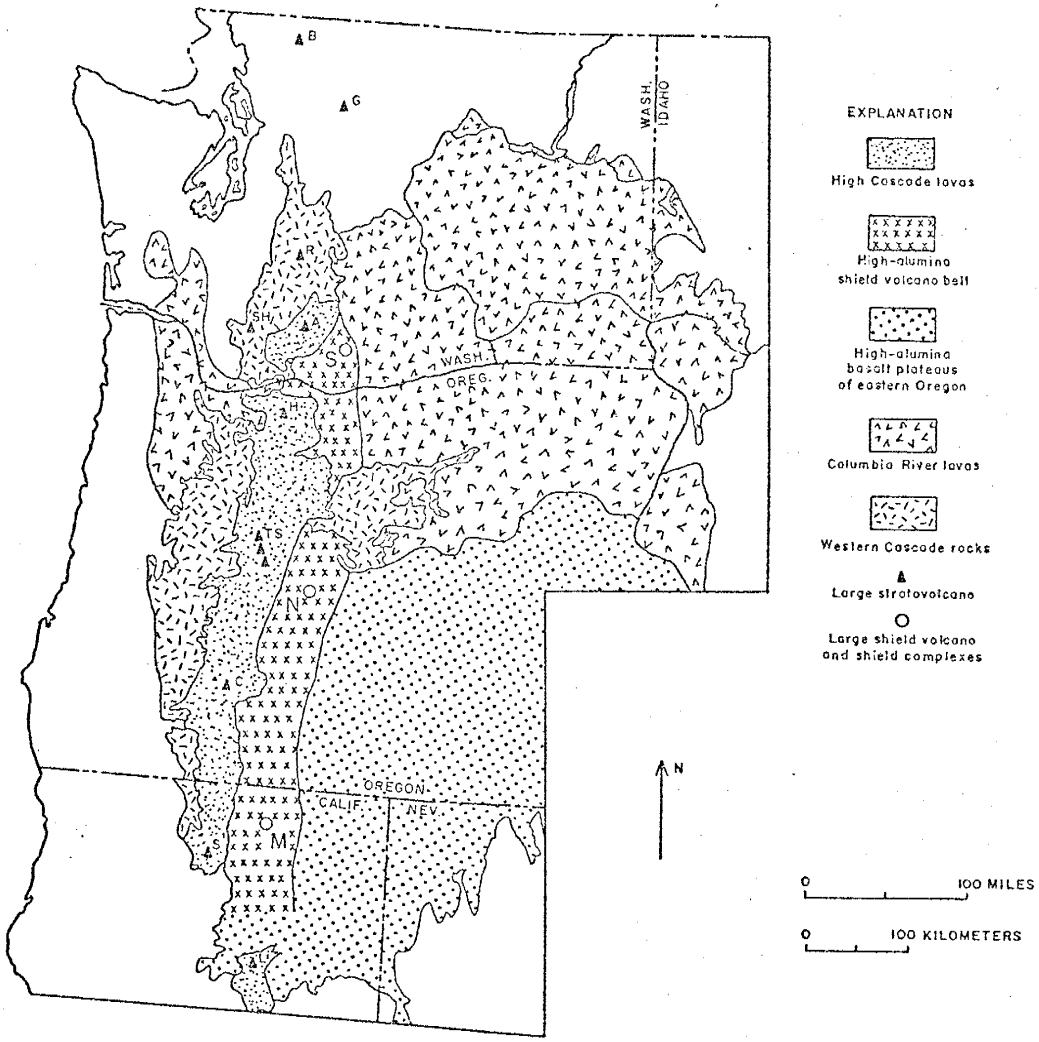

Figure 2. Generalized geologic map of volcanics in northern California, Oregon, and Washington, showing the high-alumina shield volcano belt (after Higgins, 1973). N = Newberry Volcano, M = Medicine Lake Highland Volcano, L = Lassen Peak, S = Mount Shasta, C = Crater Lake, TS = Three Sisters, H = Mount Hood, A = Mount Adams, SH = St. Helens, R = Mount Rainier, G = Glacier Peak, B = Mount Baker.

Physiography

To the north, east, and south, the Medicine Lake Highland is flanked by the Modoc plateau which has an average elevation of 4,800 feet and is occasionally broken by small fault block mountains. Westward the highland merges with the volcanics of the Cascade Range.

The Highland proper has a diameter of about 20 miles, its flanks converging at higher elevation into a central elliptical rampart of cones and domes 4 by 6 miles in diameter. Mount Hoffman, the highest dome, has an elevation of 7,913 feet. The rampart encloses a basin, the western side of which is occupied by Medicine Lake which has a surface elevation of 6,700 feet.

VOLCANIC HISTORY

Previous Investigations

Geologic inquiry concerning the Medicine Lake Highland area was initiated in 1897 when an obsidian sample collected by J. S. Diller was analysed by the U. S. Geological Survey (Clarke and Hillebrand, 1897).

The next significant mention of the Highland occurred in the five year period from 1928 to 1933. R. H. Finch (1928) postulated that a small explosive eruption had taken place at Glass Mountain in 1910. In the same year, H. T. Stearns (1928) published a description of lava tubes located in Lava Beds National Monument. M. A. Peacock (1931a) and H. A. Powers (1932) culminated a study sponsored by Harvard University which dealt with the lavas of the Modoc Lava Bed Quadrangle. Their reports included a reconnaissance geologic map of the quadrangle, petrographic descriptions, and major element analyses of samples. A brief description of the Burnt lava flow was published by R. H. Finch (1933) and the volcanic history of the Glass Mountain complex was delimited by C. A. Anderson (1933), in the same year.

At the suggestion of H. A. Powers, Anderson undertook a detailed study of the Highland in 1934. Anderson's (1941) map of the area and his geologic interpretation were of great value during the present study. Major element analyses of Powers (1932) and Anderson (1941) were used by Tilley (1950) to define hi-alumina basalt, the Medicine Lake Highland being the type-location.

Radiocarbon ages of trees killed by a pumice fall from the Glass Mountain complex were determined by Chesterman (1955). Additional radiocarbon ages were presented by Ives and others (1964), who dated the Burnt flow in a similar manner. I. Friedman (1968) dated obsidian samples from the Glass Mountain complex using hydration rates as age criteria; these compared favorably with radiocarbon dates obtained by M. Rubin (unpublished data).

Smith and Carmichael (1968) discussed and compared the petrography, mineralogy, and major element chemistry of lavas from Lassen Peak, Mount Shasta, and the Medicine Lake Highland in a paper dealing with Quaternary lavas from the southern Cascades. In a subsequent paper, Peterman, Carmichael, and Smith (1970) presented strontium isotope data from the three areas mentioned above. Oxygen isotope analyses from volcanics in the highland were reported by H. P. Taylor (1968).

In addition to the previously mentioned work currently being done in the area, A. T. Anderson, of the University of Chicago, is engaged in research concerning the chemistry of the glass phase of Recent basaltic cinders.

Summary of Volcanic History

Introduction

The following summary of the volcanic history of the thesis area is derived in large part from C. A. Anderson's (1941) Volcanoes of the Medicine Lake Highland, California. All interpretations, unless otherwise indicated, are Anderson's. However, the section on Recent volcanism contains many interpretations due to the author.

Pre-Highland Volcanism

The oldest rocks exposed in the area belong to the Miocene Cedarville series which crops out in the small fault block mountains of the lava plateau to the north and east of the Highland. The rocks of the series are basaltic and andesitic in composition and are largely of pyroclastic origin. Usually these rocks are tilted and folded and are exposed in the thesis area at Yellow and Juniper Buttes.

Unconformably overlying the Cedarville series is the Warner basalt, which is composed of a series of Pliocene basalt flows that lie nearly horizontal except where tilted by recent faulting. These basalts are the most widespread surficial rocks in northeastern California, averaging about 100 feet in total thickness in the thesis area (Powers, 1932). They are apparently the products of fissure eruptions and represent plateau volcanism on a moderate scale.

In the northwest section of the Highland, beds of massive andesite tuff are exposed and rest conformably on the Warner basalt. Anderson suggests that the tuff is the result of a Pelean type eruption emanating from vents now occupied by two rhyolite domes near Dock Well.

Distributed around the margin of the Highland are at least nine separate bodies of obsidian and massive or platy rhyolite not completely covered by later Highland lavas. The forms of these bodies indicate to Anderson that the majority of them were extruded as flows.

To the west of the Highland is a group of volcanic cones related to massive basaltic lavas. Powers (1932) referred to them as the "massive lava group" and included them with the rhyolitic bodies distributed around the Highland margin.

Although the massive basalts and most of the silicic bodies postdate the andesite tuff and are covered by later Highland lavas, Anderson finds no evidence indicating a genetic relationship between the two diverse rock types. The peripheral distribution of the obsidians indicates to him that they are related to the volcanicity centering in the present Highland. The massive basalts, on the other hand, form the eastern margin of a province of similar volcanics to the west.

Growth of the Andesite Volcano - Initiation of Highland Volcanism

Growth of the Medicine Lake Volcano was initiated by the eruption of numerous flows of fluid pyroxene-olivine andesite which built up a shield volcano about 20 miles in diameter. This lava is referred to as the older platy olivine andesite (OPOA) by Anderson. The slope of the flows in the northwest, southwest, and southern portions of the Highland is about 3 degrees, indicating a center of eruption coincident with the present center of the Highland. Extrapolation of these slopes indicates that the summit of the shield volcano was approximately 400 to 600 feet higher than the present elevation of Medicine Lake.

Collapse of the summit is postulated by Anderson in his geologic history of the area. His hypothesis for caldera formation requires the development of a magma chamber under the shield volcano, followed by subsidence of a central block bounded by outward dipping fractures. As supporting evidence for his theory, Anderson cites similarities with calderas of known collapse origin, the extrapolated elevation of the original summit, and the lack of widespread ejecta cover on the OPOA which would have indicated an explosive genesis.

Rim Volcanism

Following the formation of the caldera, viscous olivine-free andesites flowed out on the caldera floor, buried the walls of the caldera, and flowed down the outer slopes of the shield for short distances. These lavas are termed the platy andesite (PA) by Anderson. Their eruption resulted in two east-west trending ridges forming the north and south rims of the caldera basin. Pyroclastic cones capping the ridges indicate that the last phase of the eruptions were explosive. The presence of glaciated surfaces on the PA suggests its age is probably Pleistocene.

The eastern side of the caldera basin underwent a much more varied development. Three separate complexes were built up, each having a different history and volcanic assemblage. These are discussed in order of earliest formation, but during later stages of activity they may have been erupted more or less contemporaneously. The youngest of these three complexes, the Glass Mountain center, is discussed in the next section as its age is Recent.

The Red Shale Butte complex, which includes Lyons Peak, began its growth with the eruption of olivine andesite identical to the andesite forming the Medicine Lake shield volcano. Termed the later platy olivine

andesite (LPOA) by Anderson, it overlies the PA of Medicine Mountain.

The LPOA was followed by the eruption of a coarsely porphyritic olivine basalt, designated the Lake basalt by powers (1932). The Lake basalt flowed westward in the caldera basin and presently forms the eastern and northeastern of Medicine Lake.

Following the eruption of the Lake basalt, two new vents discharged viscous platy andesites forming two coalescing volcanoes, Red Shale Butte and Lyons Peak. Minor amounts of dacitic lava were also extruded with the andesite from the Lyons Peak Volcano. The lower slopes of Red Shale Butte exhibit the effects of glacial abrasion, suggesting a Pleistocene age.

The Mount Hoffman complex started its growth with the eruption of basaltic lavas. These basalts were similar to the Lake basalt, but differed by being less porphyritic. They overlie both the PA of the northern rim and the LPOA of Red Shale Butte. Overlying the basalt, the main body of the complex is essentially a circular table built by successive flows of viscous rhyolite 50 to 150 feet in thickness. The last activity at the complex consisted of the eruption of a short tongue of perlitic rhyolite about 100 feet thick, which was followed by the protrusion of a dome about 200 feet above the flow surface. Glacial erratics found on the sides of Mount Hoffman indicate a Pleistocene age for most of the rhyolite, but the small flow and dome appear to be Recent.

Recent Volcanism

The last volcanism to occur in the Highland area, that with which this study is concerned, consisted of the contemporaneous eruption of

basalts, basaltic andesites, dacites, and rhyolites. This type of association, in which rocks of intermediate composition are sparse or absent, has been termed "bimodal" by Hamilton (1965). The period of eruption of this bimodal assemblage extends from late Pleistocene to within the last few centuries. The basalts and basaltic andesites are more abundant than the dacites and rhyolites, the volume ratio being estimated at 25:1. In general, the siliceous flows are confined within or near the caldera, while the basic lavas cover the flanks of the older shield volcano. This spatial distribution also occurs at Newberry Volcano in central Oregon (Williams, 1935; Higgins and Walters, 1967, 1968, 1970; Laidley and McKay, 1971; Higgins, 1973), although Recent flows of basic composition are not as voluminous there as in the Medicine Lake Highland area.

Over 100 basaltic cinder cones are present in the thesis area. Powers (1932) referred to these cones and associated flows as the Modoc basalt. The Modoc basalts are distributed over the entire Highland, although most notably on the northern, eastern, and southern flanks of the older shield volcano. The cones limited to the caldera basin are late Pleistocene in age and do not appear to be related to the postglacial cones and flows occurring on the flanks of the Highland. Most of the basalt occurring on the flanks was erupted from vents between 5000 and 6000 feet in elevation. Usually these flows followed the construction of associated cones; but some, such as the Devil's Homestead flow, were erupted from fissures or chimneys.

Anderson separated the Modoc basalts into two groups based on texture and surface characteristics. The oldest group represents the more fluid of these lavas, as exemplified by smooth, corded, pahoehoe

surfaces and lava tubes. Intersertal texture is dominant in most of these flows. The latest Modoc flows fall into the second group which is in large part porphyritic, with plagioclase phenocrysts set in a dark aphanitic groundmass. Blocky aa surfaces characterize these later flows, although local areas of pahoehoe surface are found. The author found Anderson's groupings generally viable. In this paper, the lavas of the first group are termed "older Modoc"; while the second group is distinguished as "younger Modoc". Several flows of intermediate age were defined and are termed "intermediate Modoc". A relative age scale for the Modoc basalts and basaltic andesites discussed in this paper is given in Figure 3. These relative ages were determined by the author on the basis of surface freshness, vegetation, and pumice cover on the respective flows.

Radiocarbon analysis of a tree killed by the Burnt lava flow (possibly one of the most recent of the younger Modoc) gave an age of 200±200 years (Ives and others, 1964) for the flow. This young date is supported by the sparsity of pumice on the surface of the flow, since the nearby Glass Mountain complex, whose last dated activity occurred within the last few centuries (M. Rubin, unpublished data; I. Friedman, 1968), had numerous pumice eruptions.

The Recent silicic lavas, located within or near the caldera, are discussed in the order of their eruption (Fig. 4) as inferred by the author from surface freshness, vegetation, pumice cover, and field relationships. Much of their volcanic history is overlapping, however, and the order should not be considered absolute.

The Hoffman flow, a recent rhyolite flow, occupies the gap between Mount Hoffman and Red Shale Butte. Fronts of the flow range between 50

FIGURE 3

RELATIVE AGES OF THE MODOC FLOWS

1. YOUNGER MODOC

   a - Burnt

       Callahan[1]

   b - Schonchin[1]

   c - Devil's Homestead

   d - Paint Pot Crater

2. INTERMEDIATE MODOC[2]

   a - Black Crater

   b - Ross Chimneys

3. OLDER MODOC

   a - Three Sisters

   b - Older Modoc undifferentiated with respect to individual flows

1 - Both the Callahan and Schonchin flows were subdivided into older, intermediate, and younger sections, all of these sections being classified as younger Modoc.
2 - Using Anderson's (1941) classification the intermediate and younger Modoc would form one group; significant age differences noted between the flows, however, led the author to believe that further discrimination was needed.

FIGURE 4

RELATIVE AGES OF RECENT SILICIC FLOWS

1. Glass Mountain Complex

    a - Composite flow

        1 - Dacite section

        2 - Rhyolite obsidial section

    b - Rhyolite obsidian flow

    Little Glass Mountain

    a - First rhyolite obsidian flow

    b - Second rhyolite obsidian flow

2. Medicine Flow

3. Hoffman Flow

and 150 feet in height and a dome 1500 feet in diameter is located in the central portion. There is some variation in the lavas of the flow, the majority being subvitreous and black with local areas of pumiceous and glassy types. Numerous olivine basalt inclusions are distributed throughout the flow.

The Medicine flow, glassy black dacite, covers an area of about 1 square mile north of Medicine Lake. This small flow is very similar in appearance to the Hoffman flow, although no dome or basaltic inclusions are present.

Little Glass Mountain underwent a relatively simple volcanic history. Following significant pumice eruptions, two obsidian flows were extruded, the second almost completely covering the first. The surface of both flows is pumaceous with occasional obsidian blocks lying on them.

The Glass Mountain complex, which collectively forms the largest exposed silicic body in the area, underwent a more complicated volcanic history than the other silicic centers. Anderson (1933b) presented a detailed account of the history of the complex, a summary of which follows:

Explosive eruptions which built up several steep sided pumice cones and showered the Highland with white rhyolitic pumice were followed by voluminous extrusions of lava. Most of the lava flowed down the eastern slope of the Highland and split into two tongues around a buttress of pre-Highland obsidian and dacite. The remainder flowed to the west, covering part of the Hoffman flow. This first flow, termed the "composite flow" by Anderson, is of particular interest as the two eastern tongues are composed of a dark dacite containing inclusions of olivine basalt, while the western section of the flow is composed of rhyolitic obsidian

devoid of basaltic inclusions. In addition, the dacitic section contains numerous pods and stringers of obsidian with dimensions up to about 3 feet in thickness and 10 feet in length. A relatively narrow transition zone, defined by the author, exists between the two sections of the flow and is composed of rocks of both types. A second flow composed entirely of rhyolite obsidian forms the second "layer" of Glass Mountain. This flow was not as voluminous as the first and the flow margin stands out sharply from the underlying composite flow. Numerous eruptions of rhyolitic pumice occurred throughout the volcanic evolution of the Glass Mountain complex, although none were as extensive as those which were erupted before the emplacement of the composite flow. The last significant activity at Glass Mountain was the rise of a dome of rhyolitic obsidian, about a quarter mile in diameter and 100 to 150 feet in height.

Radiocarbon dating of the initial pumice eruption at the Glass Mountain complex gives an age of 1360±240 years (Chesterman, 1955). These dates were obtained from trees buried by the pumice. Dates for the composite flow, obtained in a similar manner, indicate ages of 390, 380, 190, and 130 years, all ±200 years (M. Rubin, unpublished data). I. Friedman (1968) dated the western obsidian section of the composite flow at 300±60 years, using hydration rinds on the obsidians as age criteria.

GEOCHEMISTRY OF THE RECENT VOLCANICS

Summary of Previous Geochemical Studies

Major Element Studies

Powers (1932) stated on the basis of major element analyses that all the basalts in the Highland area show very little variation in chemical composition and that the Modoc basalts, being erupted from the same general center, are differentiates of the same magma. In addition, he pointed out that the composition of both pre-Highland and Recent rhyolite flows is remarkably constant. He concludes that the location, mineralogy, and chemistry relates the lavas of the Highland to those of the Cascades, the volcanics being derived by fractional crystallization of a primary basaltic magma.

The analyses of Anderson (1941) showed greater variability in the composition of the basic lavas, these being more similar to the lavas of Newberry volcano with respect to Al_2O_3, MgO, and CaO content than to High Cascade lavas. Anderson stated that the older Modoc basalts have higher total Fe and MgO contents than the younger Modoc basalts and suggested that the volcanic assemblage at Medicine Lake may have been derived from a tholeiitic basalt parent.

Smith and Carmichael (1968) analyzed 4 samples of the younger Modoc and used these analyses in conjunction with those of Powers and Anderson to reach conclusions concerning the Highland area. They also compared the composition of Highland lavas to the lavas of Mount Lassen and Mount Shasta. The Modoc basalts and basaltic andesites they examined were

were classified as being the hi-alumina type based on chemical parameters developed by Kuno (1960). The higher alkali content, particularly K_2O, of the Medicine Lake lavas was noted and interpreted as being a function of increasing depth of magma formation (Kuno, 1966; Dickinson, 1968). Petrogenesis of the lavas was postulated to be the result of melting an upper mantle parent of feldspathic peridotite under either wet or dry conditions over appropriate pressure and temperature ranges, this type of genesis giving rise to all the Quaternary volcanism at Mount Shasta, Mount Lassen, and Medicine Lake.

Oxygen Isotope Data

H. P. Taylor (1968) determined oxygen isotope ratios (O^{18}/O^{16}) in whole rock samples from each of the major volcanic groups in the Highland area. The results of these analyses, shown in Figure 5, are significant with respect to the magmatic evolution of the Highland volcanics.

All the pre-Modoc flows are very low in O^{18}, the range being from δ = 5.5 to 6.3. The Recent flows are O^{18} enriched, with δ values ranging from 6.8 for the Modoc basalt to 8.5 for dacitic lavas. Values for the young obsidians lie between those of the Modoc basalt and the young dacites. Taylor suggests that the intermediate values for the young obsidians may be due to hybridization with the older, low δ value, magmas. He supports this hypothesis with mention of the composite flow at the Glass Mountain complex. Unfortunately, Taylor did not determine the O^{18}/O^{16} ratio of the dacite of the composite flow. All other dacites analyzed, from the Hoffman and Medicine flows, give high δ values (7.8 to 8.5); therefore, hybridization of these magmas with the young

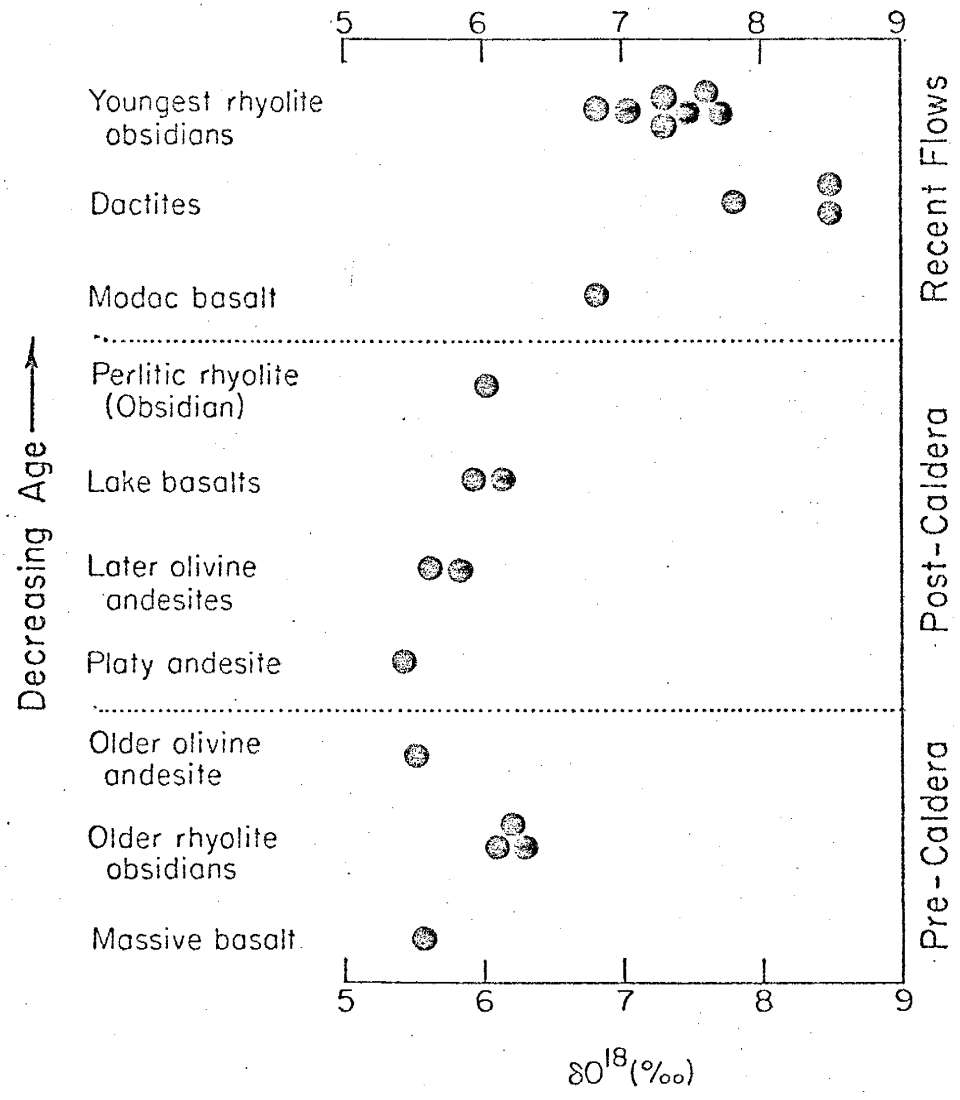

Figure 5. Oxygen isotope values of the Highland volcanics (after Taylor, 1968).

obsidians could not lower the δ values, but would have the opposite effect.

The author agrees with Taylor's postulation that the difference in O^{18}/O^{16} ratios between the older and younger lavas implies that at least two different mechanisms were involved in the evolution of the Highland magmas. The older group of lavas displays a trend in which essentially no change occurred in the O^{18}/O^{16} ratio; whereas, the Recent volcanics show a sharp increase in O^{18} with corresponding increases in SiO_2, excepting the high δ values for the dacites.

Little can be said about crustal contamination of the Highland lavas in light of oxygen isotope data. Most meta-sedimentary and almost all meta-igneous rocks have fairly low δ values and large amounts of them would have to be incorporated in the magma before any significant increase in O^{18} values could be realized.

The Recent dacites, however, are similar in O^{18} content to plutonic tonalities and granodiorites from the Sierra Nevada and Southern California batholiths. It is possible that they could have been formed by the same type of process as the granites or be re-fused material from a hypothetical batholith underlying the Highland. These mechanisms are not viable for the young obsidians however, as they are much lower in O^{18} than corresponding quartz monzonites and granites of these batholiths.

Strontium Isotope Data

Peterman and others (1970) reported Sr^{87}/Sr^{86} ratios for the samples from Mount Shasta, Mount Lassen, and Medicine Lake previously discussed by Smith and Carmichael (1968). Two additional analyses of Recent Highland rhyolites performed by Hedge and Wathall (1963) were also incorporated in their discussion.

The range of Sr^{87}/Sr^{86} for the Recent Highland lavas ranges from 0.7032 to 0.7043. These ratios fall in the range reported for volcanic rocks from oceanic islands (Hedge, 1966; Powell and DeLong, 1966; Pushkar, 1968; Hedge and Knight, 1969) suggesting an upper mantle source. No evidence from the strontium isotope data implies that the Recent Highland volcanics were contaminated significantly by the incorporation of old sialic crustal material. However, the possibility of contamination with young sialic crust derived from the mantle cannot be eliminated.

Analytical Methods

Sampling

Samples collected in the field for geochemical analysis were chosen chiefly on the basis of geology and freshness. Sample locations are shown on the enclosed map of the thesis area. At each location samples were collected in triplicate, providing a specimen for thin section, chemical analysis, and reference. Locations were mapped on U.S. Geological Survey 15-minute quadrangle maps; the Medicine Lake, Timber Mountain, and portions of the Mount Dome, Tulelake, Hambone, and White-horse quadrangles being used for this purpose. Aerial photographs were used as guides to the location and form of flow units.

Sample Preparation

Preparation of rock samples for chemical analysis was accomplished by the procedure outlined below. Figure 6 is a flow diagram of the various procedures performed on the samples.

1. The sample was reduced to pieces approximately 0.5 inches in their maximum dimension using a sledge and stainless steel plate.

2. After elimination of pieces exhibiting any signs of weathering, about 50 grams of the material was fed through a Lemaire Model 150 jaw crusher (equipped with ceramic plates) four times; twice with an 1/8 inch aperature at the discharge opening and twice with an 1/6 inch aperature.

3. About 15 grams of sample was then ground by hand on a mullite

FIGURE 6

FLOW DIAGRAM OF SAMPLE PREPARATION METHODS

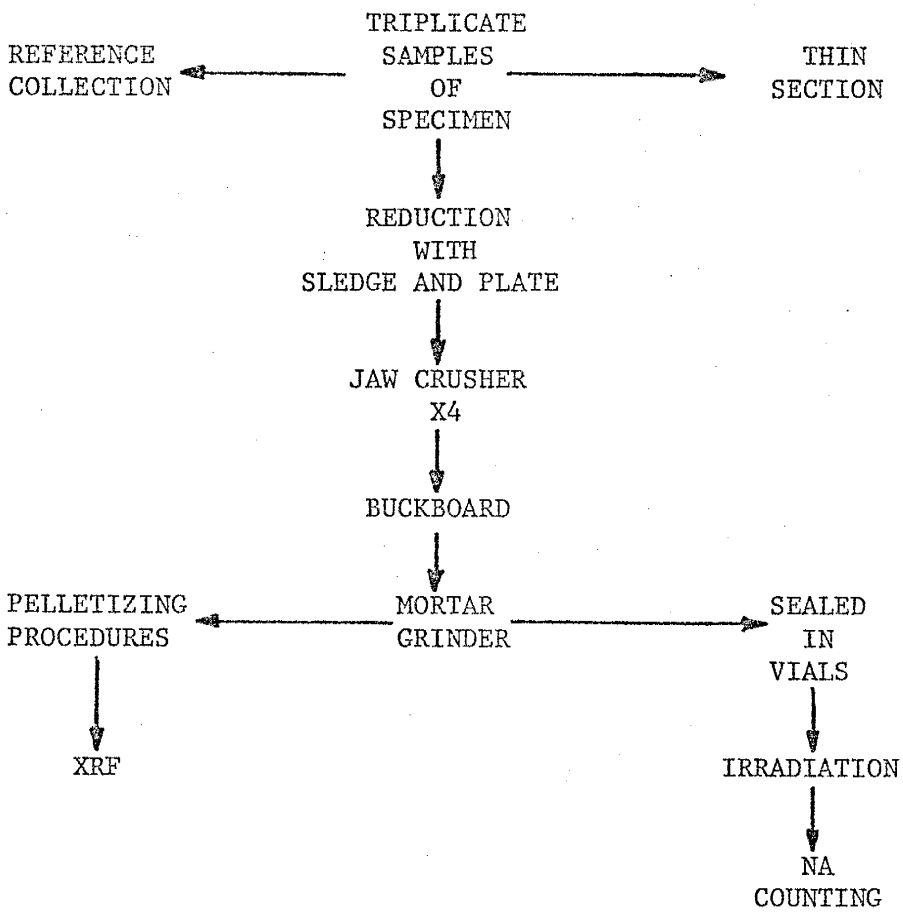

XRF = X-RAY FLUORESCENCE
NA = NEUTRON ACTIVATION

buckboard until the individual particles were approximately 2 millimeters or less in size.

4. The buckboard material was ground in a Fisher Model 155 mortar grinder until a particle size of 97 microns or less, as suggested by Volborth (1963), was achieved. This size was determined by optically comparing the sample with a standard whose particle size was $\leq$ 97 microns.

5. Pellets of the samples were prepared for X-ray fluorescence in the following manner:

a- Six grams of sample were diluted with 1 gram of ground bakalite powder using a Mettler Model H 10 TW analytical balance, the weighing being carried out to the nearest 0.0001 of a gram.

b- This mixture was then transferred to a plastic vial along with a polyethylene ball and homogenized for 10 minutes in a Spex Model 8000 Mixer/Mill.

c- The powder was placed in a stainless steel die which was inserted in a heating jacket and put into a Research and Industrial Instrument Company 25 ton ring press. A temperature of 120°C and pressure of 12 tons was maintained for 8 minutes to produce a solid pellet for X-ray fluorescense.

6. Samples for neutron activation analysis were derived by sealing 0.5 grams of ground sample from step 4 in a ½ inch by ¼ inch polyethylene vial. Again, weighing was carried out to the nearest 0.0001 of a gram.

During all the above steps care was taken to prevent any undue con-

tamination of the samples. The preparation equipment was throughly washed with distilled water between samples to avoid any contamination from one sample to the next. The most likely sources of contamination were Fe from the sledge and stainless steel plate, alumina from the jaw crusher and buckboard, and Si from the mortar grinder. Since all of these cases involve major elements and very minor amounts of contamination, their influence on the analyses was considered negligible.

Major and Trace Element Determinative Methods

Analyses were performed by non-destructive X-ray fluorescence (XRF) and neutron activation (NA). Over 200 samples from basalt, basaltic andesite, dacite, and rhyolite flows in the thesis area were analyzed for Si and K by XRF to identify gross geochemical trends. One hundred and two samples were then selected for more complete analysis.

X-ray fluorescence data were obtained on a Philips 8-position vacuum spectrograph equipped with a simultaneous output printer. Counting was done entirely in the fixed time mode. The major elements Si, Ti, Al, Fe, Mg, Ca, and K and the trace elements Rb, Sr, Zr, Cu, and Ni were analyzed for by XRF using methods previously described (Condie, 1967a,b). U.S. Geological Survey standard rocks W-1, BCR-1, T-1, GSP-1, AGV-1, SY-1, and G-2 and the French granite standard rocks GH and GR were used to construct major element calibration curves. Trace element analyses were made using W-1 and BCR-1 as standards for the basalts and basaltic andesites and G-2 for the dacites and rhyolites. Instrumental parameters for the XRF work and major element calibration curve statistics are listed in Tables 1 and 2, respectively.

TABLE 1

X-RAY FLUORESCENCE INSTRUMENTAL PARAMETERS

ELEMENT	PEAK	TARGET	CRYSTAL	DETECTOR	GAS	COLLIMATOR	PATH	KV	mA	FT[2]
Si	Kα	Cr	EDDT	FPC	P-10	Coarse	VAC	45	25	10
Ti	Kα	W	LiF(200)	Scin	-	Coarse	VAC	45	35	10
Al	Kα	Mo	Gyp	FPC	P-10	Fine	VAC	45	35	10
Fe	Kα	W	LiF(200)	Scin	-	Coarse	AIR	45	35	10
Mg	Kα	Cr	ADP	FPC	Nat.	Coarse	VAC	50	28	10
Ca	Kα	Cr	EDDT	FPC	P-10	Coarse	VAC	45	25	10
K	Kα	Cr	EDDT	FPC	P-10	Coarse	VAC	45	25	10
Cu	Kα	Mo	LiF(200)	Scin[1]	-	Fine	AIR	50	40	20
Ni	Kα	Mo	Lif(200)	Scin[1]	-	Fine	AIR	50	40	50
Zr	Kα	W	Lif(200)	Scin	-	Coarse	AIR	50	40	10
Rb	Kα	Mo	LiF(200)	Scin	-	Coarse	AIR	50	40	10
Sr	Kα	Mo	LiF(200)	Scin	-	Coarse	AIR	50	40	10

1 0.0005" Ti Filter Used

2 Ft = Fixed time in seconds

Each sample was counted 10 times, each time for the number of seconds indicated

TABLE 2

MAJOR ELEMENT CALIBRATION CURVE STATISTICS

ELEMENT	CORRELATION COEFFICIENT	EQUATION	STANDARD ERROR OF ESTIMATE
Si	0.994	Y = 0.028X + 7.491	0.609
Ti	0.999	Y = 0.007X + 0.024	0.016
Al	0.988	Y = 0.025X + 1.960	0.228
Fr	0.999	Y = 0.002X - 0.705	0.100
Mg	0.997	Y = 0.022X + 0.034	0.182
Ca	0.991	Y = 0.001X - 0.023	0.246
K	0.998	Y = 0.001X - 0.077	0.057

X = Average counts

Y = Concentration

Standard Error of Extimate = Sy/x

Neutron activation analyses were performed using a Canberra 4,096 channel gamma ray spectrometer with a Li drifted Ge detector system. Again, counting was done in the fixed time mode. The method described by Condie and Lo (1971) was used in the determination of Na, Co, and Ba concentrations. W-1 and G-2 were used as standards for the basalts and basaltic andesites and dacites and rhyolites, respectively. Data pertinent to the NA analytical work are presented in Table 3.

Instrumental precision was determined prior to the use of the analytical equipment by M. Murray (1971) and K. C. Condie (personal communication) and was found to be satisfactory. An additional check of the precision was made during the XRF analytical work on the elements Si, K, Rb, and Sr; the results of this check are given in Table 4. Accuracy of the XRF analyses was determined by treating U.S. Geological Survey standard rocks as unknowns. The data obtained from the accuracy tests are listed in Table 5. Lower detection limits for the XRF analyses were calculated according to Jenkins and De Vries (1966) and analytical results falling below these limits were deleted from final data compilations.

Due to the necessity of a limited number of samples per run on the gamma ray spectrometer, precision and accuracy tests were not performed for the NA analytical work. Results of immediately prior work (K. C. Condie, personal communication), however, gave a total analytical error ± 5 percent for Na and Co, and ± 10 percent for Ba. Several U.S. Geological Survey standard rocks were treated as unknowns during the NA analytical work, the results falling well within the limits given above.

Thin Sections

Thin sections were made of most samples and modal estimates were

TABLE 3

NEUTRON ACTIVATION ANALYTICAL PARAMETERS

ELEMENT	IRRADIATION FLUX	LENGTH OF IRRADIATION (min)	COOLING PERIOD (Days)	PEAK (KEV)	COUNTING TIME (sec)
Na	1. X 10^{14}n/cm^2	3.33	0.5	1369	6.0 X 10^2
Co	9. X 10^{15}n/cm^2	60.0	98.0	1173	4.0 X 10^4
Ba	9. X 10^{15}n/cm^2	60.0	14.0	496	1.0 X 10^4

TABLE 4

X-RAY FLUORESCENCE INSTRUMENTAL PRECISION FOR Si, K, Rb and Sr[1]

Sample: H127 - Basaltic Andesite from Burnt Lava Flow.

	SiO_2	K_2O	Rb	Sr
Min.	55.37	1.48	62	195
Max.	55.61	1.53	69	210
Mean	55.49	1.50	65	203
S.D.[2]	0.13	0.02	2.95	5.37
CV (%)[3]	0.23	1.18	4.52	2.64

Sample: H296 - Dacite from Composite Flow, Glass Mountain Complex

	SiO_2	K_2O	Rb	Sr
Min.	63.21	2.49	96	276
Max.	63.66	2.54	112	287
Mean	63.46	2.52	105	282
S.D.[2]	0.15	0.02	5.62	3.54
CV (%)[3]	0.24	0.73	5.34	1.25

[1] Calculated from a total of 8 analyses of each sample; 4 pellets of each sample were made and both sides used during the XRF analytical work.

[2] S. D. = Standard Deviation

[3] CV (%) = Coefficient of variation in percent

TABLE 5

ACCURACY OF X-RAY FLUORESCENCE ANALYSES

Element	W-1			G-2		
	Accepted Value	XRF-1	XRF-2	Accepted Value	XRF-1	XRF-2
Si	52.64	52.31	52.85	69.19	68.95	69.21
Ti	1.07	1.03	1.08	0.53	0.50	0.51
Al	14.85	14.76	14.87	15.34	15.42	15.40
Fe	11.09	11.15	11.02	2.76	2.68	2.82
Mg	6.62	6.65	6.60	1.44	1.45	1.39
Ca	10.96	10.82	10.79	1.98	1.96	2.01
K	0.64	0.66	0.65	4.51	4.58	4.55
Cu	110	94	91	13	14	10
Ni	78	68	75	-	-	-
Zr	100	98	103	316	304	311
Rb	22	21	26	170	161	179
Sr	190	192	189	480	475	484

XRF-1 and XRF-2 are replicate analyses of W-1 and G-2, treated as unknowns

Major element concentrations are given in oxide weight percent; trace element concentrations are given in ppm

made of representative samples from flows considered pertinent to the present study. The anorthite content of plagioclase in several samples was determined by the Michel-Levy method. The author feels that a more detailed study of the thin sections would greatly enhance the value of the investigation.

Analytical Results

Bimodality and Chemical Classification

The bimodal character of the Recent Highland volcanics is clearly shown in the SiO_2 frequency diagram (fig. 7). It is interesting to note the extensive overlap in SiO_2 variation of the older, intermediate, and younger Modoc flows. No simple age relationship between SiO_2 variation and field estimates of relative ages of the flows is apparent. Variation within a single Modoc flow, such as the Callahan, covers a range up to 6.0 percent. This intra-flow variation is not expected however, as most of the younger Modoc exhibit characteristics (surface freshness, pumice cover, vegetation) interpreted by the author as indicating several periods of eruption contributing to the formation of a multiple flow unit.

With the exception of the dacite flow, the silicic lavas (rhyolites) exhibit very little variation in SiO_2. The Mount Hoffman flow, previously termed a dacite by Anderson (1941), seems more analogous to the rhyolites with respect to SiO_2 content. The dacite section of the composite flow exhibits an SiO_2 range of 9 percent. This wide range most probably reflects the effect of numerous olivine basalt inclusions which were impossible to totally eliminate from the samples during the analytical preparation stage.

Several common geochemical plots were used to classify the young Highland volcanics. The first of these is an AMF diagram (not illustrated), which shows the subdued Fe enrichment typical of calc-alkaline associations (Irvine and Baragar, 1971). Also interesting is the fact that the intermediate and younger Modoc generally plot as distinctive groups with respect to individual flows.

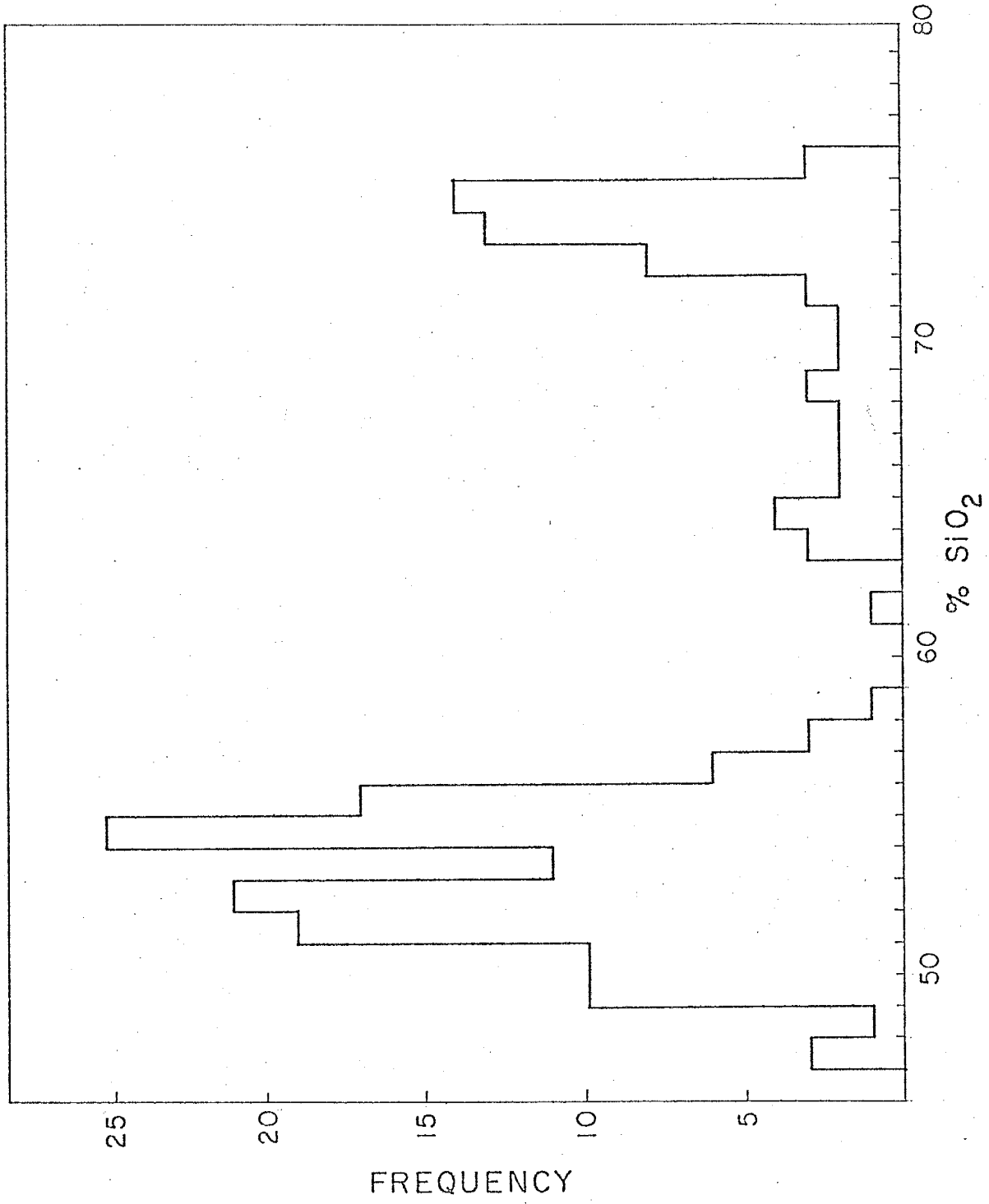

Figure 7. SiO_2 frequency diagram of the Recent Highland volcanics.

Figure 8 is a total alkali-SiO_2 diagram developed by Kuno (1966a) to distinguish between volcanics of the tholeiitic, high-alumina, and alkali series. On the basis of this plot practically all of the Modoc basalts and basaltic andesites are classified as high-alumina. The Recent Highland silicic rocks, however, plot in an intermediate zone between the high-alumina and alkali fields.

Another, more sensitive plot, was developed by Kuno (1960) to distinguish between basalts of the three above mentioned series at specified SiO_2 levels. In this diagram total alkalies are plotted against Al_2O_3 concentration (Fig. 9) and with minor exceptions the Modoc basalts plot in the high-alumina field.

Major Element Chemistry of the Modoc Basalts and Basaltic Andesites

Major element Harker variation diagrams for K_2O, Na_2O, Al_2O_3, CaO, TiO_2, total Fe (as Fe_2O_3), and MgO are presented in Figures 10 through 16, respectively. In these plots a general age relationship between the flows and composition becomes more apparent, especially with respect to the intermediate and younger Modoc. This relationship is most pronounced in the K_2O variation diagram (Fig. 10), where, with the exception of the Schonchin flow, an increase in K_2O with increasing SiO_2 content is observed to be a function of age; progressing from the intermediate Ross Chimneys to the younger Burnt and Callahan flows. This trend is also observed within multiple flow units, notably the Schonchin and Callahan, in which component flows of different ages were discerned. An increase in SiO_2 with K_2O content remaining fairly constant is observed in the Ross Chimneys, Black Crater, and Paint Pot Crater flows. The older Modoc exhibits an overlapping relationship with most of the intermediate and

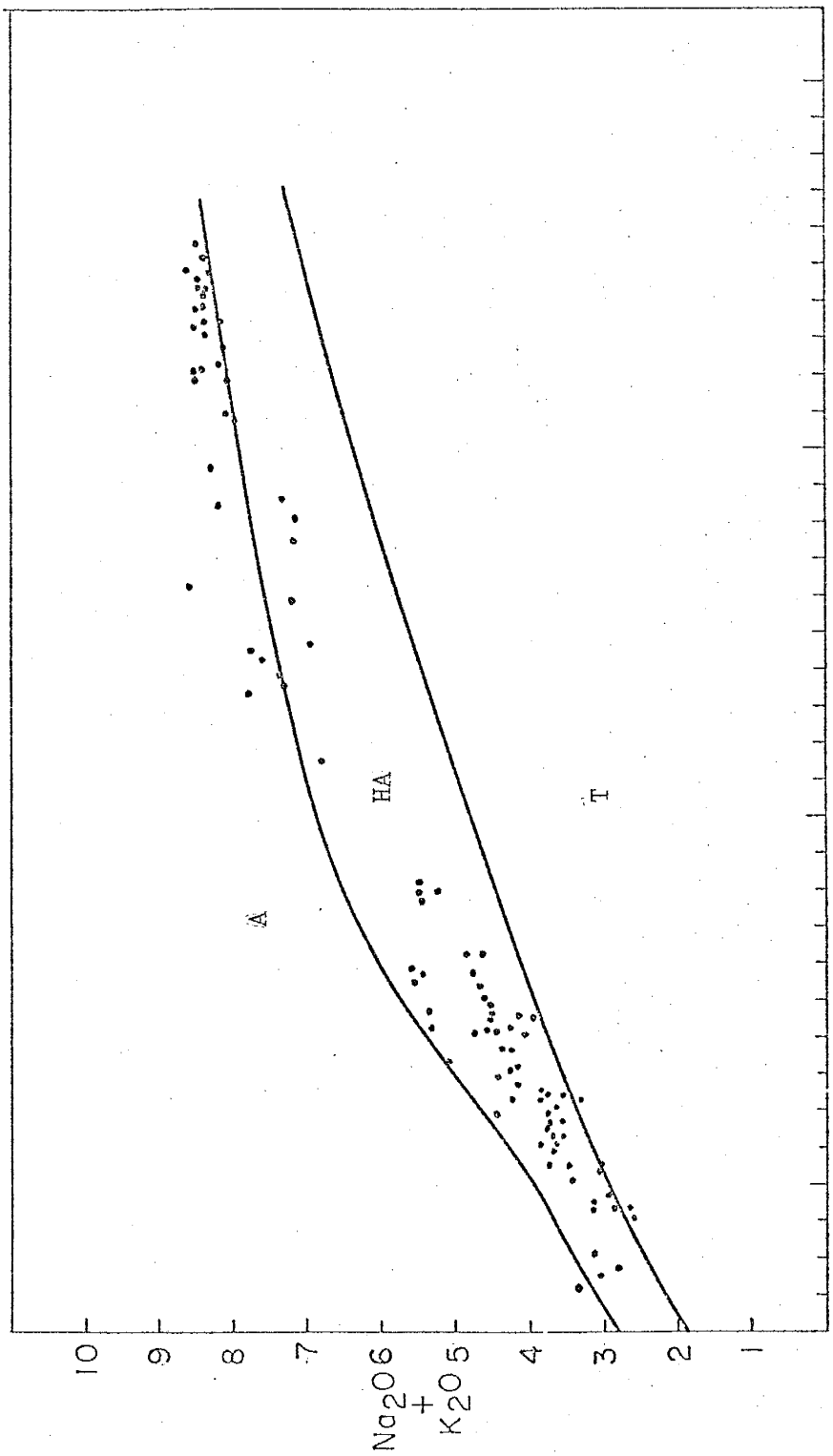

Figure 8. Total alkali-silica variation diagram. T = Tholeiite, HA = High Alumina, A = Alkali

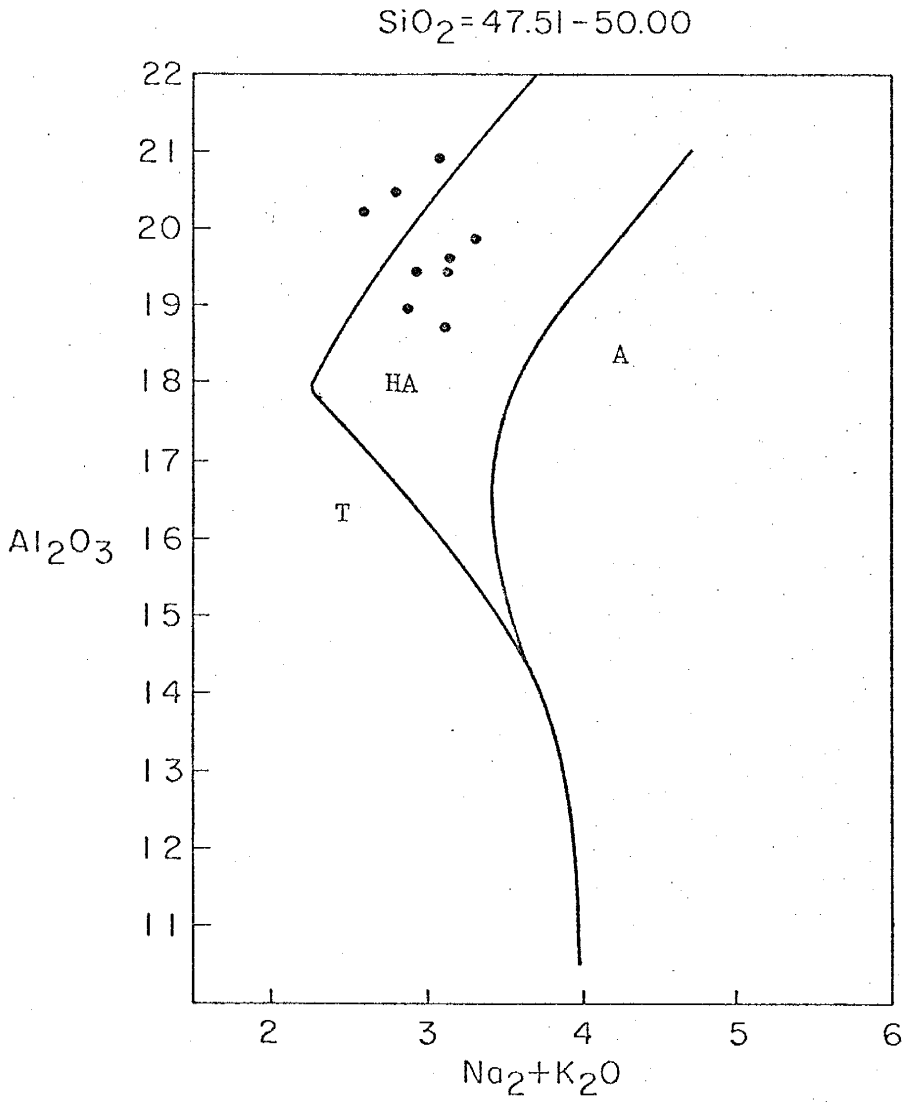

Figure 9. Total alkali-alumina variation diagram. T = Tholeiite, HA = High Alumina, A = Alkali.

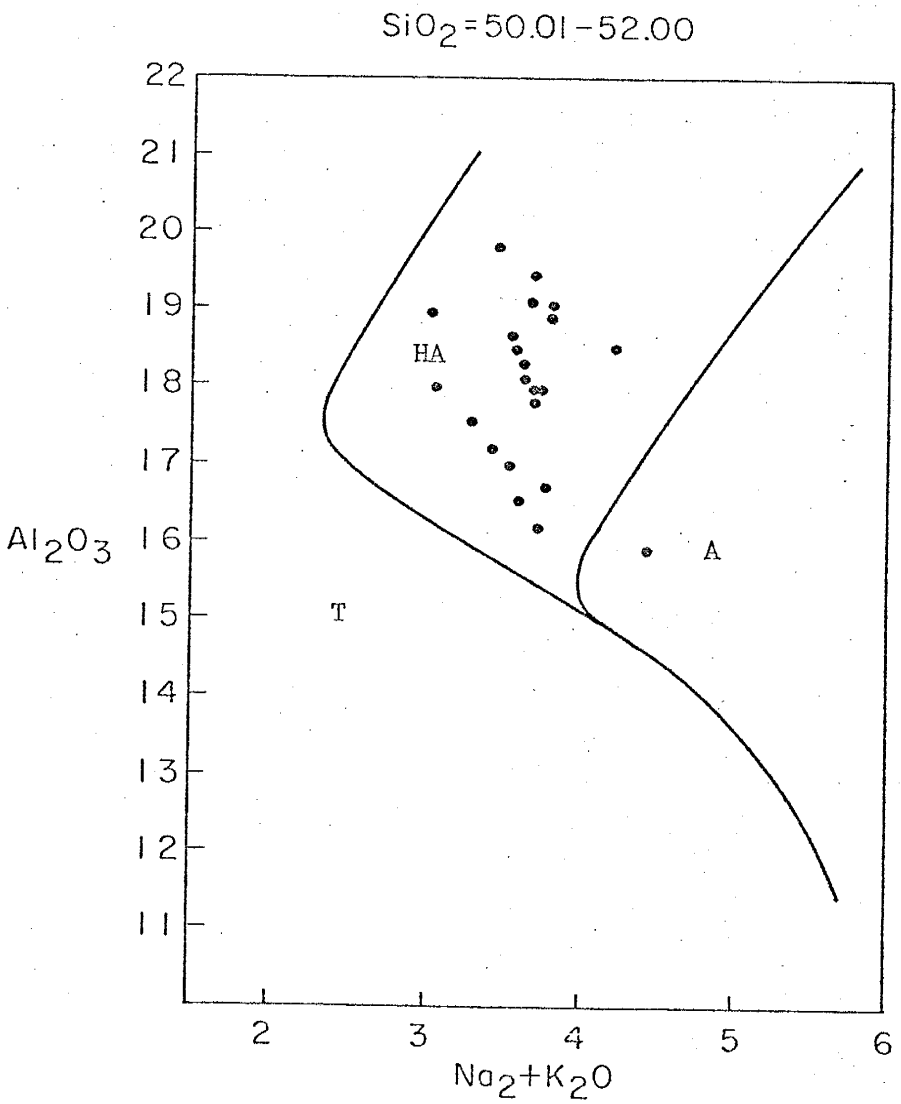

Figure 9. Continued.

SiO_2 = 52.51 - 55.00

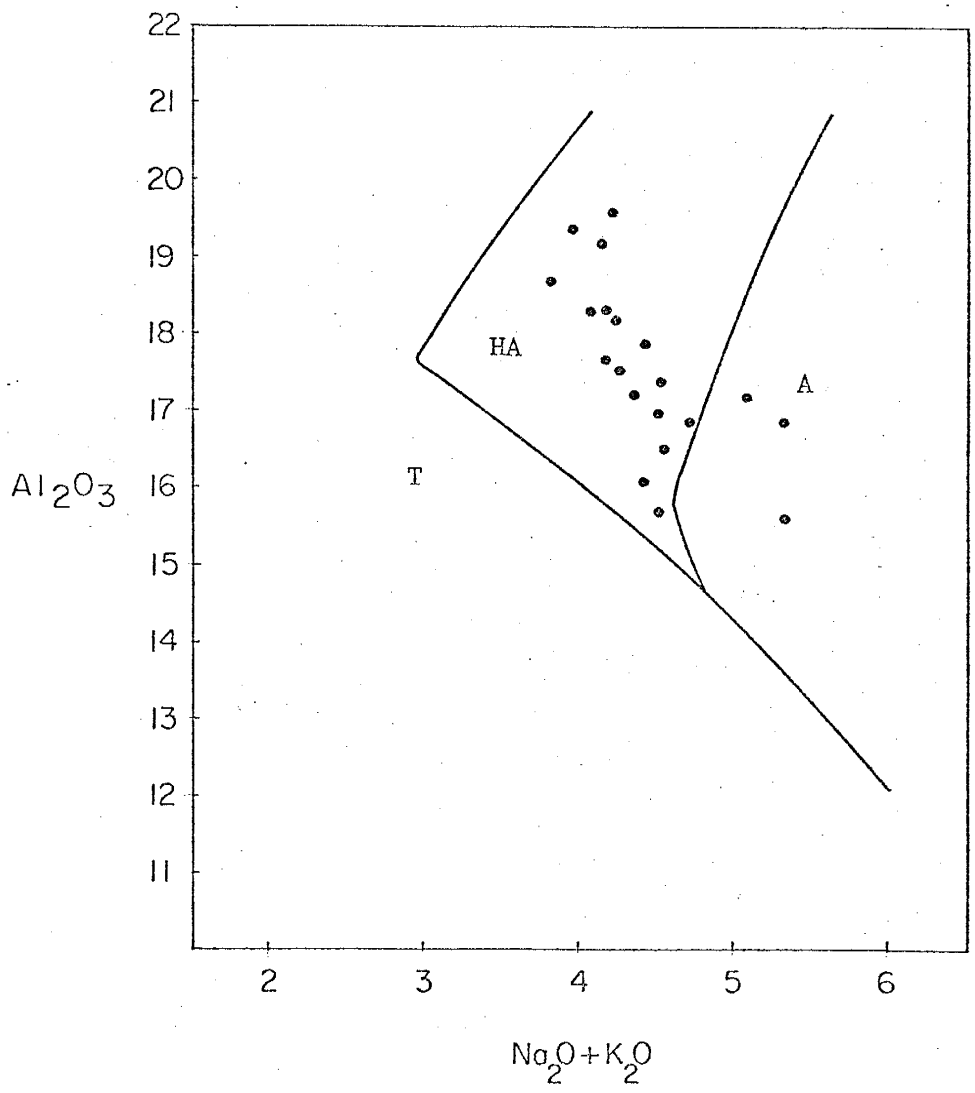

Figure 9. Continued.

Figure 10. Potassium-silica variation diagram.

MODOC BASALTS

+ DEVIL'S HOMESTEAD FLOW
· BLACK CRATER FLOW
△ ROSS CHIMNEYS FLOW
x SCHONCHIN FLOW
□ THREE SISTERS FLOW
o CALLAHAN FLOW
⊕ PAINT POT CRATER FLOW
⊹ BURNT FLOW
⊙ OLDER MODOC

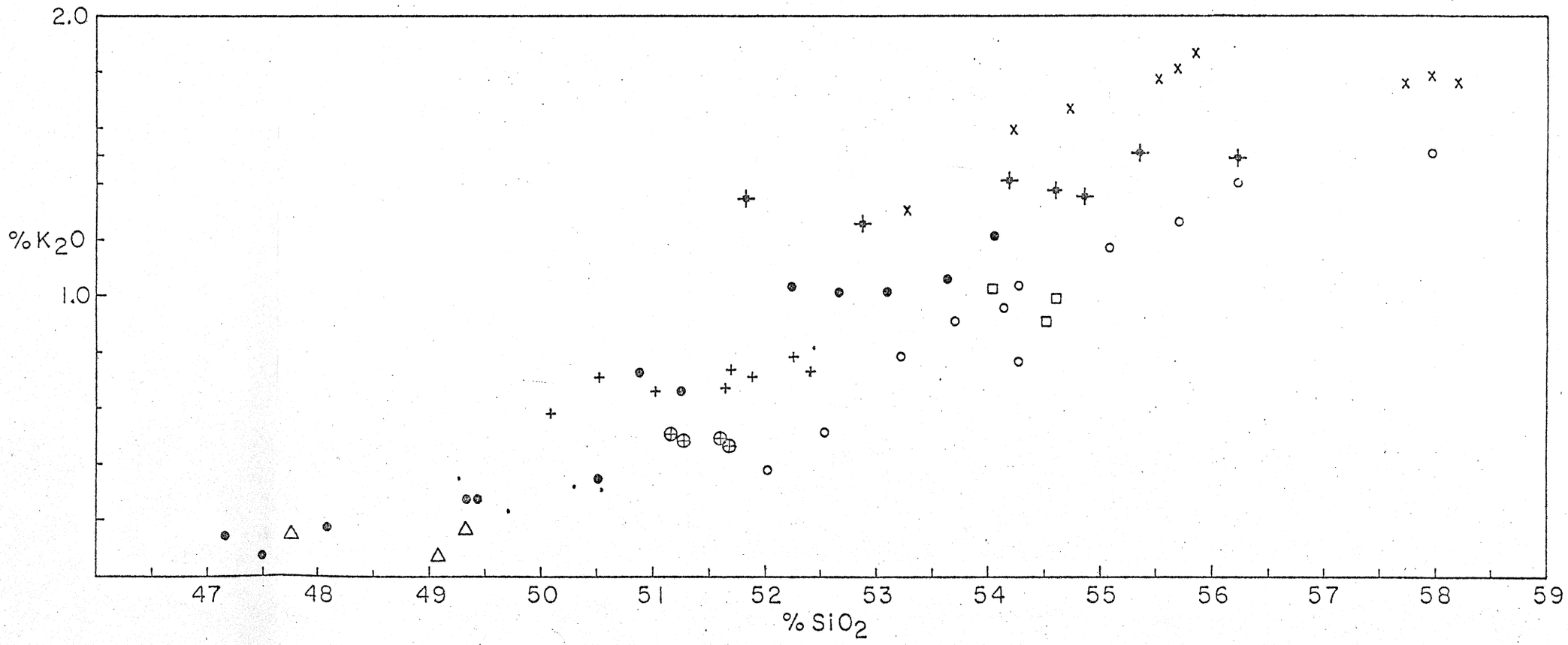
2.0
1.0
%K2O
47
48
49
50
51
52
53
54
55
56
57
58
59
%SiO2

younger Modoc; the youngest flows however, show significantly higher K_2O contents than the older Modoc flows.

The variation of Na_2O with SiO_2 (Fig. 11) is similar, but less pronounced, than that of K_2O with respect to the age relationships mentioned above. A rather constant Na_2O content within a flow or flow unit of given age is observed for essentially all the Modoc flows.

Alumina exhibits a significant degree of scatter when plotted against SiO_2 (Fig. 12). All the Modoc flows are high in Al_2O_3 content, ranging from 21 to 16 percent and showing a general decrease with increasing SiO_2. The trends of two flows, the Devil's Homestead and Burnt, are anomalous with respect to the others in that they show a definite increase in Al_2O_3 with a corresponding increase in SiO_2. The younger sections of the Schonchin and Callahan flows also exhibit this trend with respect to their older component flows.

The Modoc flows show a very coherent trend in CaO variation (Fig. 13), decreasing SiO_2 content. The trends of the Devil's Homestead, Burnt, and the intermediate age section of the Schonchin flow are exceptions in that CaO remains at a constant level with increasing SiO_2.

Titanium shows a very interesting distribution in the Modoc flows (Fig. 14). With the exception of the intermediate age section of the Schonchin, all the flow units exhibit nearly constant TiO_2 concentrations over their respective SiO_2 ranges, with concentration levels varying between flows. The older Modoc flows show two distinct levels of TiO_2 concentration: a group from the northern section of the thesis area (0.75 to 0.90 percent), and a group from the northeastern and eastern section (1.10 to 1.15 percent). The intermediate and younger Modoc flows

Figure 11. Sodium-silica variation diagram.

MODOC BASALTS

+ DEVIL'S HOMESTEAD FLOW
· BLACK CRATER FLOW
△ ROSS CHIMNEYS FLOW
x SCHONCHIN FLOW
□ THREE SISTERS FLOW
○ CALLAHAN FLOW
⊕ PAINT POT CRATER FLOW
✢ BURNT FLOW
● OLDER MODOC

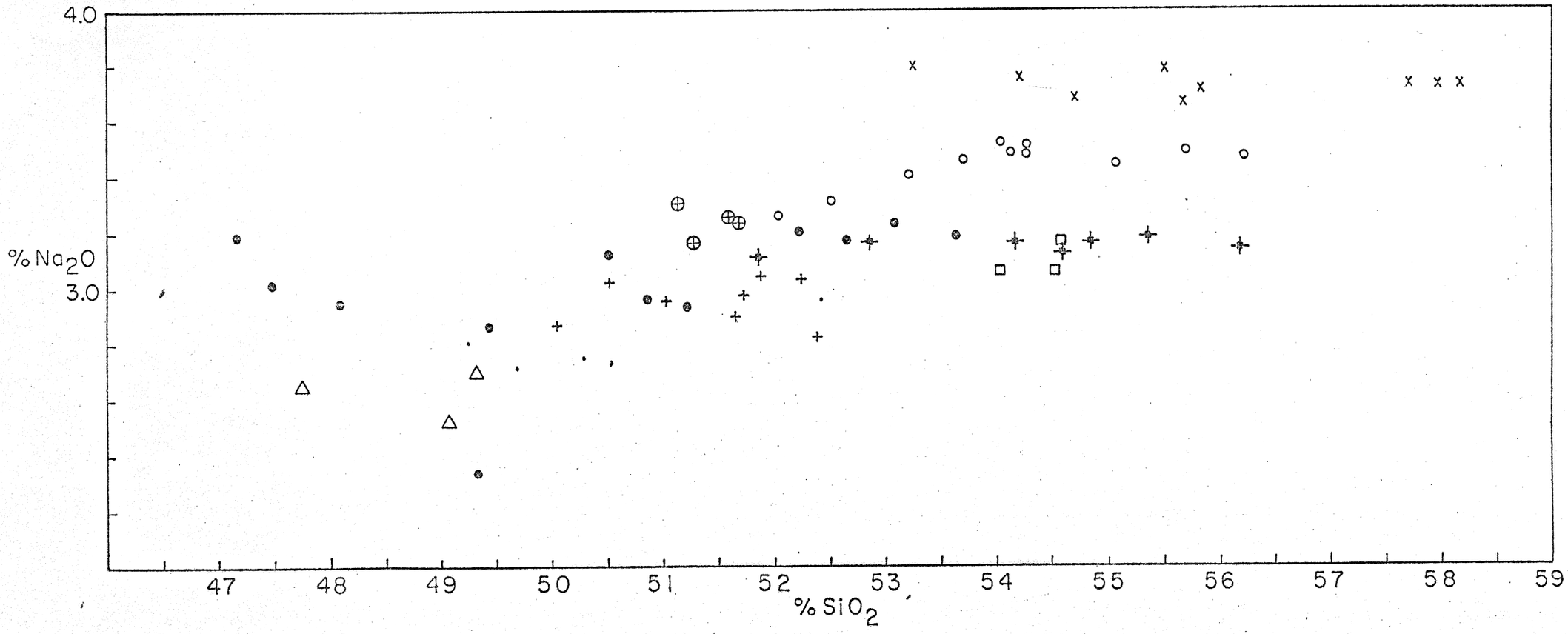
4.0
3.0
% Na2O
47
48
49
50
51
52
53
54
55
56
57
58
59
% SiO2

Figure 12. Alumina-silica variation diagram.

MODOC BASALTS

+ DEVIL'S HOMESTEAD FLOW
· BLACK CRATER FLOW
△ ROSS CHIMNEYS FLOW
x SCHONCHIN FLOW
□ THREE SISTERS FLOW
o CALLAHAN FLOW
⊕ PAINT POT CRATER FLOW
⊹ BURNT FLOW
● OLDER MODOC

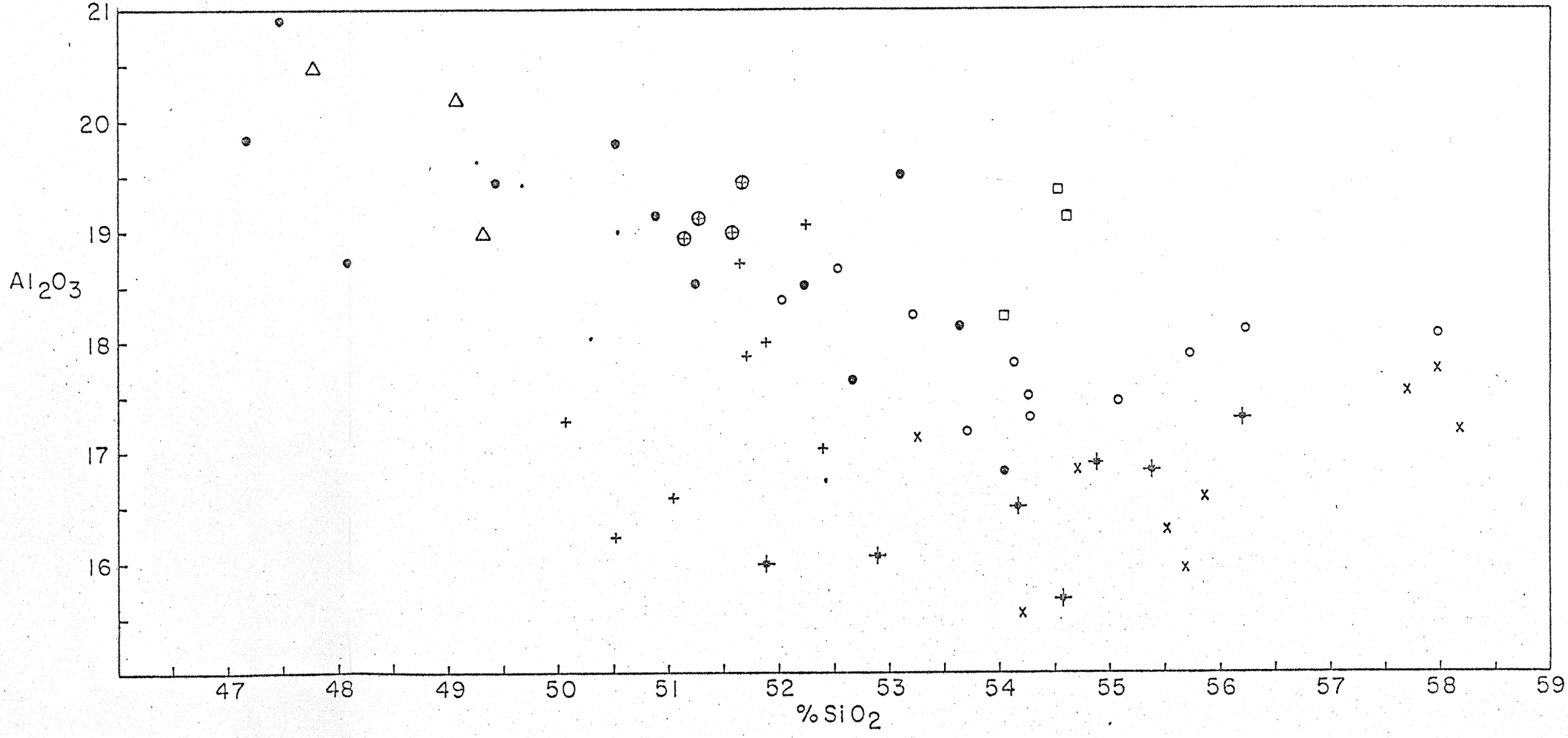
21
20
19
18
17
16
Al_2O_3
47
48
49
50
51
52
53
54
55
56
57
58
59
% SiO_2

Figure 13. Calcium-silica variation diagram.

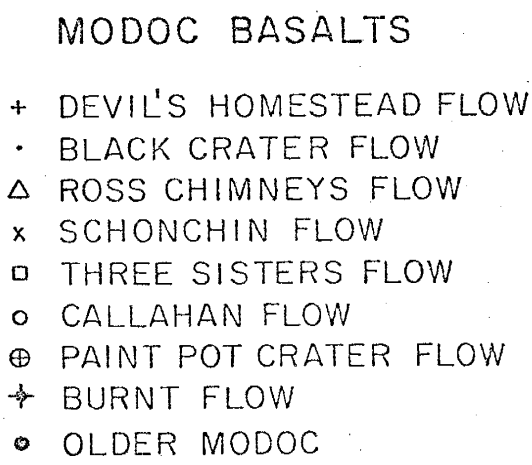

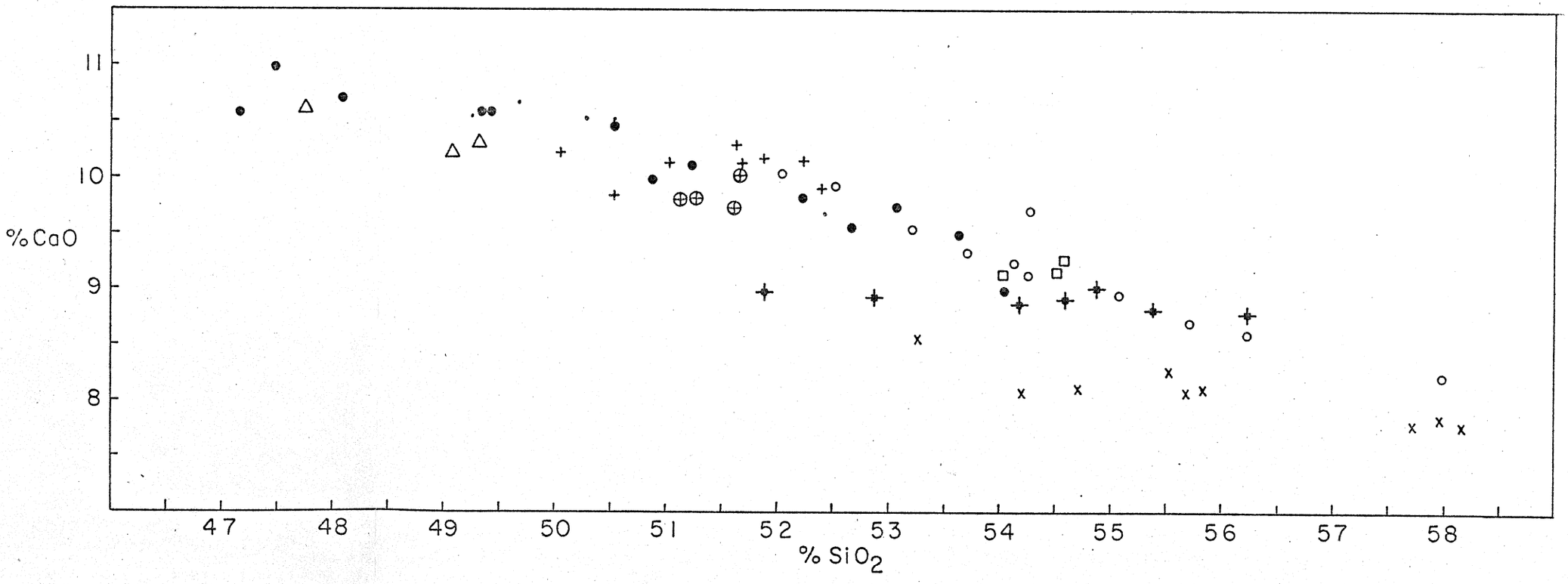
11
10
9
8
% CaO
47
48
49
50
51
52
53
54
55
56
57
58
% SiO2

Figure 14. Titanium-silica variation diagram.

MODOC BASALTS

+ DEVIL'S HOMESTEAD FLOW
· BLACK CRATER FLOW
△ ROSS CHIMNEYS FLOW
x SCHONCHIN FLOW
□ THREE SISTERS FLOW
o CALLAHAN FLOW
⊕ PAINT POT CRATER FLOW
✣ BURNT FLOW
● OLDER MODOC

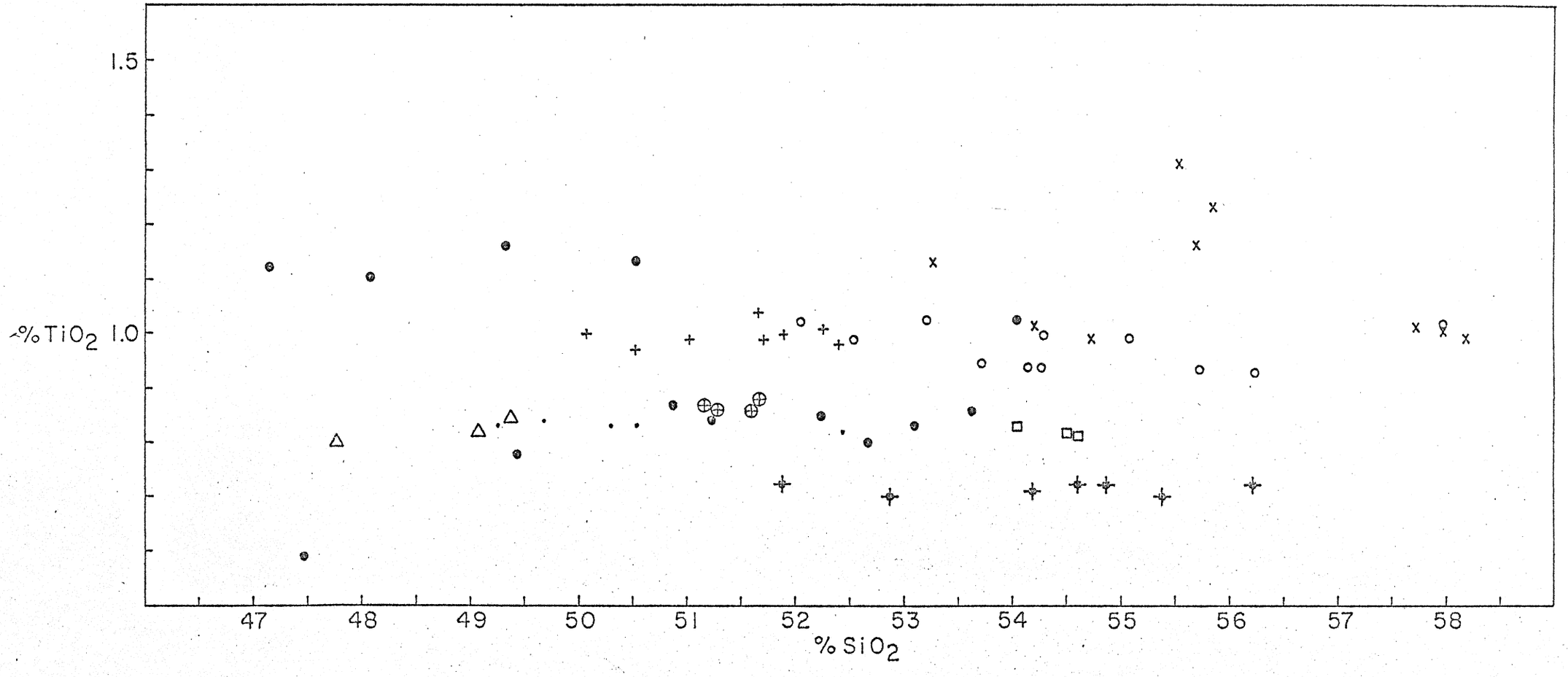
1.5
1.0
% TiO2
47
48
49
50
51
52
53
54
55
56
57
58
% SiO2

exhibit a general increase in TiO_2 content with increasing SiO_2 and decreasing age. The Burnt flow is an exception to this last statement as it has the lowest TiO_2 content of all the Modoc flows.

The variation of total Fe (as Fe_2O_3, Fig. 15) exhibits a general decrease with increasing SiO_2. Age relationships between flows are not as pronounced on this plot as on others, although a trend from older to younger Modoc does correspond to decreasing Fe. The Devil's Homestead and Callahan flows appear somewhat anomalous, having higher Fe concentrations than would be expected based on the trend of the other Modoc flows. Total Fe remains nearly constant over the SiO_2 ranges of the Ross Chimneys, Black Crater, and Burnt flows; while the intra-flow variation between the older, intermediate, and younger sections of the Schonchin and Callahan flows show decreasing Fe with a corresponding decrease in age. In addition, the Burnt flow has the lowest Fe content of all the Modoc.

Magnesium variation (Fig. 16) also exhibits a general trend of decreasing MgO content with increasing SiO_2 and decreasing age. Both the Burnt and intermediate age section of the Schonchin flow show fairly constant MgO levels across their SiO_2 ranges, while the Devil's Homestead and older Modoc flows display trends of increasing MgO content with increasing SiO_2.

Major Element Chemistry of the Recent Silicic Flows

Major element variation diagrams for K_2O, Na_2O, Al_2O_3, CaO, TiO_2, total Fe (as Fe_2O_3), and MgO are presented in Figures 17 through 23, respectively. In addition to analyses from individual silicic flows, separate analyses of the western rhyolite obsidian and eastern dacite

Figure 15. Total iron-silica variation diagram.

MODOC BASALTS

+ DEVIL'S HOMESTEAD FLOW
· BLACK CRATER FLOW
△ ROSS CHIMNEYS FLOW
x SCHONCHIN FLOW
□ THREE SISTERS FLOW
o CALLAHAN FLOW
⊕ PAINT POT CRATER FLOW
✣ BURNT FLOW
● OLDER MODOC

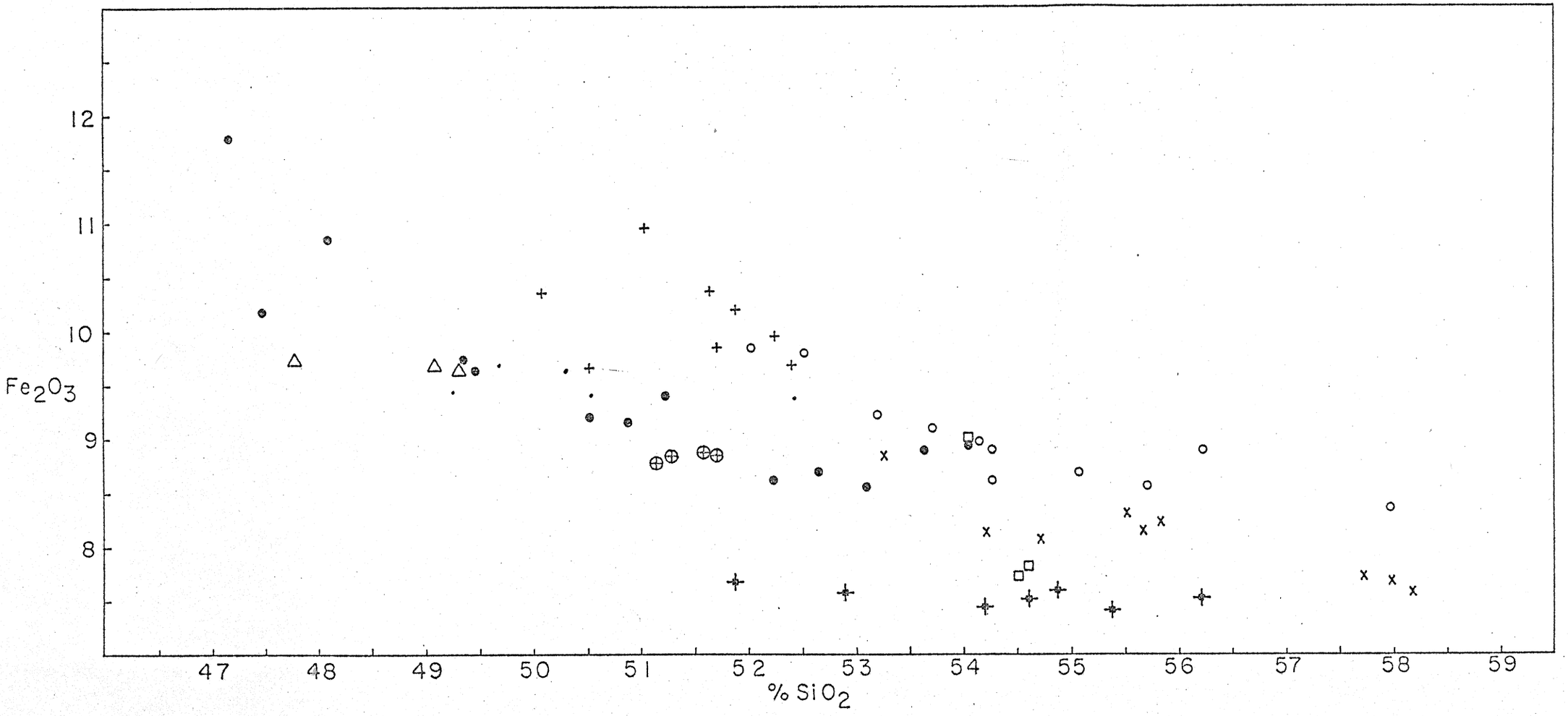
12
11
10
9
8
Fe_2O_3
47
48
49
50
51
52
53
54
55
56
57
58
59
% SiO_2

Figure 16. Magnesium-silica variation diagram.

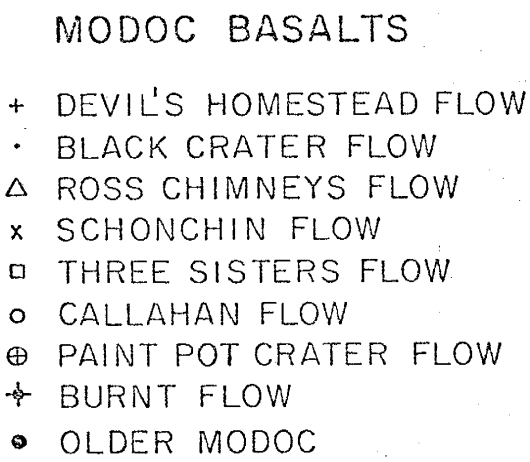

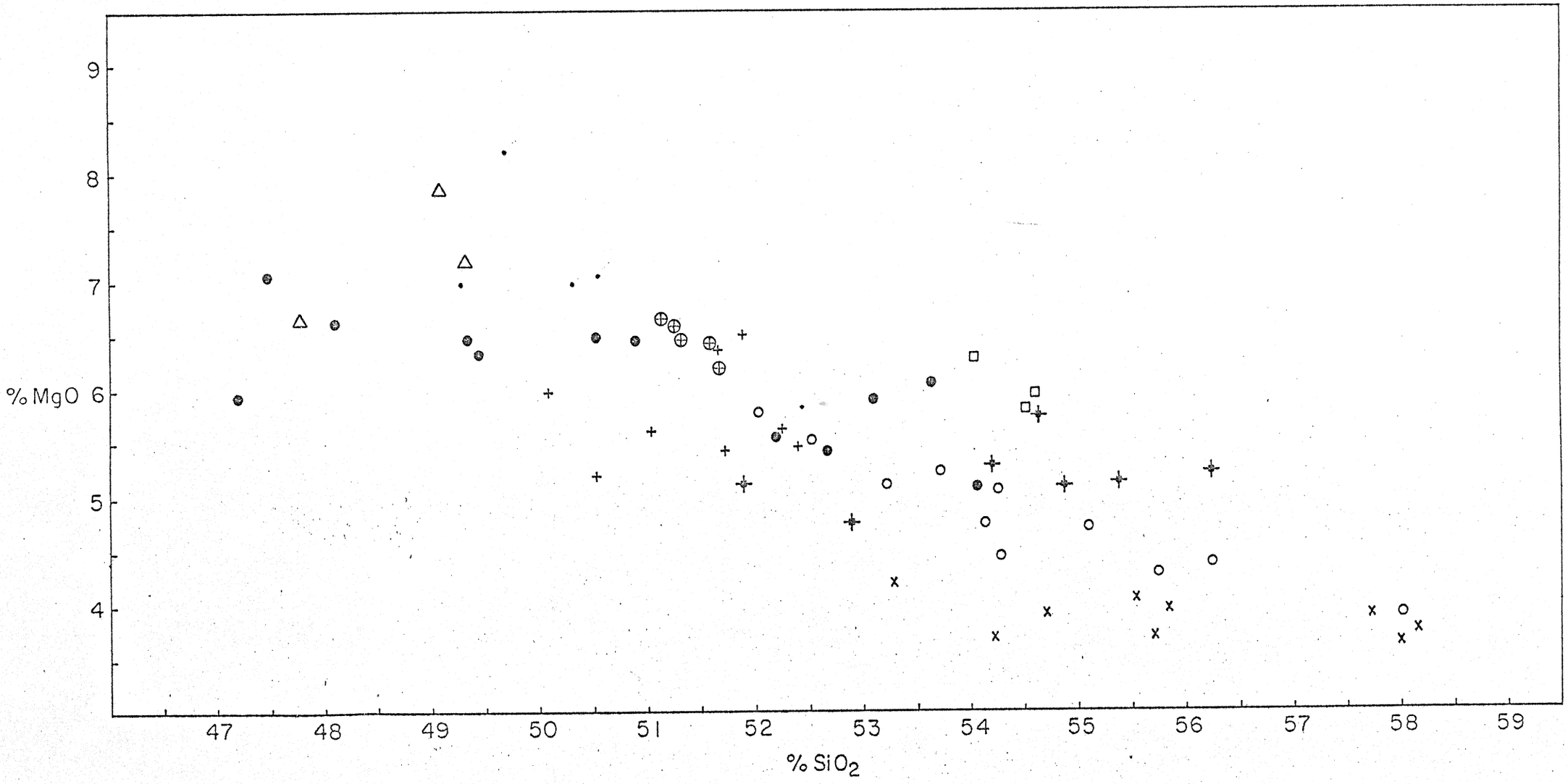
9
8
7
6
5
4
% MgO
47
48
49
50
51
52
53
54
55
56
57
58
59
% SiO2

sections of the composite flow are presented. The dacite sections of the composite is subdivided further by the presentation of separate analyses of the dacite and of the pods and stringers of rhyolite obsidian which occur as inclusions in the dacite. In the following discussion only the dacite is referred to when the dacite section of the composite flow is mentioned; the rhyolite obsidian inclusions are discussed as belonging in the same category as the other rhyolites.

A relative age relationship between composition and the ages suggested by the author for the Recent silicic flows is generally exhibited by the K_2O variation diagram (Fig. 17) which shows a trend of increasing K_2O with increasing SiO_2 and decreasing age, the major exception to this scheme being the composition of the dacite section of the composite flow. The Hoffman flow displays constant K_2O levels in its SiO_2 range, being lower in K_2O content than the other rhyolites which tend to cluster in an area defined by a SiO_2 range of 71 to 75 percent, with K_2O levels between 4.00 and 4.25 percent.

Sodium systemmatically increases with silica (Fig. 18) with the exception of the dacite section of the composite flow which exhibits Na_2O concentrations significantly higher than the other Recent dacites and obsidians. This high Na_2O level cannot be attributed to contamination by the olivine basalt inclusions as the opposite effect would be seen. The rhyolites tend to plot at rather constant Na_2O levels within their SiO_2 ranges.

Calcium displays a systemmatic decrease with decreasing SiO_2 content (Fig. 19), the dacite section of the composite flow being lower in CaO_2 at equivalent SiO_2 levels than the Medicine Lake dacite.

Figure 17. Potassium-silica variation diagram.

SILICIC FLOWS

- LITTLE GLASS MOUNTAIN
- MEDICINE LAKE GLASS FLOW
- HOFFMAN FLOW
- MT. HOFFMAN
- GLASS MOUNTAIN -DOME
- GLASS MOUNTAIN -COMPOSITE FLOW RHYOLITE OBSIDIAN SECTION
- GLASS MOUNTAIN -COMPOSITE FLOW TRANSITION ZONE
- GLASS MOUNTAIN -COMPOSITE FLOW DACITE SECTION
- GLASS MOUNTAIN -COMPOSITE FLOW DACITE SECTION (OBSIDIAN INCLUSIONS)

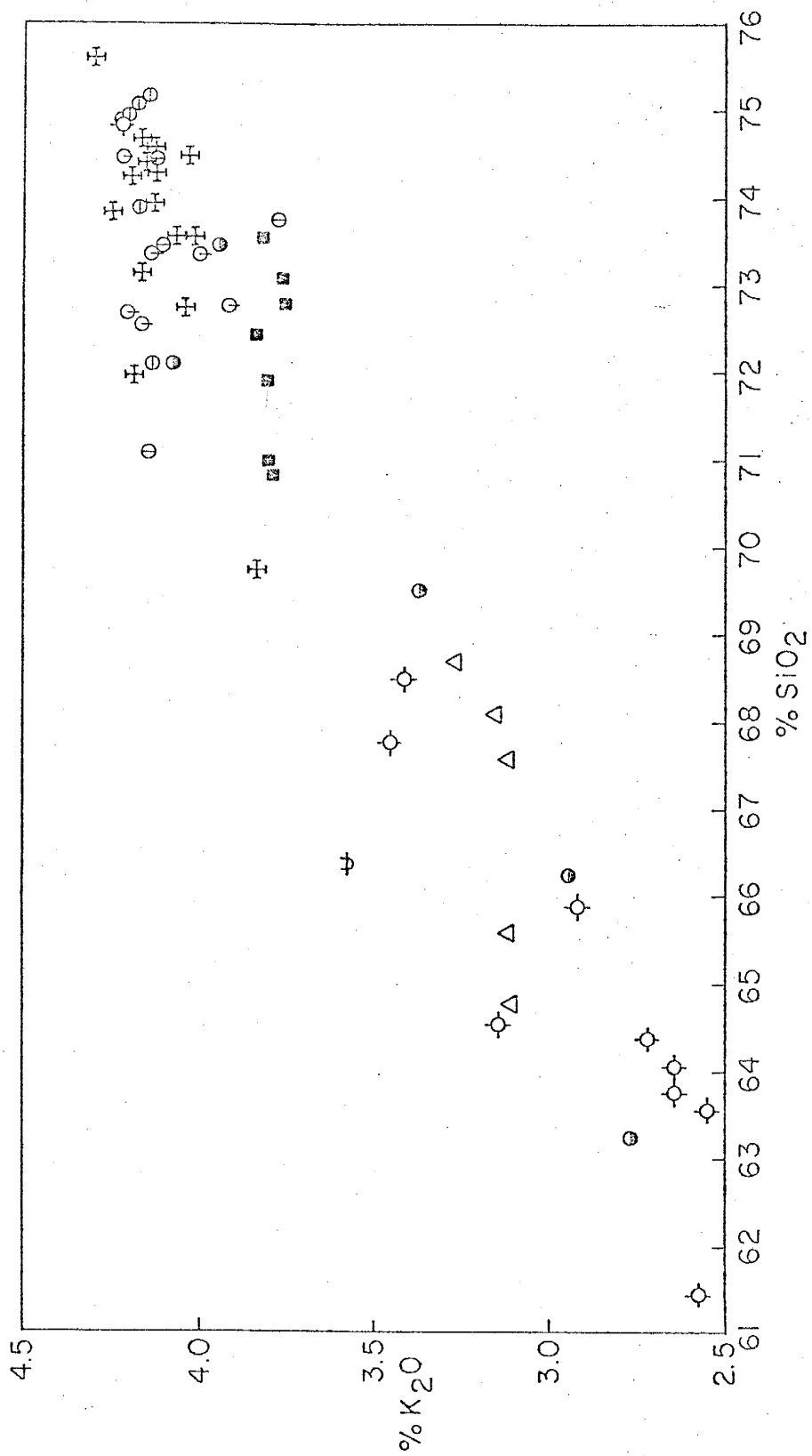
4.5
4.0
3.5
3.0
2.5
% K_2O
61
62
63
64
65
66
67
68
69
70
71
72
73
74
75
76
% SiO_2

Figure 18. Sodium-silica variation diagram.

SILICIC FLOWS

- LITTLE GLASS MOUNTAIN
- MEDICINE LAKE GLASS FLOW
- HOFFMAN FLOW
- MT. HOFFMAN
- GLASS MOUNTAIN -DOME
- GLASS MOUNTAIN -COMPOSITE FLOW RHYOLITE OBSIDIAN SECTION
- GLASS MOUNTAIN -COMPOSITE FLOW TRANSITION ZONE
- GLASS MOUNTAIN -COMPOSITE FLOW DACITE SECTION
- GLASS MOUNTAIN -COMPOSITE FLOW DACITE SECTION (OBSIDIAN INCLUSIONS)

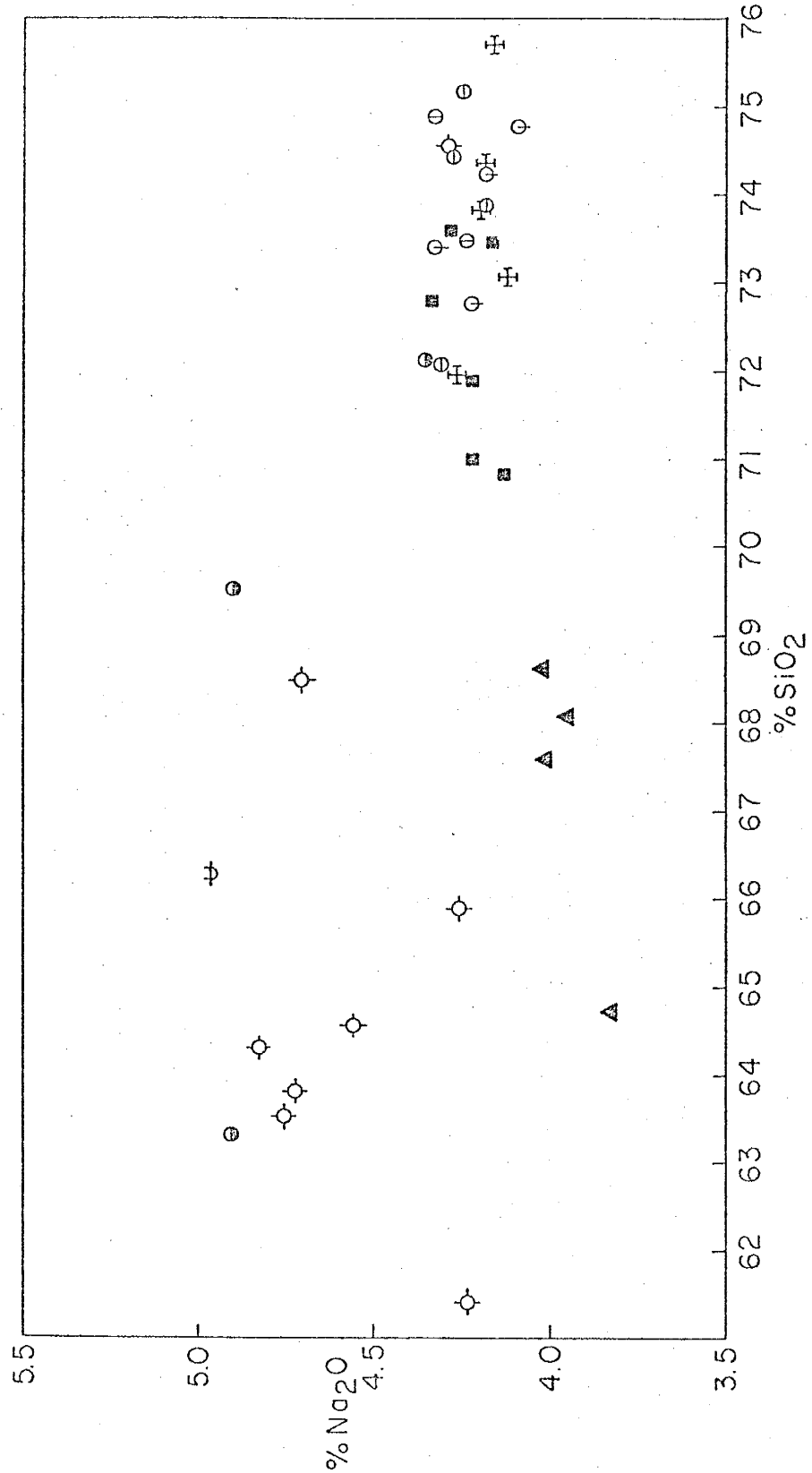
5.5
5.0
4.5
4.0
3.5
% Na2O
62
63
64
65
66
67
68
69
70
71
72
73
74
75
76
% SiO2

Figure 19. Calcuim-silica variation diagram.

SILICIC FLOWS

- LITTLE GLASS MOUNTAIN
- MEDICINE LAKE GLASS FLOW
- HOFFMAN FLOW
- MT. HOFFMAN
- GLASS MOUNTAIN -DOME
- GLASS MOUNTAIN -COMPOSITE FLOW RHYOLITE OBSIDIAN SECTION
- GLASS MOUNTAIN -COMPOSITE FLOW TRANSITION ZONE
- GLASS MOUNTAIN -COMPOSITE FLOW DACITE SECTION
- GLASS MOUNTAIN -COMPOSITE FLOW DACITE SECTION (OBSIDIAN INCLUSIONS)

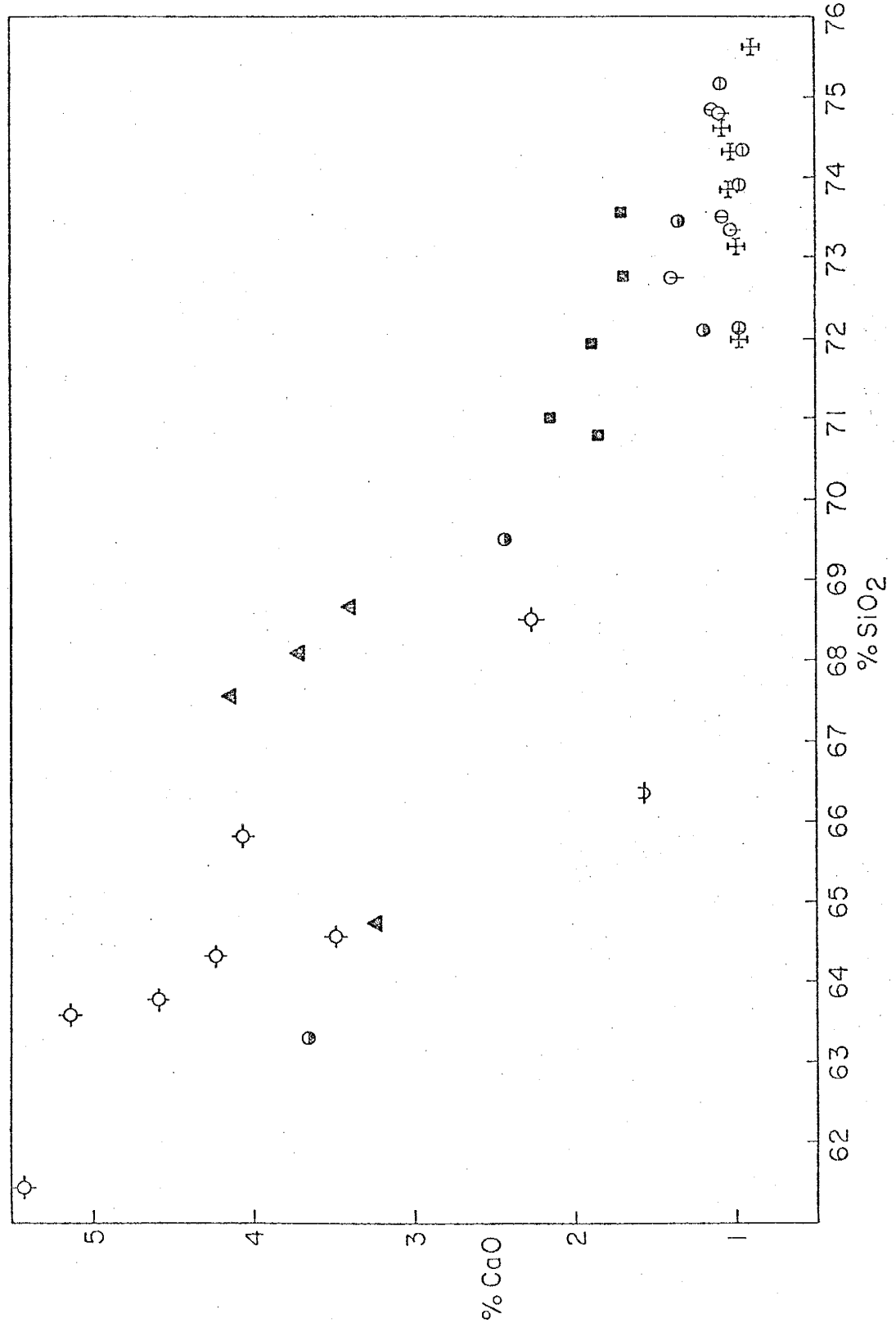
% CaO
% SiO2
1
2
3
4
5
62
63
64
65
66
67
68
69
70
71
72
73
74
75
76

Alumina, TiO_2, total Fe (as Fe_2O_3), and MgO all exhibit fairly coherent systemmatic decreases in their content with increasing SiO_2.

Trace Element Chemistry of the Modoc and Recent Silicic Flows

The elements Rb, Sr, and Ba are plotted against the SiO_2 content of the Recent volcanics in Figures 24 through 26. Barium is only plotted for the Modoc basalts and basaltic andesites as it remains at fairly constant levels for the dacites and obsidians.

Rubidium (Fig. 24) exhibits a coherent trend for nearly all the Recent volcanics, both the Modoc and silicic flows showing a general increase in Rb content with decreasing age. The Burnt and Schonchin flows are somewhat anomalous, as they respectively plot above and below the trend defined by the rest of the Modoc flows.

Strontium (Fig. 25), while showing a well defined trend of decreasing Sr with increasing SiO_2 for the silicic flows, exhibits a great deal of scatter relative to the Modoc flows, although the individual older, intermediate, and younger Modoc flows plot as coherent units. No consistent age relationship is displayed by the Modoc flows. The Callahan

Figure 20. Alumina-silica variation diagram.

SILICIC FLOWS

- LITTLE GLASS MOUNTAIN
- MEDICINE LAKE GLASS FLOW
- HOFFMAN FLOW
- MT. HOFFMAN
- GLASS MOUNTAIN -DOME
- GLASS MOUNTAIN -COMPOSITE FLOW RHYOLITE OBSIDIAN SECTION
- GLASS MOUNTAIN -COMPOSITE FLOW TRANSITION ZONE
- GLASS MOUNTAIN -COMPOSITE FLOW DACITE SECTION
- GLASS MOUNTAIN -COMPOSITE FLOW DACITE SECTION (OBSIDIAN INCLUSIONS)

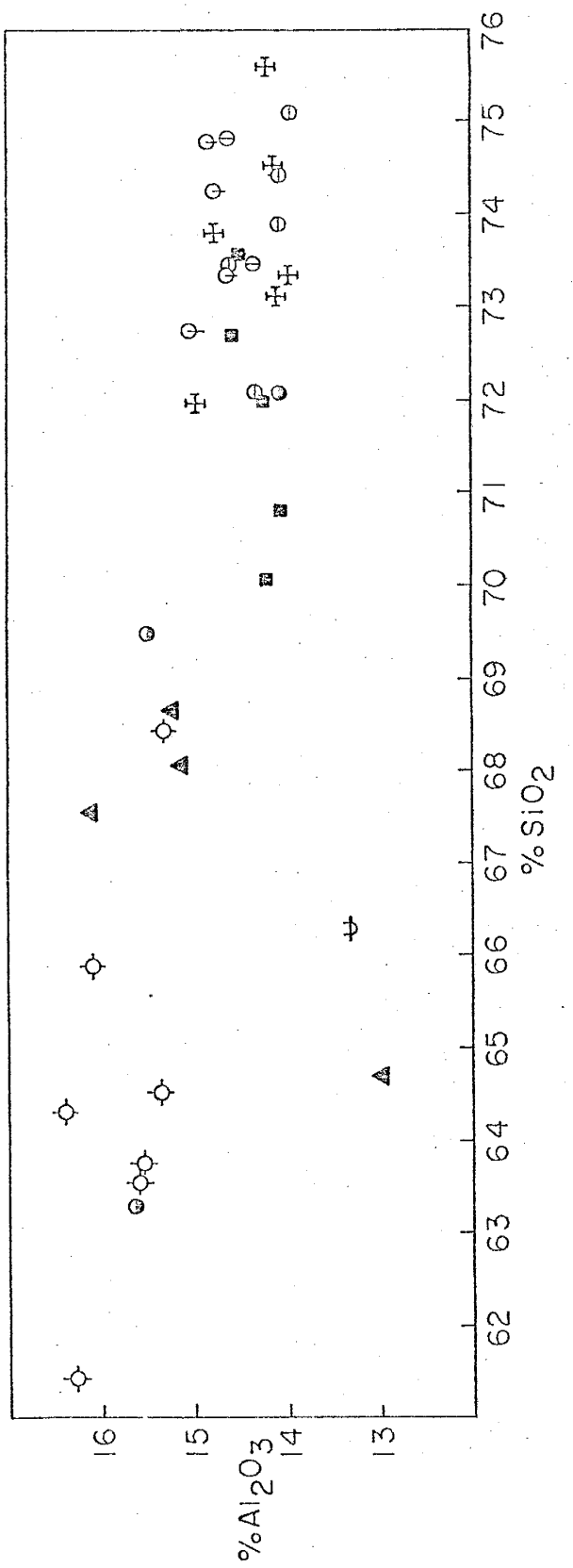
% Al_2O_3
16
15
14
13
% SiO_2
62
63
64
65
66
67
68
69
70
71
72
73
74
75
76

Figure 21. Titanium-silica variation diagrams.

SILICIC FLOWS

- ⊙ LITTLE GLASS MOUNTAIN
- ⧋ MEDICINE LAKE GLASS FLOW
- ▣ HOFFMAN FLOW
- ⊎ MT. HOFFMAN
- ⊖ GLASS MOUNTAIN -DOME
- ⧾ GLASS MOUNTAIN -COMPOSITE FLOW RHYOLITE OBSIDIAN SECTION
- ⊜ GLASS MOUNTAIN -COMPOSITE FLOW TRANSITION ZONE
- ⊹ GLASS MOUNTAIN -COMPOSITE FLOW DACITE SECTION
- ⊙ GLASS MOUNTAIN -COMPOSITE FLOW DACITE SECTION (OBSIDIAN INCLUSIONS)

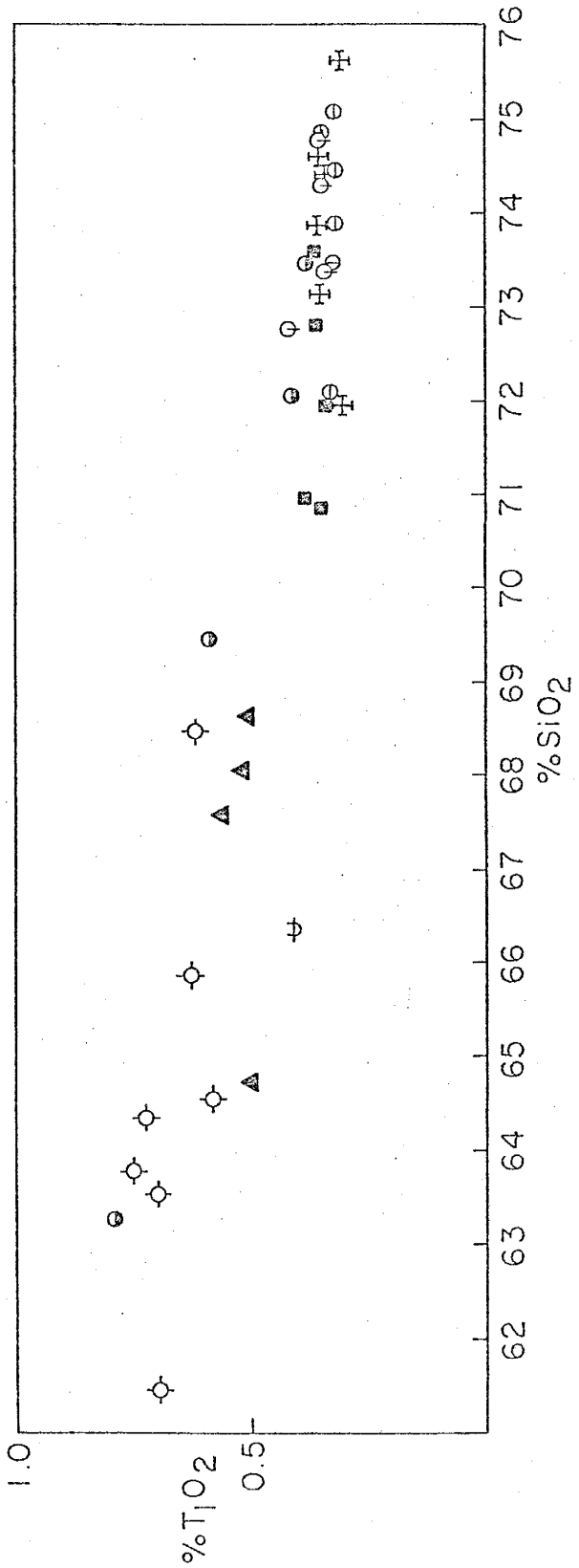
1.0
0.5
%TiO2
62
63
64
65
66
67
68
69
70
71
72
73
74
75
76
%SiO2

Figure 22. Total iron-silica variation diagram.

SILICIC FLOWS

- LITTLE GLASS MOUNTAIN
- MEDICINE LAKE GLASS FLOW
- HOFFMAN FLOW
- MT. HOFFMAN
- GLASS MOUNTAIN -DOME
- GLASS MOUNTAIN -COMPOSITE FLOW RHYOLITE OBSIDIAN SECTION
- GLASS MOUNTAIN -COMPOSITE FLOW TRANSITION ZONE
- GLASS MOUNTAIN -COMPOSITE FLOW DACITE SECTION
- GLASS MOUNTAIN -COMPOSITE FLOW DACITE SECTION (OBSIDIAN INCLUSIONS)

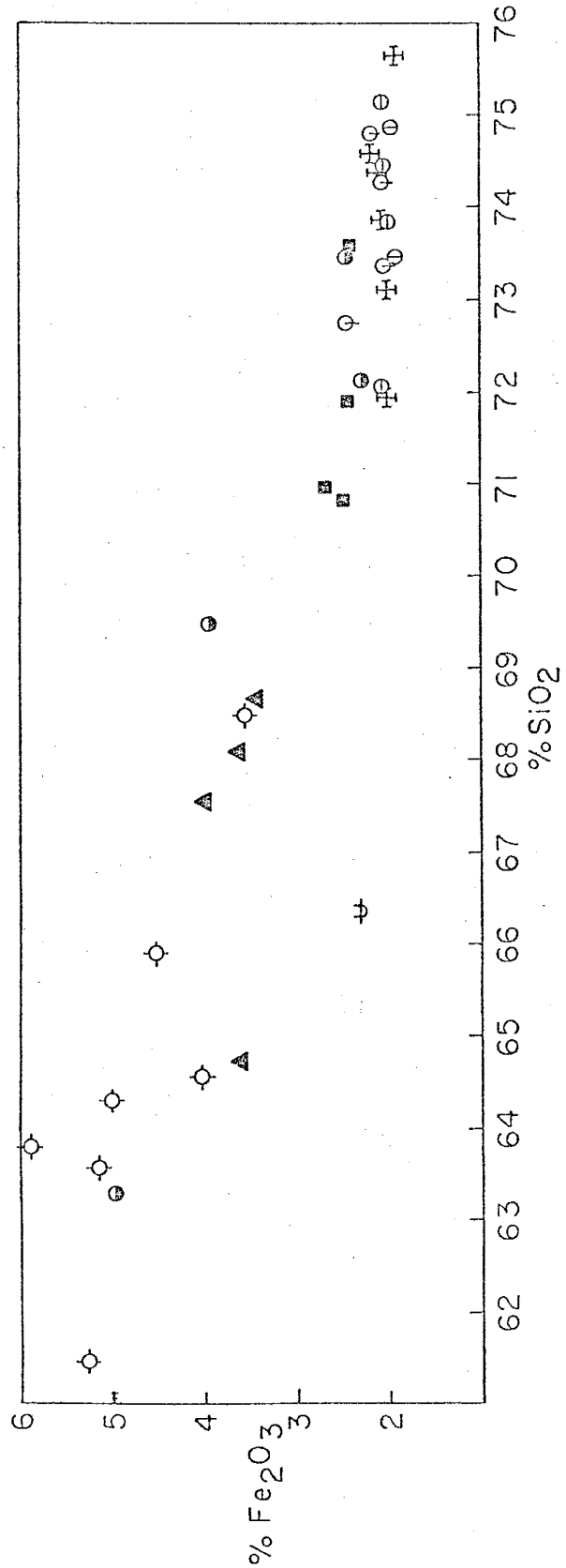
% Fe_2O_3
6
5
4
3
2
62
63
64
65
66
67
68
69
70
71
72
73
74
75
76
% SiO_2

Figure 23. Magnesium-silica variation diagram.

SILICIC FLOWS

- LITTLE GLASS MOUNTAIN
- MEDICINE LAKE GLASS FLOW
- HOFFMAN FLOW
- MT. HOFFMAN
- GLASS MOUNTAIN -DOME
- GLASS MOUNTAIN -COMPOSITE FLOW RHYOLITE OBSIDIAN SECTION
- GLASS MOUNTAIN -COMPOSITE FLOW TRANSITION ZONE
- GLASS MOUNTAIN -COMPOSITE FLOW DACITE SECTION
- GLASS MOUNTAIN -COMPOSITE FLOW DACITE SECTION (OBSIDIAN INCLUSIONS)

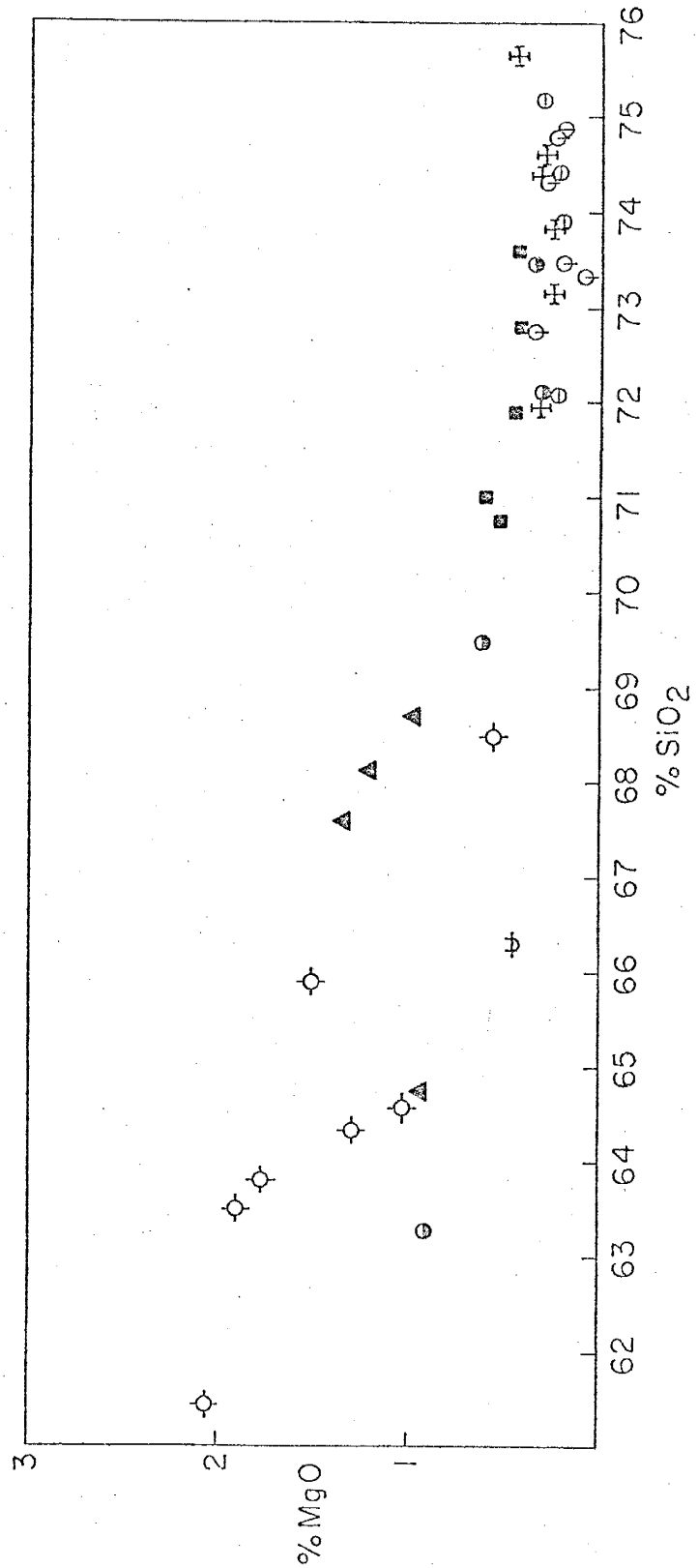
% MgO
3
2
1
62
63
64
65
66
67
68
69
70
71
72
73
74
75
76
% SiO2

Figure 24. Rubidium-silica variation diagram.

MODOC BASALTS

+ DEVIL'S HOMESTEAD FLOW
· BLACK CRATER FLOW
△ ROSS CHIMNEYS FLOW
x SCHONCHIN FLOW
□ THREE SISTERS FLOW
○ CALLAHAN FLOW
⊕ PAINT POT CRATER FLOW
⊹ BURNT FLOW
● OLDER MODOC

SILICIC FLOWS

⊙ LITTLE GLASS MOUNTAIN
▲ MEDICINE LAKE GLASS FLOW
■ HOFFMAN FLOW
⊎ MT. HOFFMAN
⊖ GLASS MOUNTAIN -DOME
⧾ GLASS MOUNTAIN -COMPOSITE FLOW
RHYOLITE OBSIDIAN SECTION
⊜ GLASS MOUNTAIN -COMPOSITE FLOW
TRANSITION ZONE
⌖ GLASS MOUNTAIN -COMPOSITE FLOW
DACITE SECTION
⚲ GLASS MOUNTAIN -COMPOSITE FLOW
DACITE SECTION (OBSIDIAN INCLUSIONS)

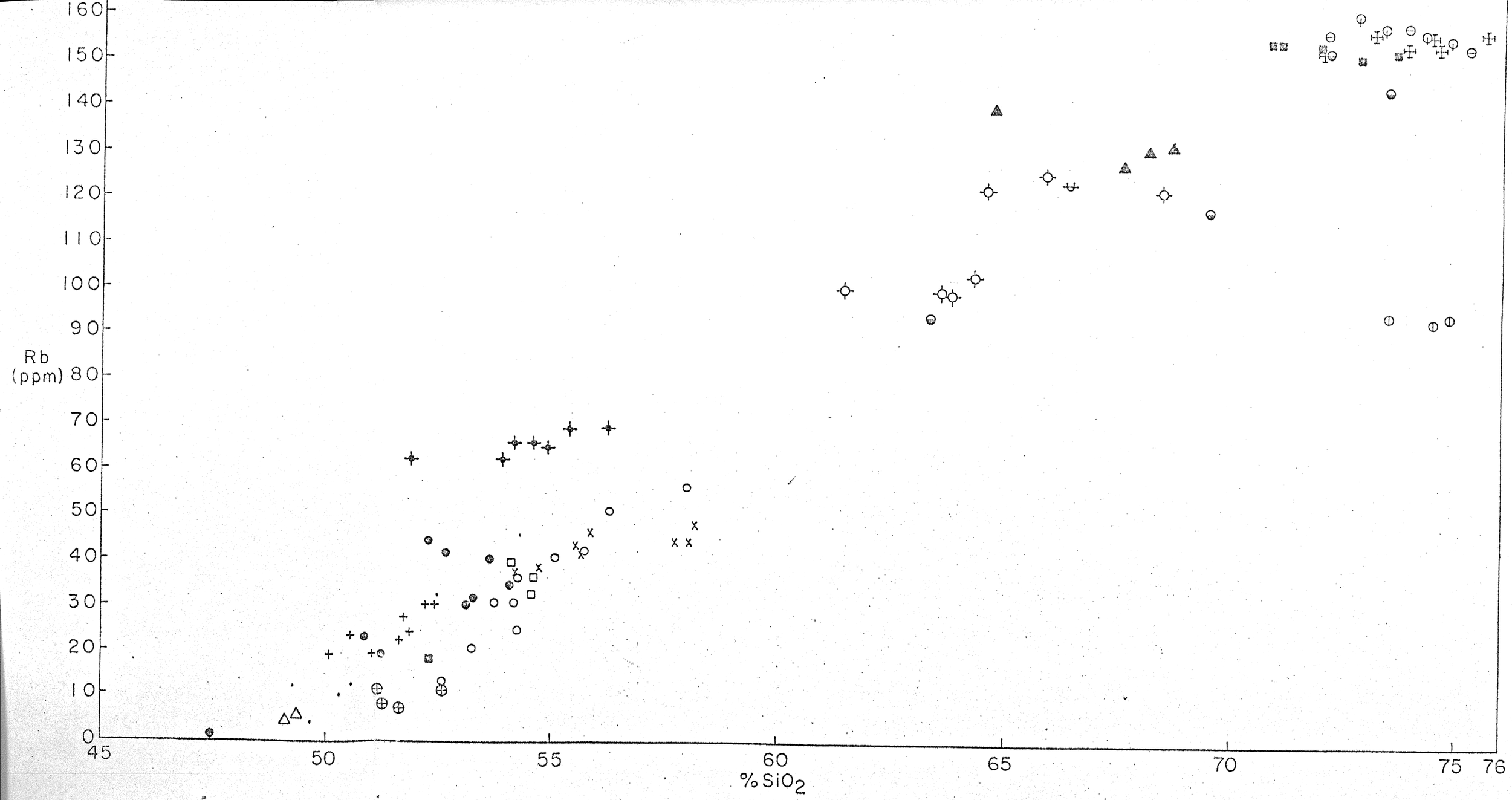
160
150
140
130
120
110
100
90
Rb
(ppm) 80
70
60
50
40
30
20
10
0
45
50
55
60
65
70
75
76
% SiO2

Figure 25. Strontium-silica variation diagram.

MODOC BASALTS

+ DEVIL'S HOMESTEAD FLOW
· BLACK CRATER FLOW
△ ROSS CHIMNEYS FLOW
x SCHONCHIN FLOW
□ THREE SISTERS FLOW
○ CALLAHAN FLOW
⊕ PAINT POT CRATER FLOW
⊹ BURNT FLOW
◎ OLDER MODOC

SILICIC FLOWS

◐ LITTLE GLASS MOUNTAIN
▲ MEDICINE LAKE GLASS FLOW
■ HOFFMAN FLOW
⊎ MT. HOFFMAN
⊖ GLASS MOUNTAIN -DOME
⧾ GLASS MOUNTAIN -COMPOSITE FLOW
RHYOLITE OBSIDIAN SECTION
◒ GLASS MOUNTAIN -COMPOSITE FLOW
TRANSITION ZONE
⊹ GLASS MOUNTAIN -COMPOSITE FLOW
DACITE SECTION
⚲ GLASS MOUNTAIN -COMPOSITE FLOW
DACITE SECTION (OBSIDIAN INCLUSIONS)

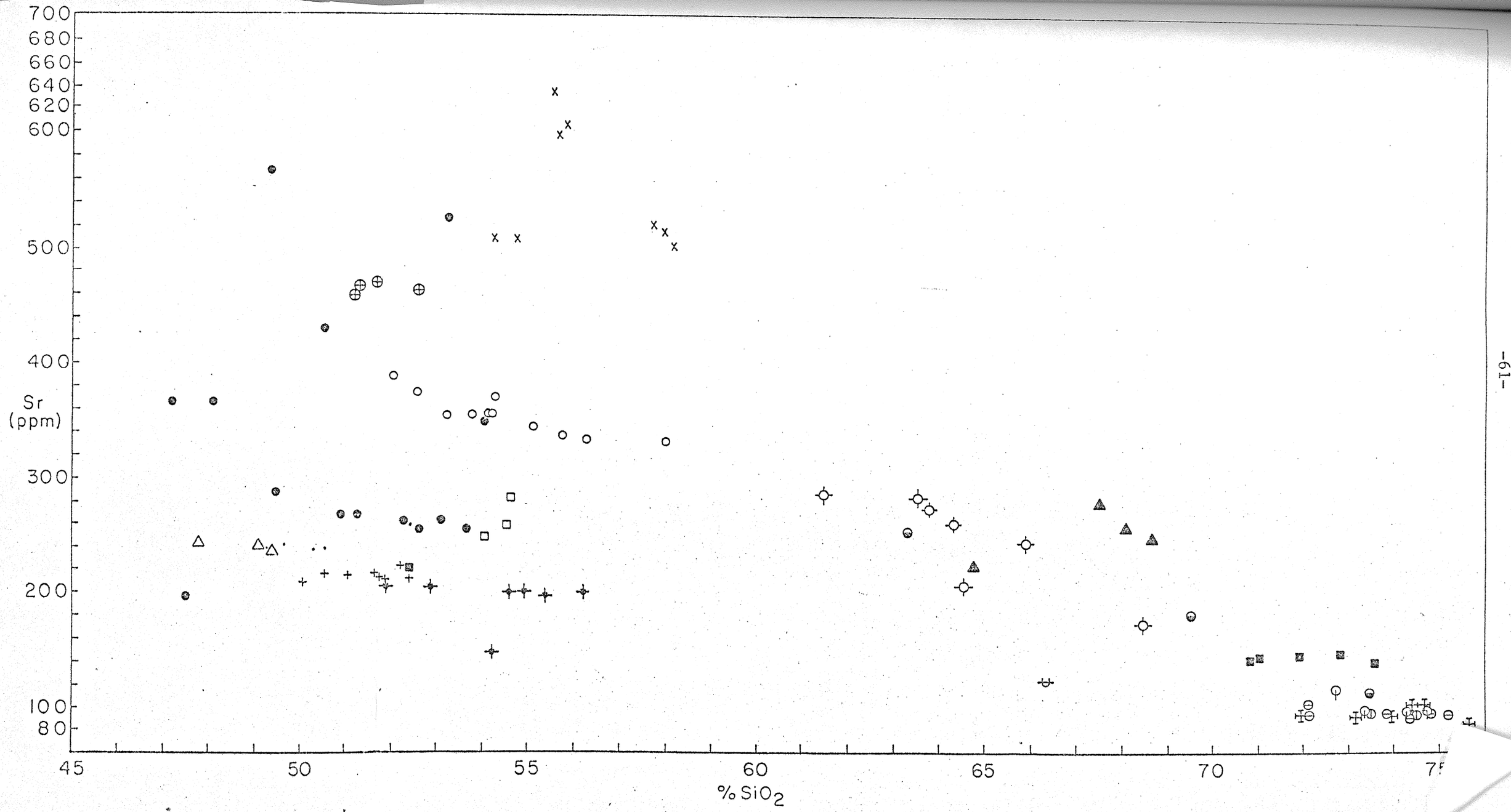
700
680
660
640
620
600
500
400
Sr
(ppm)
300
200
100
80
45
50
55
60
65
70
% SiO2

flow shows a trend of decreasing Sr with increasing SiO_2 as do the Older Modoc flows; however, these trends are not well defined. Of particular interest is the high Sr level exhibited by the Schonchin flow (500 to 640 ppm) as compared to the other intermediate and younger Modoc flows.

Barium (Fig. 26), although showing some scatter, displays an increase in concentration with increasing SiO_2, this trend corresponding to a general decrease in the age of the Modoc flows.

Figures 27 through 29 are log-log plots of percent K versus Rb, Sr versus Rb, and Ba versus Rb, respectively, for the Modoc flows.

Figure 27, percent K versus Rb, exhibits a decrease in the K/Rb ratio for the Modoc flows, with some scatter occurring at lower Rb concentrations. The Schonchin flow is an exception, as it has a higher K/Rb ratio than that defined by the trend of the other Modoc flows. Both K and Rb show a general increase with increasing eruptive age for the intermediate and younger Modoc flows.

Strontium versus Rb (Fig. 28) shows the relationship of Sr concentration levels remaining fairly constant within individual flows while Rb varies. The Ross Chimneys, Black Crater, Devil's Homestead, and Burnt flows all show about the same level of Sr concentration, while Rb increases with decreasing age. Most of the undifferentiated older Modoc and the Three Sisters flow also display this relationship, while the Callahan, Paint Pot Crater, and Schonchin flows exhibit distinctive Sr concentration levels.

Barium, although showing considerable scatter when plotted against Rb (Fig. 29), displays an increase with increasing Rb concentration, the Ba/Rb ratio decreasing with decreasing eruptive age.

Strontium, when displayed on a log-log plot against percent K

Figure 26. Barium-silica variation diagram.

MODOC BASALTS

+ DEVIL'S HOMESTEAD FLOW
· BLACK CRATER FLOW
△ ROSS CHIMNEYS FLOW
x SCHONCHIN FLOW
□ THREE SISTERS FLOW
o CALLAHAN FLOW
⊕ PAINT POT CRATER FLOW
⊹ BURNT FLOW
● OLDER MODOC

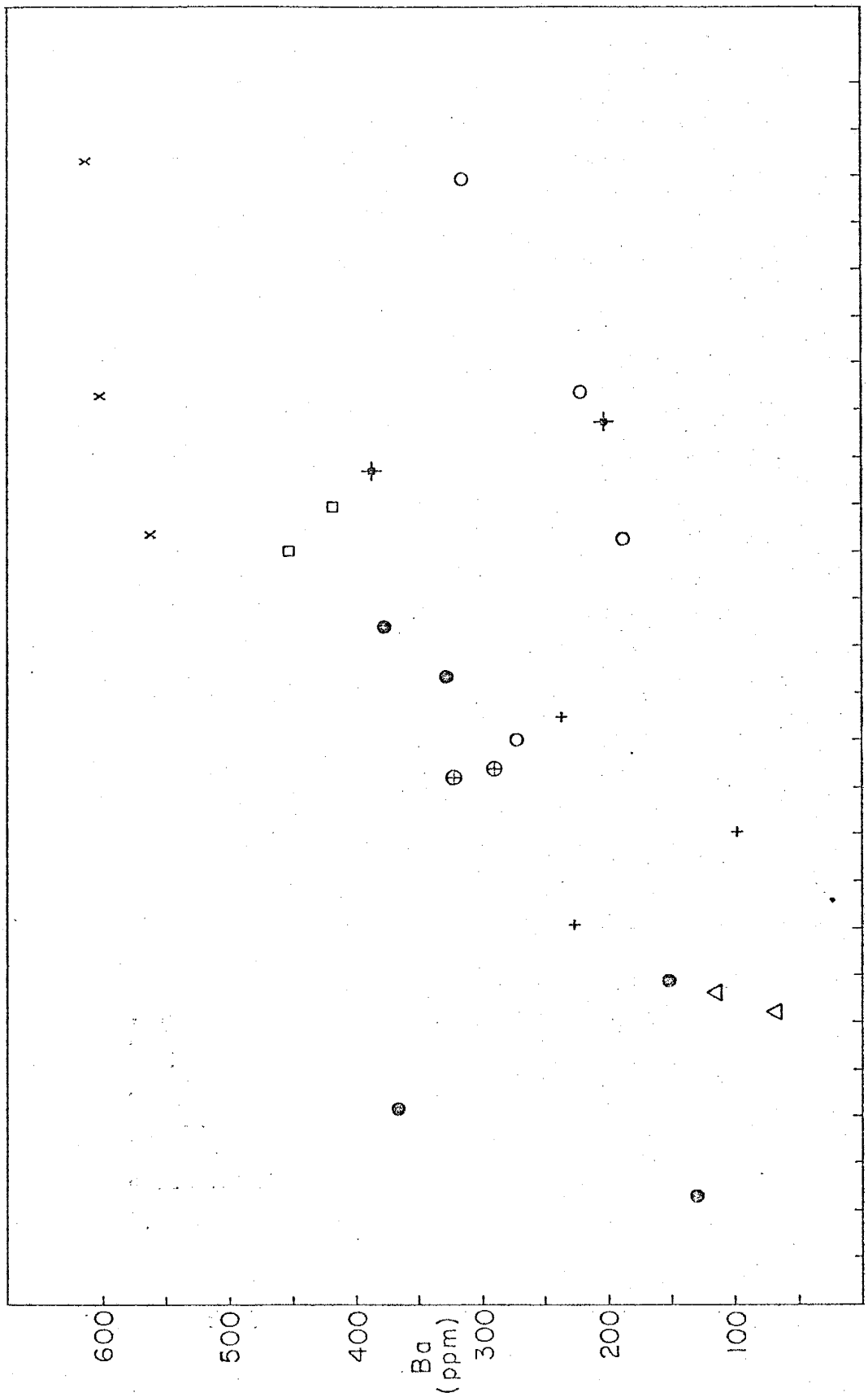
Ba (ppm)
600
500
400
300
200
100
47
48
49
50
51
52
53
54
55
56
57
58
59
% SiO_2

Figure 27. Log-log plot of percent K versus Rb.

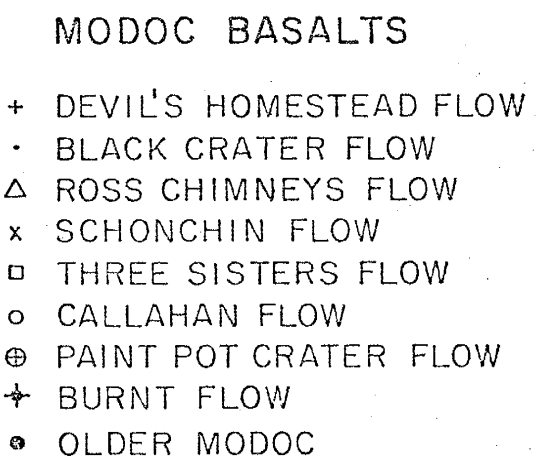

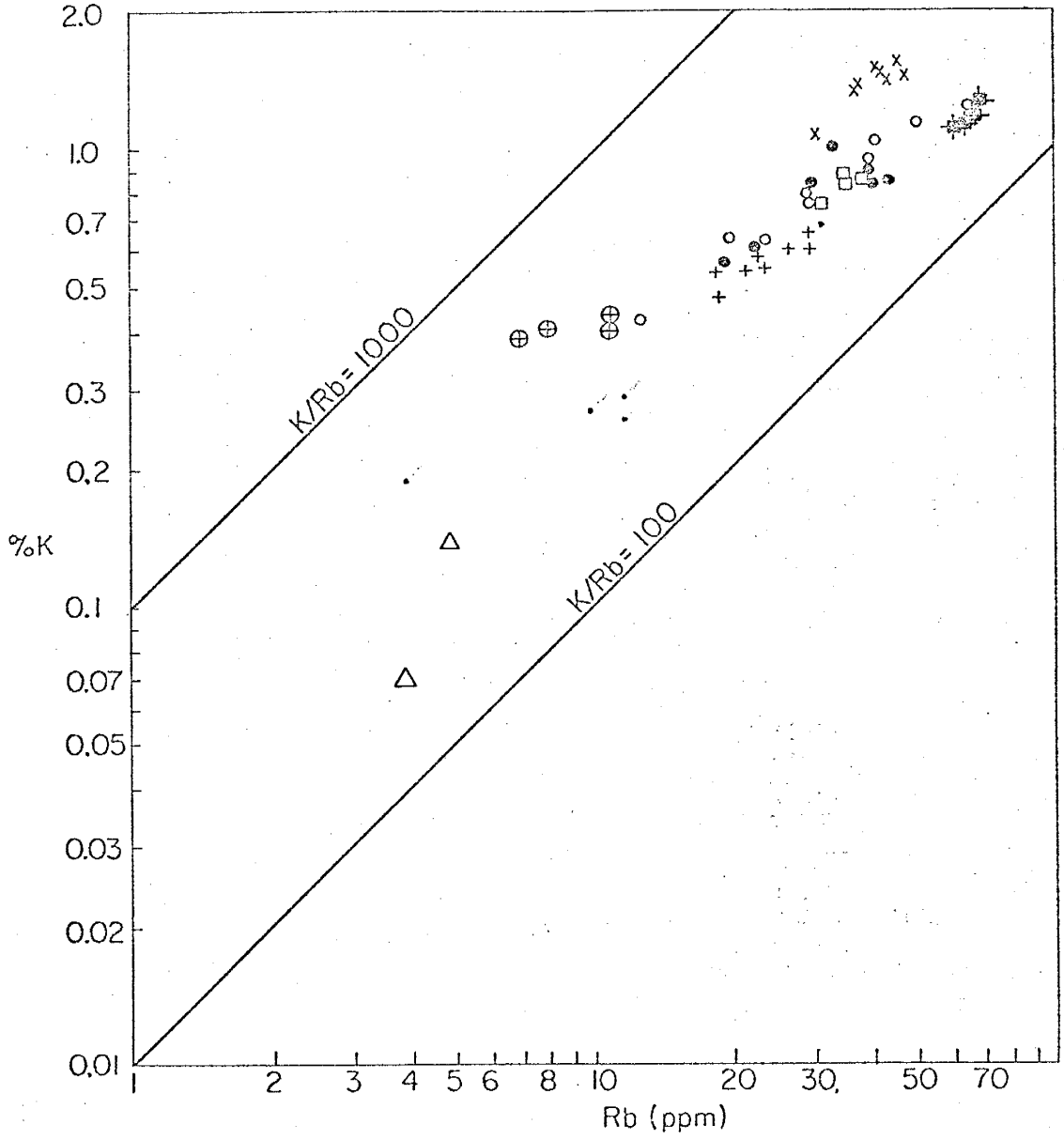
2.0
1.0
0.7
0.5
0.3
0.2
%K
0.1
0.07
0.05
0.03
0.02
0.01
K/Rb= 1000
K/Rb= 100
1
2
3
4
5
6
8
10
20
30
50
70
Rb (ppm)

Figure 28. Log-log plot of Sr versus Rb.

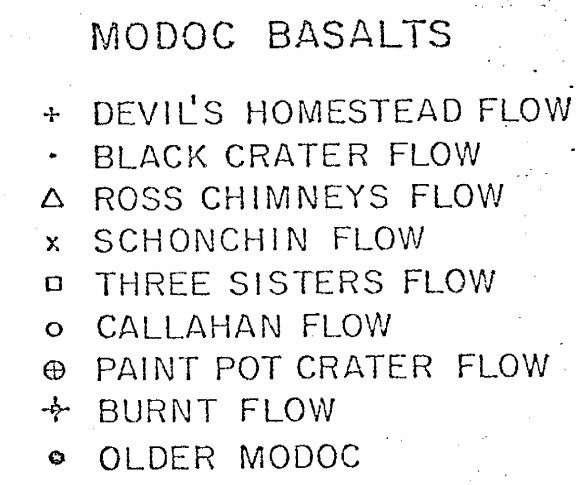

Figure 29. Log-log plot of Ba versus Rb.

MODOC BASALTS

+ DEVIL'S HOMESTEAD FLOW
· BLACK CRATER FLOW
△ ROSS CHIMNEYS FLOW
x SCHONCHIN FLOW
□ THREE SISTERS FLOW
o CALLAHAN FLOW
⊕ PAINT POT CRATER FLOW
✣ BURNT FLOW
● OLDER MODOC

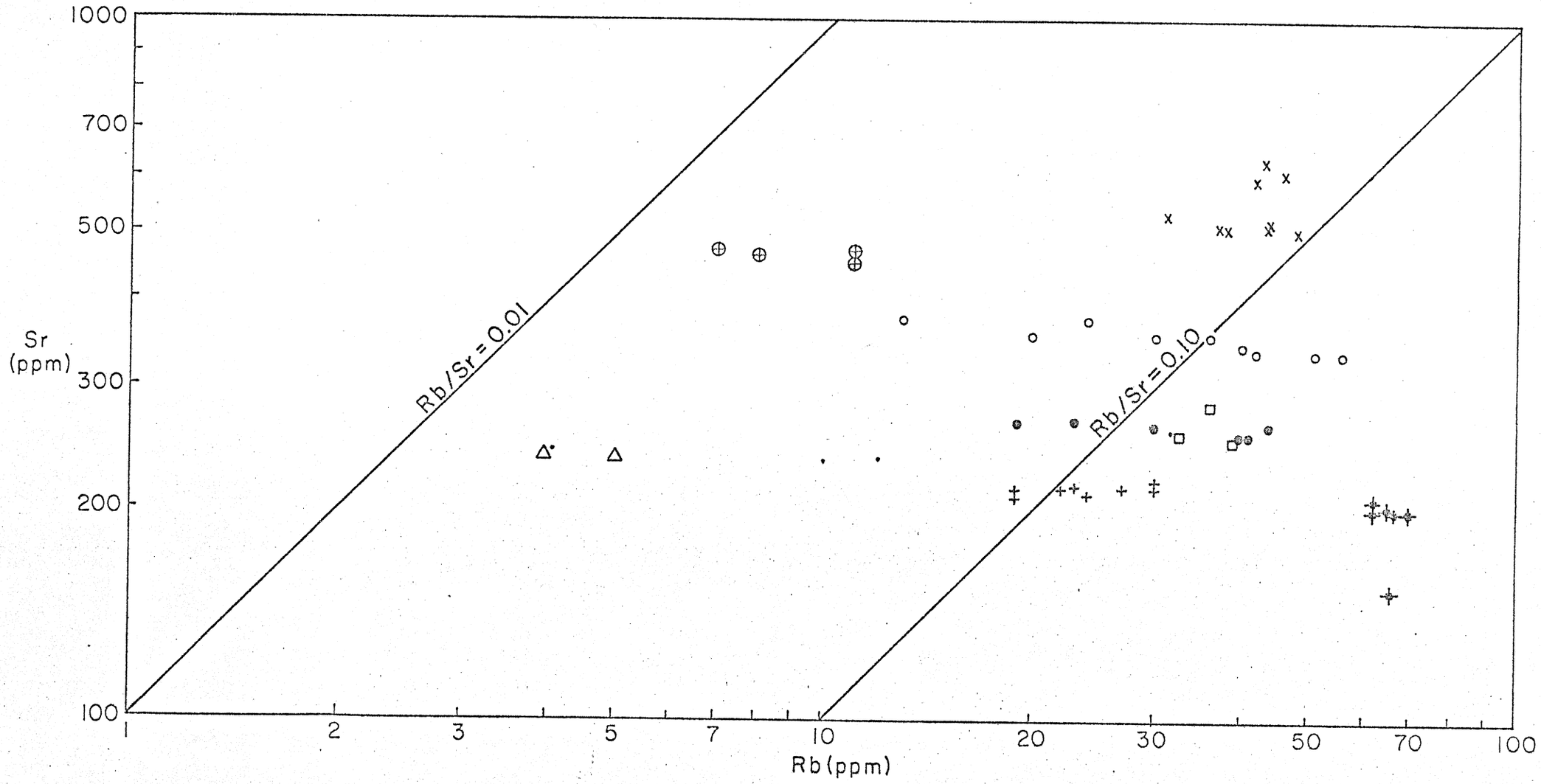
1000
700
500
300
200
100
Sr
(ppm)
Rb/Sr=0.01
Rb/Sr=0.10
1
2
3
5
7
10
20
30
50
70
100
Rb(ppm)

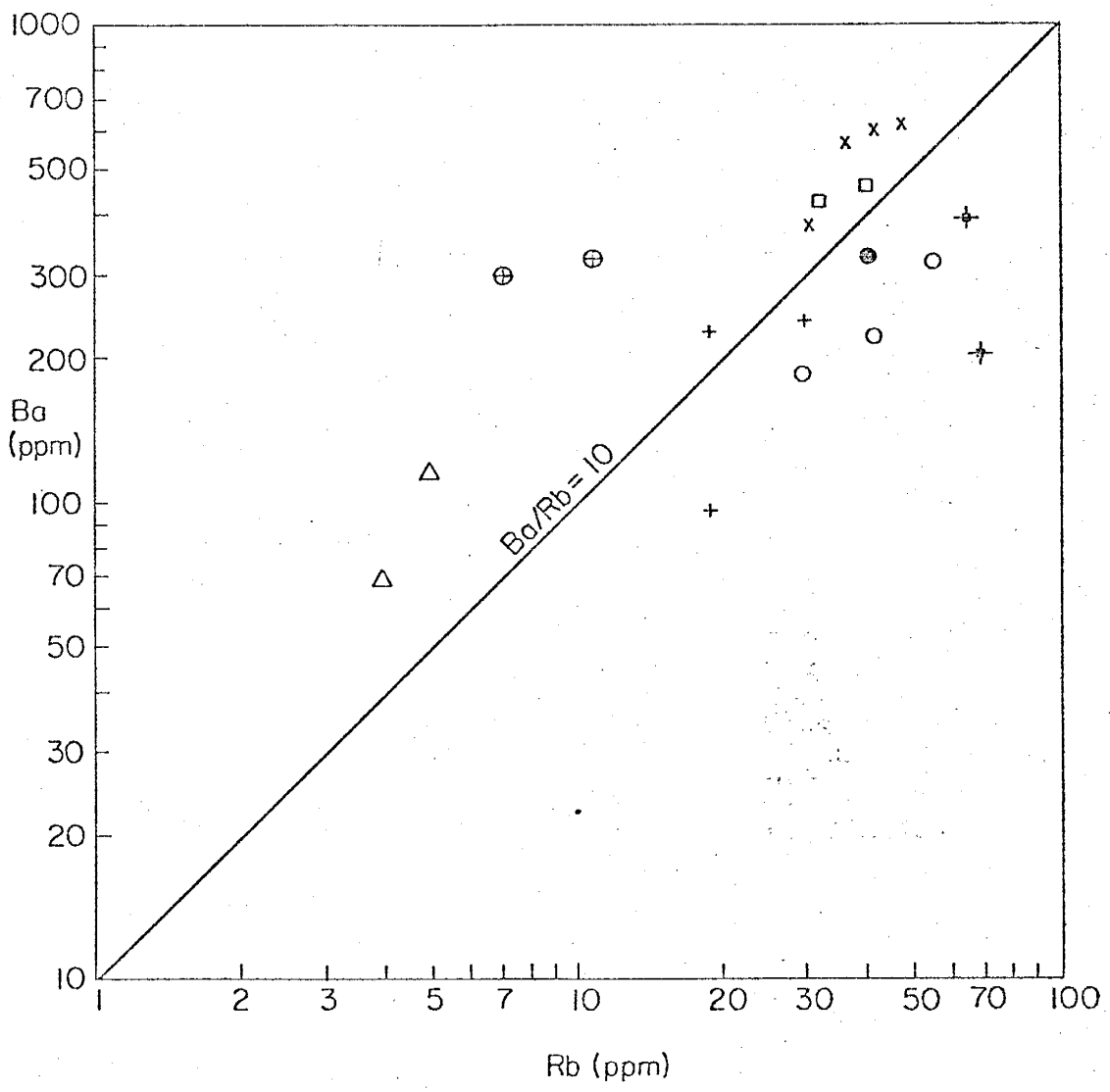
1000
700
500
300
200
Ba
(ppm)
100
70
50
30
20
10
Ba/Rb=10
1
2
3
5
7
10
20
30
50
70
100
Rb (ppm)

(Fig. 30), exhibits essentially the same features as the Sr versus Rb plot, reinforcing the previously shown (Fig. 27) coherence between Rb and K.

Nickel and Co are plotted against SiO_2 for the Modoc flows in Figures 31 and 32, respectively. Nickel was not determined for the dacites and rhyolites and Co shows little variation in these rocks and is not plotted. Both Ni and Co exhibit decreasing concentrations with respect to increasing SiO_2, the Ni data showing significantly more scatter than Co. Of particular interest in the Ni diagram (Fig. 31) is the constant concentration of Ni in the Callahan flow over its SiO_2 range and the increase in Ni with increasing SiO_2 exhibited by the Devil's Homestead flow. General age relationships previously appear viable, with both Ni and Co decreasing with decreasing eruptive age. Nickel decreases more rapidly than Co as shown in Figure 33, a log-log plot of Ni versus Co.

Copper variation with SiO_2 is illustrated in Figure 34. A coherent trend of decreasing Cu with increasing SiO_2 is observed. Age relationships generally hold throughout this trend with the exception of the Devil's Homestead flow being high in Cu content for its SiO_2 range as compared to the trend of the rest of the Modoc flows.

Figure 35 is a plot of Zr versus SiO_2 for the Modoc flows. Zirconium exhibits very little variation in the Recent dacites and obsidians and therefore is not plotted for these rocks. A trend of increasing Zr with increasing SiO_2 is exhibited by the Modoc flows, the Schonchin and Burnt flows appearing to have Zr concentrations respectively higher and lower than those that would be predicted by the trend of the other Modoc flows.

Figure 30. Log-log plot of Sr versus percent K.

MODOC BASALTS

+ DEVIL'S HOMESTEAD FLOW
· BLACK CRATER FLOW
△ ROSS CHIMNEYS FLOW
x SCHONCHIN FLOW
□ THREE SISTERS FLOW
o CALLAHAN FLOW
⊕ PAINT POT CRATER FLOW
⊹ BURNT FLOW
● OLDER MODOC

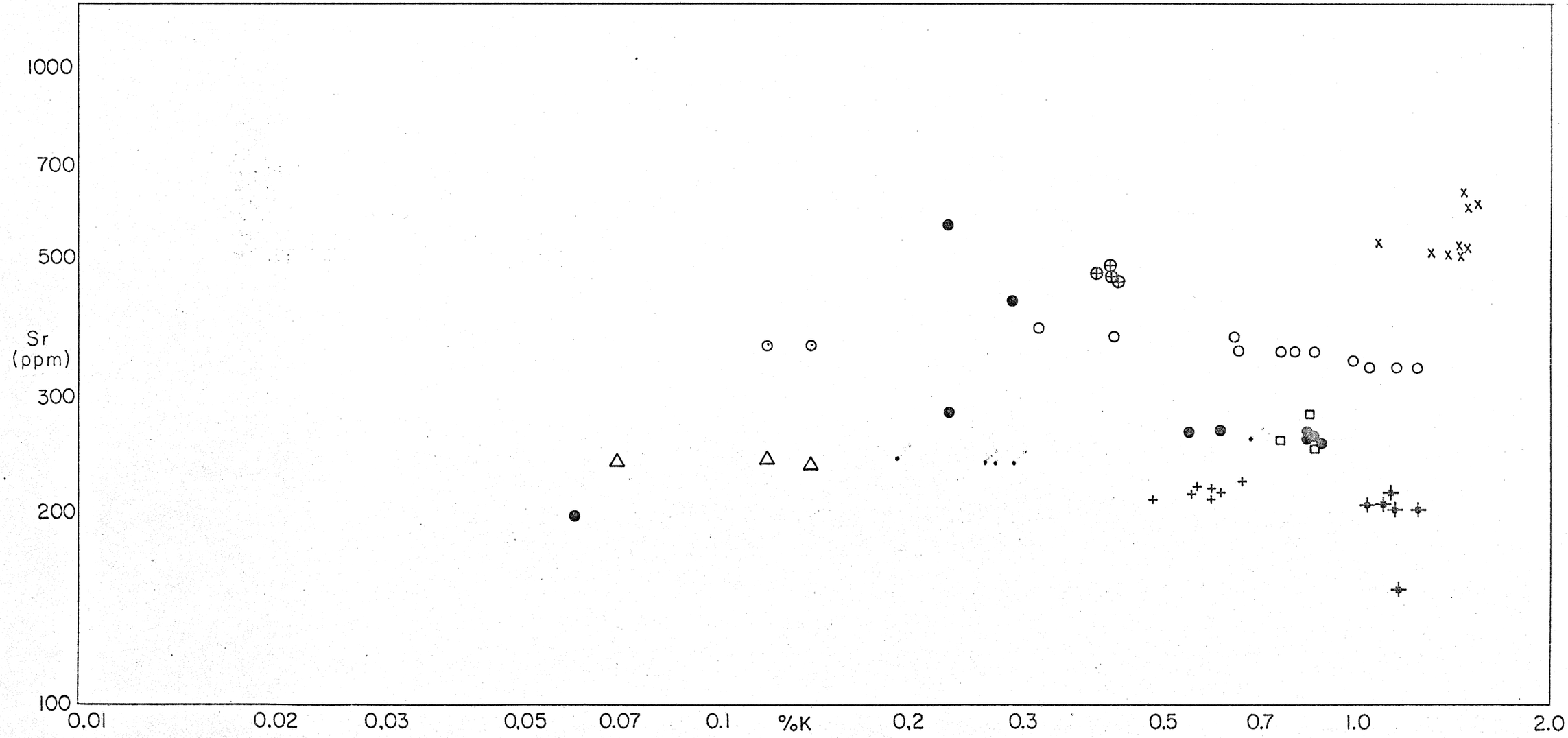
1000
700
500
Sr
(ppm)
300
200
100
0.01
0.02
0.03
0.05
0.07
0.1
%K
0.2
0.3
0.5
0.7
1.0
2.0

Figure 31. Nickel-silica variation diagram.

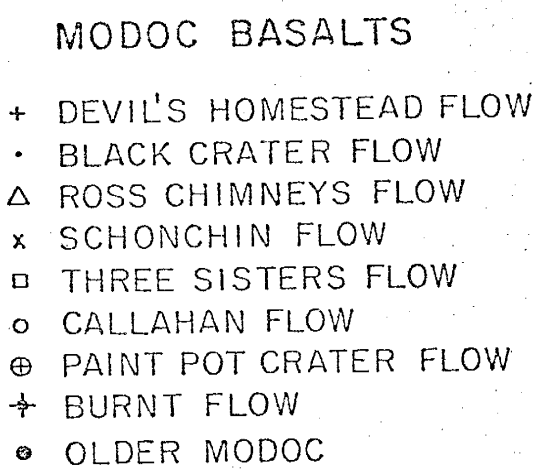

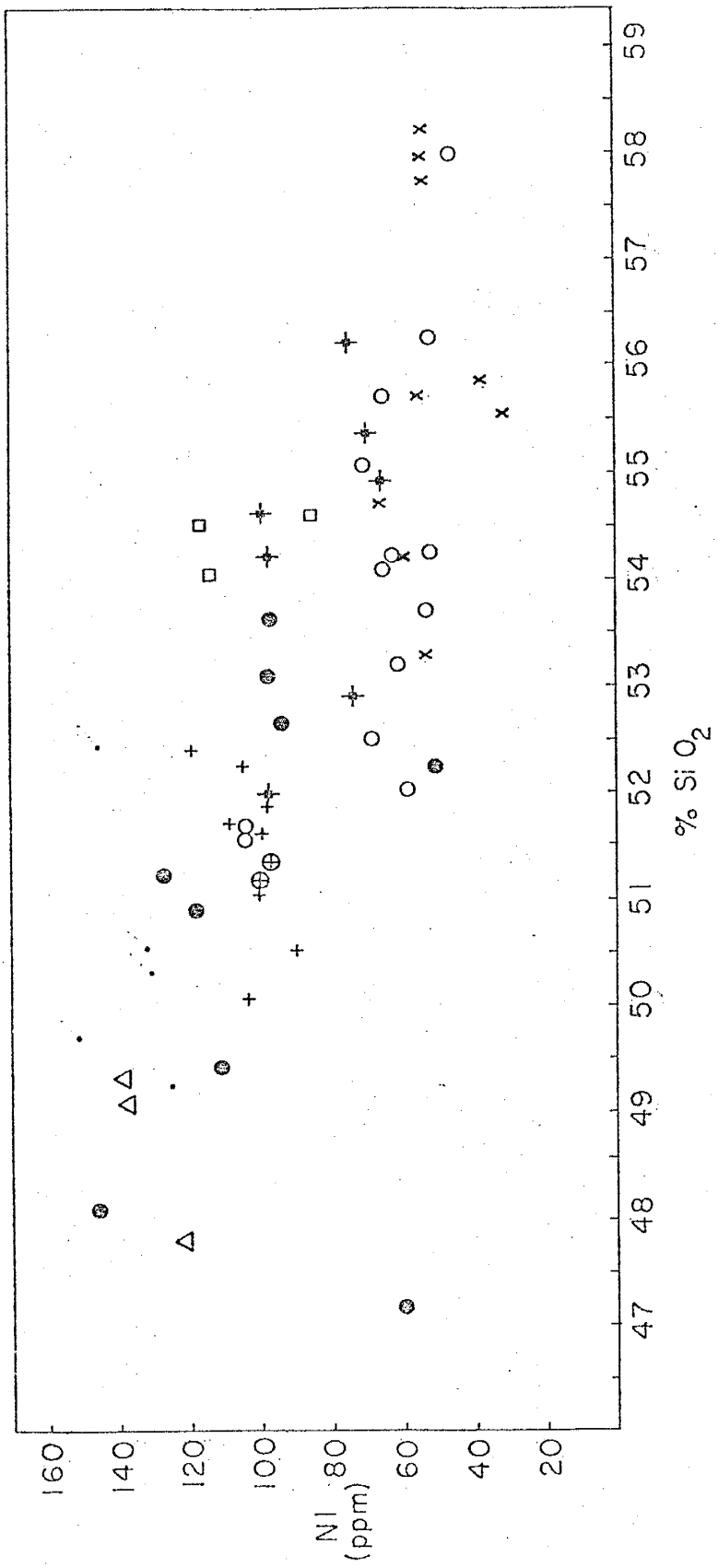
Ni (ppm)
160
140
120
100
80
60
40
20
47
48
49
50
51
52
53
54
55
56
57
58
59
% Si O_2

Figure 32. Cobalt-silica variation diagram.

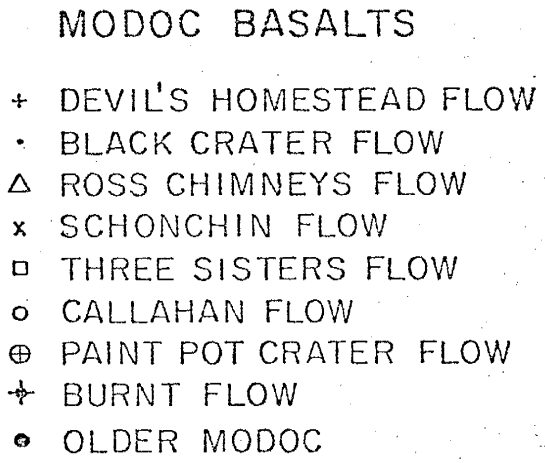

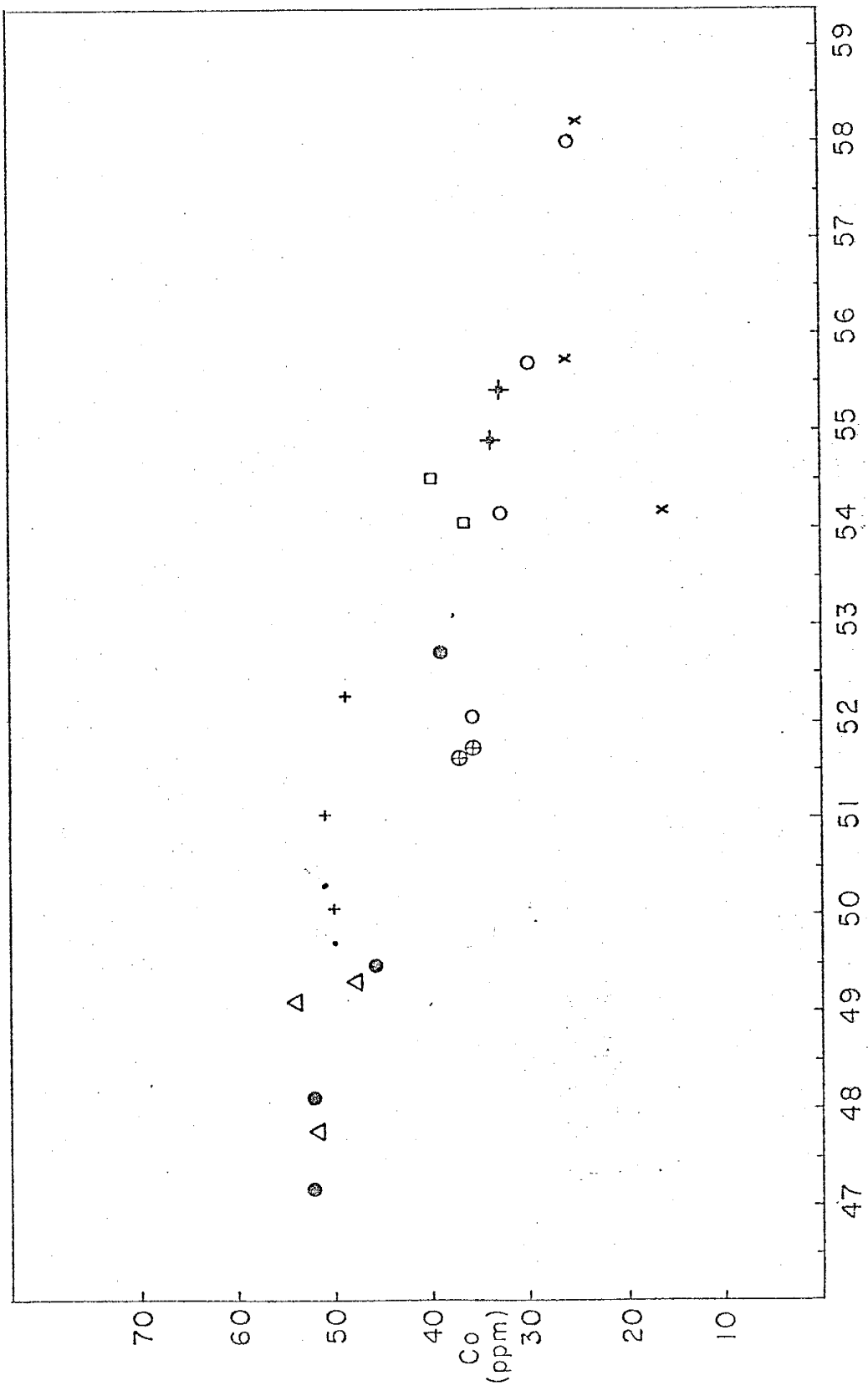
70
60
50
40
30
20
10
Co
(ppm)
47
48
49
50
51
52
53
54
55
56
57
58
59
% Si O2

Figure 33. Log-log plot of Ni versus Co.

MODOC BASALTS

+ DEVIL'S HOMESTEAD FLOW
· BLACK CRATER FLOW
△ ROSS CHIMNEYS FLOW
x SCHONCHIN FLOW
□ THREE SISTERS FLOW
o CALLAHAN FLOW
⊕ PAINT POT CRATER FLOW
⊹ BURNT FLOW
● OLDER MODOC

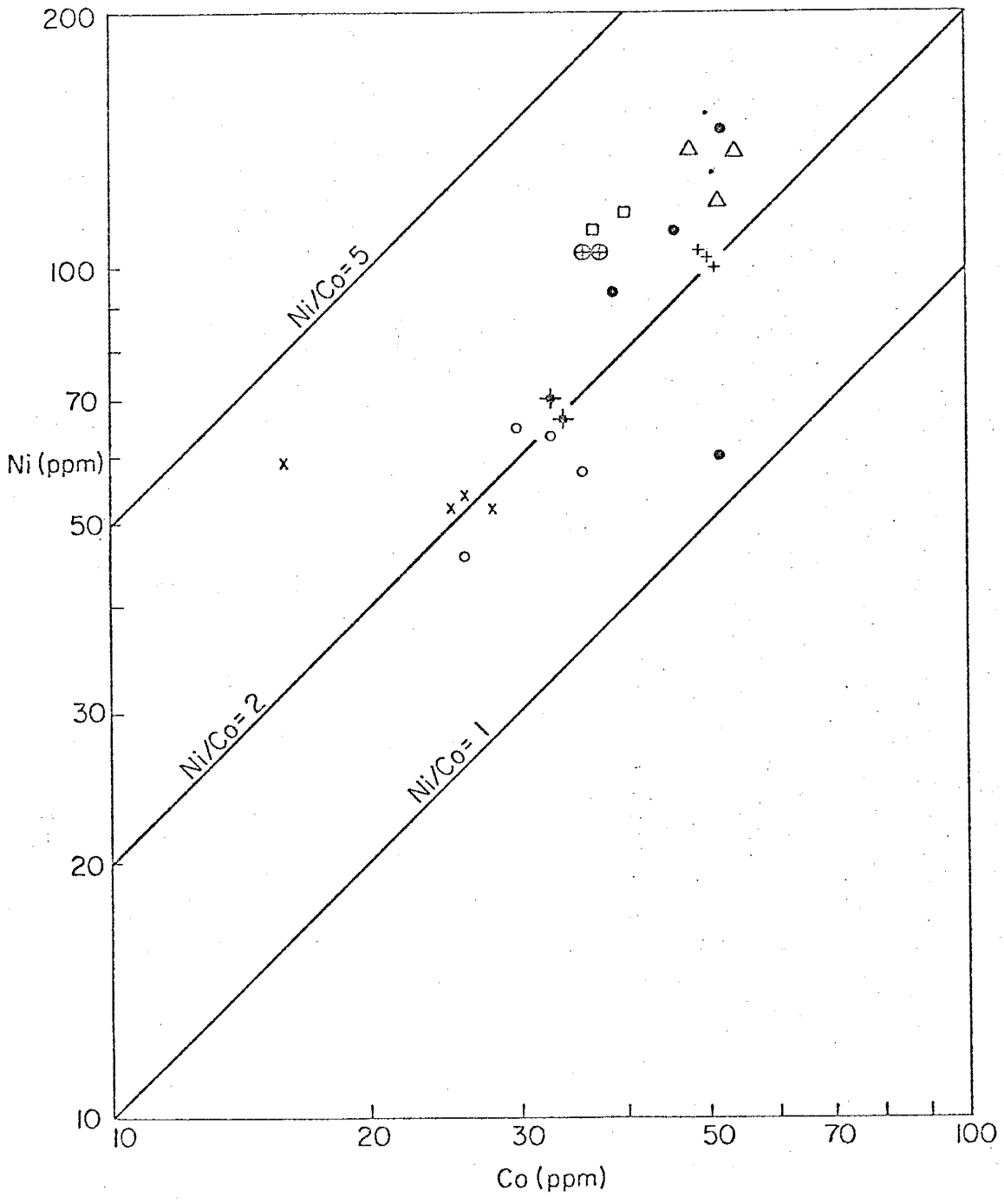
200
100
70
50
30
20
10
Ni (ppm)
Ni/Co=5
Ni/Co=2
Ni/Co=1
10
20
30
50
70
100
Co (ppm)

Figure 34. Copper-silica variation diagram.

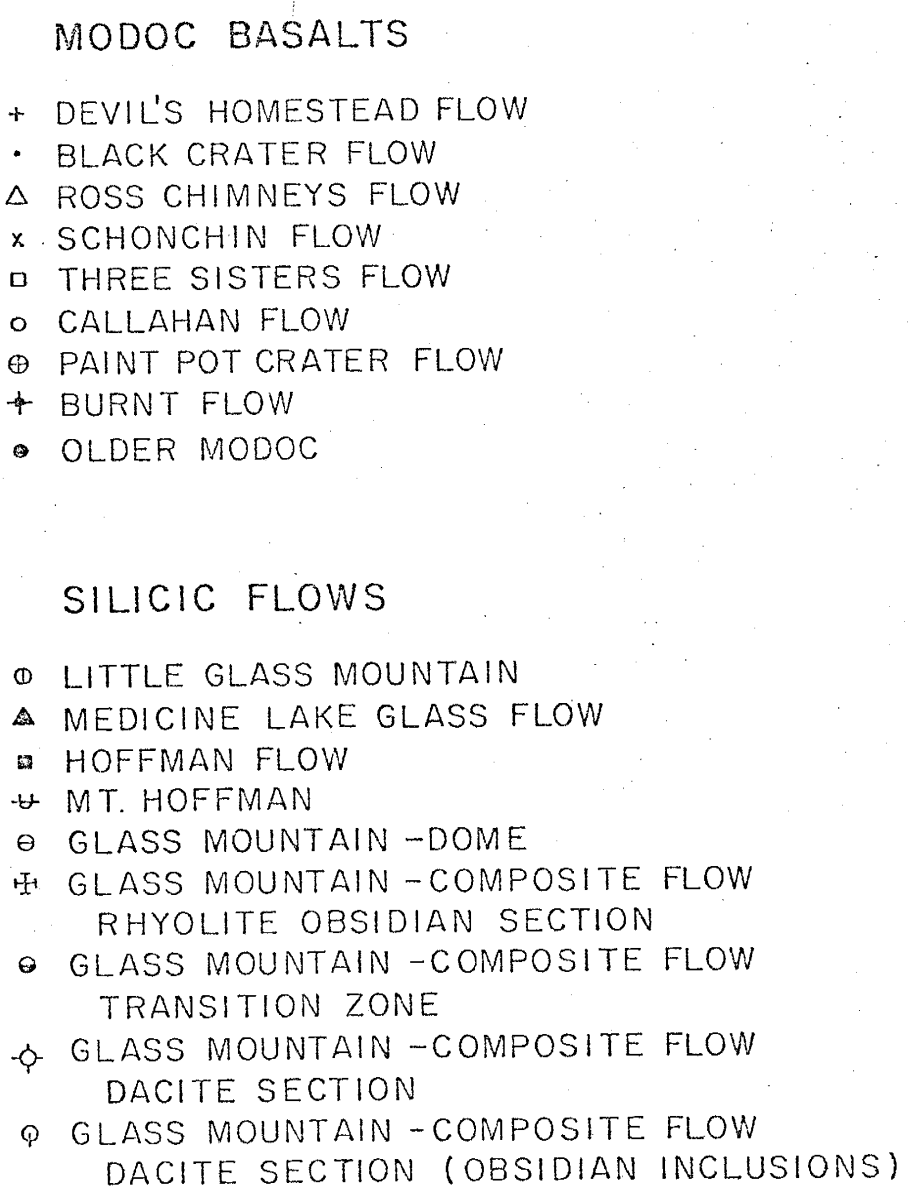

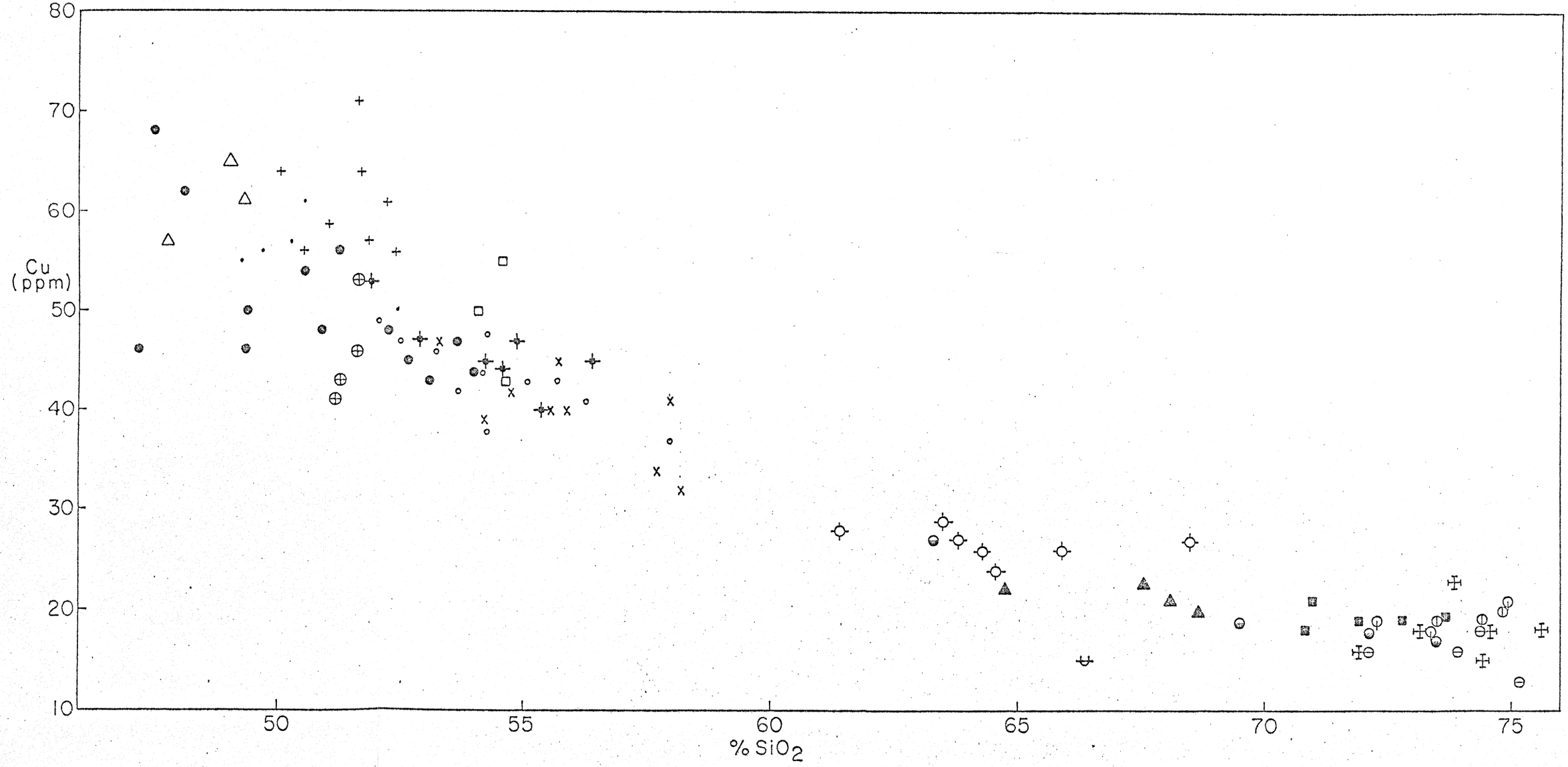
80
70
60
50
40
30
20
10
Cu
(ppm)
50
55
60
65
70
75
% SiO2

Figure 35. Zirconium-silica variation diagram.

MODOC BASALTS

+ DEVIL'S HOMESTEAD FLOW
· BLACK CRATER FLOW
△ ROSS CHIMNEYS FLOW
x SCHONCHIN FLOW
□ THREE SISTERS FLOW
o CALLAHAN FLOW
⊕ PAINT POT CRATER FLOW
✢ BURNT FLOW
● OLDER MODOC

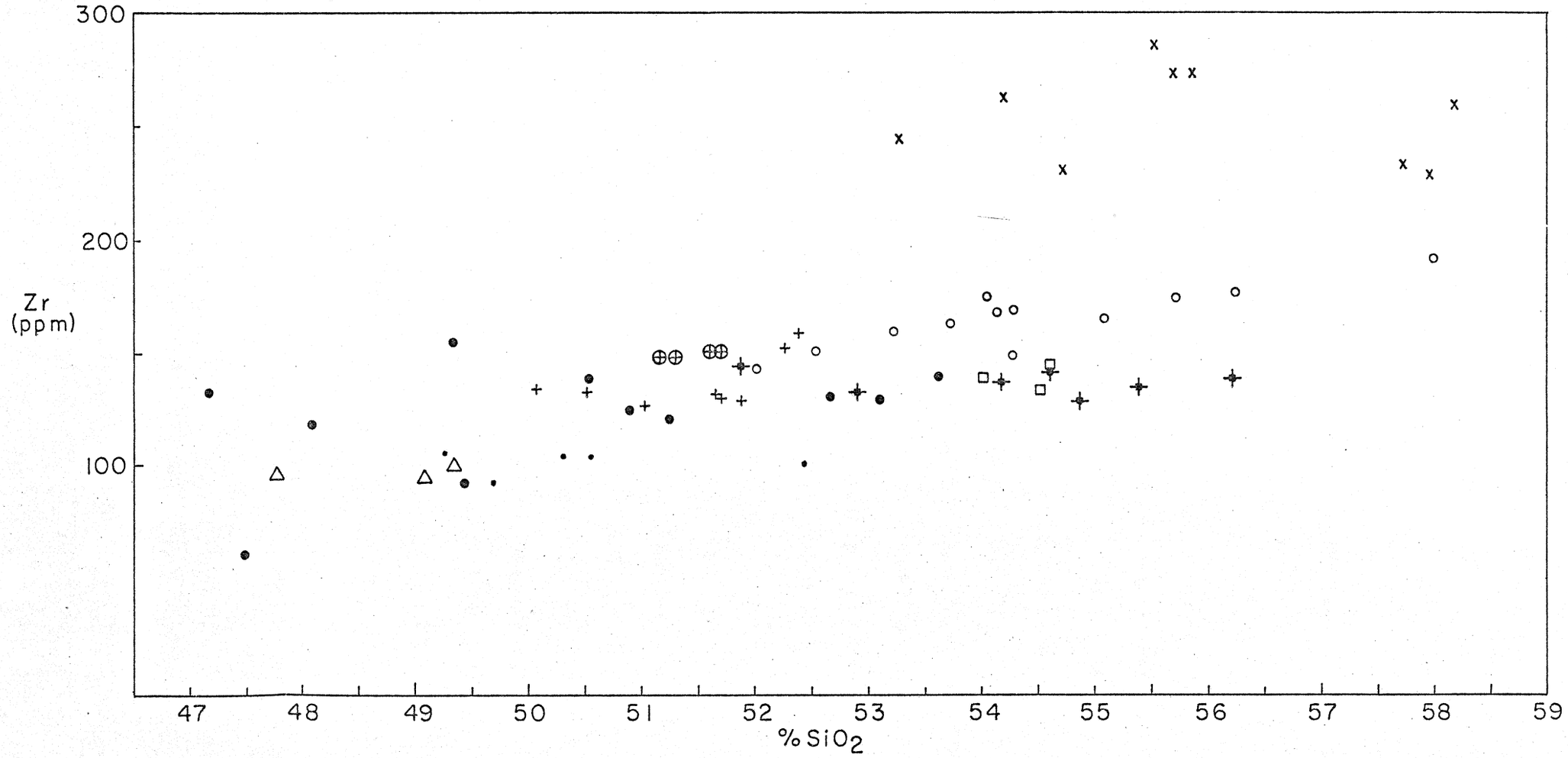
300
200
100
Zr
(ppm)
47
48
49
50
51
52
53
54
55
56
57
58
59
% SiO2

DISCUSSION OF RESULTS

Modoc Basalts and Basaltic Andesites

Introduction

The proposed volcanic history of the Modoc flows is complex with respect to inter- and intra-flow variations, but fairly simple in overall view. Gross major element trends of increasing K_2O and Na_2O and decreasing Al_2O_3, CaO, total Fe, and MgO with respect to increasing SiO suggest that fractional crystallization is the dominant process involved in the differentiation of the Modoc lavas. Two major fractionation histories appear to be represented, the first being the older Modoc, while the intermediate and younger Modoc form the second. The compositional overlap of the major element trends of the two groups and the temporal gap between them support this hypothesis, the temporal span separating the intermediate and younger Modoc being insignificant when comparing the age of either to the older Modoc.

Titanium

The distribution of TiO_2 in the Modoc flows is particularly interesting with respect to the experimental work of MacGregor (1969) who demonstrated that in the system MgO-SiO_2-TiO_2 the TiO content of a liquid derived by partial melting of an ultramafic parent rock should increase with increasing total pressure. The compositional change in TiO_2 content is most rapid in the pressure range from 1 atm to 20 kb with minor changes occurring at greater pressures.

Differences in the TiO_2 distribution in the Modoc flows could be obtained by either derivation from a homogenous parent at various depths, different degrees of partial melting in a homogenous parent at a common depth, derivation from a heterogenous parent, fractional crystallization in separate or zoned magma chambers, contamination of the magma by sialic material, or some combination of these processes.

As previously mentioned, the older Modoc is divided into two groups on the basis of TiO_2 distributions, one group from the northern section of the Highland (including the Three Sisters flow) and a group from the northeastern and eastern section of the Highland. The intermediate and younger Modoc flows are also divided into two groups, the Ross Chimneys, Black Crater, Paint Pot Crater, and Burnt flows forming the first group which is almost identical in TiO_2 with the older Modoc flows from the northern section of the Highland. The Devil's Homestead and Callahan flows form the second group, while the Schonchin flow exhibits a wide range in TiO_2 (almost equivalent to the total range exhibited by all the Modoc flows).

Assuming uncontaminated magma was derived from a homogenous parent at a common depth, the TiO_2 distributions reflect either differences in the initial compositions of batches of magma derived by different degrees of partial melting in separate and/or zoned magma chambers, or both.

Rubidium, Strontium, Barium, and Potassium

Trends of increasing Rb, Ba, and K with decreasing ages for the flows of the two eruptive groups is consistent with a model of fractional crystallization (Prinz, 1967). Rubidium is enriched relative to K and Ba with increasing fractionation as evidenced by decreases in the K/Rb and

the Ba/Rb ratios. The increase of the Rb/Sr ratio at constant Sr levels is also indicative of a normal fractional crystallization trend (Condie and others, 1969).

The variation of Sr levels between individual or groups of flows with fairly constant Sr concentrations within each flow or group is evidence for fractionation occurring in several distinct magma chambers. Several groups of flows are defined by constant Sr levels and increasing Rb with decreasing age within both eruptive groups:

Older Modoc

1. The older Modoc from the northern section of the Highland and the Three Sisters flow.
2. The Ross Chimneys, Black Crater, Devil's Homestead, and Burnt flows.
3. The Paint Pot Crater and Callahan flows.
4. The Schonchin flow.

The slight depletion in Sr with increasing Rb observed in groups 1 and 2 of the intermediate and younger Modoc is believed to be a function of the fractional crystallization of plagioclase (Condie and others, 1969).

The similarities between the flow group formed by the older Modoc, the first group listed for the intermediate and younger Modoc and the groupings formed by distinct TiO_2 levels should be obvious. Exceptions to the TiO_2 groupings are most easily explained by zonation of the magma chambers in which fractional crystallization took place. The viability of zonation as a process occurring in these magma chambers is supported by the systematic increase in Al_2O_3 with increasing SiO_2 observed in the Devil's Homestead and Burnt flows, which suggests the floatation of plagioclase.

Several processes or combination of processes could be responsible for the difference in Sr levels between the flow groups of the intermediate and younger Modoc. These are essentially the same as those used to explain the variation in the TiO_2 distributions. Again, assuming an uncontaminated magma derived from a homogenous parent at a common depth, two fundamental processes seem most viable:

1. Batches of magma, differing in initial composition due to varying degrees of partial melting, were emplaced in separate magma chambers and underwent fractional crystallization, subsequent eruptions from each reservoir forming distinct flow groups with respect to Rb/Sr variation.
2. One, or more, batches of magma were emplaced in central magma chambers which were zoned by the floatation of plagioclase and tapped at different levels or times. The derived magma was channeled into secondary reservoirs where further fractionation took place subsequent to or during the eruption of distinct flow groups.

The zonation of Sr in a magma chamber by the floatation of plagioclase is consistent with published partition coefficient data (Condie and others, 1969; Higuchi and Nagasawa, 1969; Condie and Barsky, 1972), Sr being partitioned into the plagioclase and depleted in the residual melt.

Nickel and Cobalt

Nickel and Cobalt show systematic decreases from the oldest to the youngest rocks of both eruptive groups, Ni exhibiting a more rapid decrease than Co. This results in decreasing Ni/Co ratios with decreasing age.

Such behavior is consistent with that observed for fractionation in igneous rock series and stratiform sheets (Nockolds and Allen, 1953; Wagner and Brown, 1967; Walker, 1969). The relative depletion rates are similar to those predicted from total bond energies and crystal field theory (Damon, 1968; Curtis, 1964).

The low, constant trend for Ni in the Callahan flow is somewhat puzzling, as both the Paint Pot Crater and Callahan flows are postulated to have fractionated from a common chamber prior to the extrusion of the Callahan flow. That the Paint Pot Crater flow contains only olivine as a phenocryst phase tends to support this argument.

Copper

Copper exhibits a rapid decrease in concentration from the oldest to the youngest Modoc flows of both eruptive groups. This distribution is extremely anomalous when compared to trends of stratiform sheets which show increasing Cu with fractionation until very late stages (Wagner and Brown, 1967; Walker, 1979). Crystal field theory predictions (Curtis, 1964) indicate that Cu^{+2} should be preferentially rejected from octahedral sites relative to Mg^{+2} and most divalent transition elements during fractional crystallization.

In basaltic melts undergoing fractionation Cu may enter olivine, pyroxenes, and iron ores (Wagner and others, 1957; Prinz, 1967), but not normally in sufficient amounts to deplete the residual magma with respect to Cu.

Copper, in the Cu^{+1} state, may be extracted to a limited extent by the crystallization of plagioclase (Taylor, 1965; Damon, 1968). Removal

of Cu by this process may have been significant in the Modoc lavas where plagioclase was the dominant crystallizing phase. This is suggested by the high Cu values exhibited by the Devil's Homestead flow, whose previously discussed Al_2O_3 - SiO_2 variation suggests the floatation of plagioclase.

Zirconium

Zirconium displays a steady enrichment from the oldest to the youngest rocks of both eruptive groups. This trend is consistent with the trends of other basaltic series undergoing fractional crystallization (Prinz, 1967).

Taylor (1965) states that Zr may be expected to substitute to some extent for Ti. The Schonchin and Burnt flows which exhibit Zr levels respectively higher and lower than the trend of the other Modoc flows somewhat parallel this distribution in their Ti concentrations.

Chemical Comparison of the Two Eruptive Groups

Except for having a slightly smaller SiO_2 range the older Modoc basalts and basaltic andesites show no significant differences in chemical composition when compared to the intermediate and younger Modoc flows. The textural and surficial characteristics defining the two groups may be largely due to differences in eruptive temperatures and volitile content of the two groups. Higher eruptive temperatures and a greater content of volitile constituents would be consistent with the fluid surficial features and lack of phenocryst phases which characterize the older Modoc lavas.

Recent Silicic Flows

With the exception of the dacite section of the composite flow, the major and trace element trends of the siliceous flows are consistent with fractional crystallization being the dominant process occurring with decreasing eruptive age.

Although the dacite of the composite flow may be somewhat contaminated by olivine basalt inclusions, its more basic composition relative to the Hoffman flow seems to preclude Anderson's (1941) hypothesis that the dacite was derived from the same magma as the Hoffman flow by fractionation, especially since the western section of the composite flow overlies the Hoffman flow. In addition, the dacite section of the composite flow is higher in Na and Co and lower in Ca, Rb, and Sr at equivalent SiO_2 levels than the Medicine Lake dacite flow. The distribution of Na and Ca in the two flows is reflected in an average plagioclase composition of An30 for the composite flow dacite, while the plagioclase of the Medicine Lake flow has an average composition of An48.

The author is hesistant to make further evaluations concerning the relationships between the siliceous flows or their possible genetic relationships to the older pre-Modoc andesites or the Modoc eruptive groups prior to detailed petrographic studies and partition coefficient determinations. Partition coefficient samples from the Medicine Lake, Mount Hoffman, and composite (dacite section) flows were collected and now are in various stages of preparation. When determinations of phenocryst and groundmass concentrations are completed the various relationships suggested above may be quantitatively evaluated through the use of

the Raleigh distribution law.

Hydrological Implications

Higgins (1973), using the arguments of Osborn and his co-workers (Osborn and Roeder, 1960; Roeder and Osborn, 1966; Osborn, 1969), postulated that the presence of significant volumes of water in the calderas at Newberry Volcano and Medicine Lake were responsible for the low Fe enrichment trends observed at both volcanic centers in the post-caldera lavas. He also suggests that the high O^{18}/O^{16} ratios of the Recent Medicine Lake volcanics is produced by the same mechanism.

Considerable doubt has been shed on the primary role of a high or constant oxygen fugacity in producing a trend of low Fe enrichment in high-alumina (calc-alkaline) associations (Carmichael, 1967; Green and Ringwood, 1968). Additionally, it is difficult to quantitatively evaluate the role of meteoric water from the cladera in controlling the O^{18}/O^{16} ratios of the Recent volcanics. This sort of mechanism does seem viable however, in explaining the anomalously high O^{18}/O^{16} ratios observed in the Medicine Lake and Hoffman flows. These being the first of the Recent siliceous flows to be extruded, it appears reasonable to assume that they may have had more significant interaction with meteoric water than subsequent rhyolite obsidian flows.

PETROGENESIS

Temporal and Tectonic Relationships

The Modoc Plateau, which flanks the Highland to the north, east, and south, is characterized by a series of northwest- to north-trending block-faulted ranges, with the intervening basins filled by high-alumina flood basalts (Macdonald, 1966). The faulting has continued into Recent time and the plateau region is best regarded as part of the Great Basin province which has been flooded by volcanics (Macdonald, 1966; Christiansen and Lipman, 1972).

The High Cascades to the west of the Highland were built up in Pliocene and Pleistocene times (Williams, 1949; Macdonald, 1966). This age is contemporaneous with that for the upbuilding of the Medicine Lake andesite shield volcano (Anderson, 1941).

Eaton (1966) determined a crustal thickness of 32 km for the Highland area on the basis on seismic studies.

Magma Genesis

The author feels that the andesites forming the shield and rim lavas were derived by the same mechanism as the High Cascade andesites. This hypothesis is subject to further evaluation and will not be discussed in this paper.

Higgins (1973) supports Waters' (1962) suggestion that the high-alumina basalts at the Newberry and Medicine Lake volcanic complexes differentiated from the same magma type as the high-alumina basalts that

characterize the plateaus to the east of these centers. Chemical analyses of the Warner basalt (C. Barsky, unpublished data) show Ba and Zr concentrations that are too high for the Modoc flows to have been derived from a magma of this composition by normal fractionation processes. Similar arguments apply to the Lake basalt whose Ba and Zr concentrations are too high and Ni concentration too low. These arguments do not preclude derivation from a mantle parent at different depths or degrees of partial melting, ignoring the Ni concentration of the Lake basalt.

Tentative calculations based on the batch partial melting data of Griffin and Murthy (1969) suggest a mantle parent of plagioclase peridotite, the magma being derived by small amounts of partial melting (3 to 5 percent). These calculations are based on K, Rb, Sr, and Ba concentrations observed in the most mafic of the Modoc lavas (lowest SiO_2), as these had undergone some degree of fractionation, the validity of this parent determination is questionable.

A plagioclase peridotite parent is helpful however, in explaining the differences in Sr levels between different flow groups. Griffin and Murthy (1969) give plagioclase peridotite a melting proportion of plagioclase: clinopyroxene: orthopyroxene 2:2:1. Since Sr is strongly enriched in the plagioclase differing amounts of partial melting could cause part of the Sr variation observed between flow groups.

In terms of the experimental work of Green and Ringwood (1967) the high-alumina Modoc basalts could have been produced by the fractionation of mantle derived olivine tholeiite magma in a deep crustal reservoir or reservoirs 15 to 35 km in depth. The evolved high-alumina basalts may then have been tapped into more shallow reservoirs underneath the Highland and undergone the various processes previously discussed.

BIBLIOGRAPHY

Anderson, C. A., 1933, Volcanic history of Glass Mountain, northern California: Am. Jour. Sci., v. 26, no. 155, p. 485-506.

Anderson, C. A., 1941, Volcanoes of the Medicine Lake Highland, California: California Univ. Pubs. Geol. Sci. Bull., v. 25, no. 7, p. 347-422.

Carmichael, I. S. E., 1967, Iron-titanium oxides and oxygen fugacities in volcanic rocks: Jour. Geophys. Res., v. 72, p. 4665-4687.

Chesterman, C. W., 1955, Age of the obsidian flow at Glass Mountain, Siskiyou County, California: Am. Jour. Sci., v. 253, no. 7, p. 418-424.

Christiansen, R. L., and Lipman, P., 1972, Cenozoic volcanism and plate tectonic evolution of western United States, pt. 2, Late Cenozoic: Royal Soc. London Trans., 91 p.

Clark, F. W., and Hillebrand, W. F., 1897, Analyses of rocks: U.S. Geol. Survey Bull. 148, p. 228.

Condie, K. C., 1967a, Geochemistry of early Precambrian graywackes from Wyoming: Geochim. Cosmochim. Acta, v. 31, p. 2135-2149.

Condie, K. C., 1967b, Petrology of the late Precambrian tillite association in northern Utah: Geol. Soc. America Bull., v. 78, p. 1317-1344.

Condie, K. C., Barsky, C. K., and Mueller, P. A., 1969, Geochemistry of Precambrian diabase dikes from Wyoming: Geochim. Cosmochim. Acta, v. 33, p. 1371-1388.

Condie, K. C., and Lo, H. H., 1971, Trace element geochemistry of the Louis Lake batholith of early Precambrian age, Wyoming: Geochim. Cosmochim. Acta, v. 35, p. 1099-1119.

Condie, K. C., and Barsky, C. K., 1972, Origin of Quaternary basalts from the Black Rock Desert region, Utah: Geol. Soc. America Bull., v. 83, p. 333-352.

Curtis, C. D., 1964, Applications of the crystal-field theory to the inclusion of trace transition elements in minerals during magmatic differentiation: Geochim. Cosmochim. Acta, v. 28, p. 389-403.

Damon, P. E., 1968, Behavior of some elements during magmatic crystallization: Geochim. Cosmochim. Acta, v. 32, p. 564-567.

Dickinson, W. R., 1968, Circumpacific andesite types: Jour. Geophys. Res., v. 73, p. 2261-2269.

Eaton, J. P., 1966, Crustal structure in northern and central California from sesimic evidence: Bull. Calif. Div. Mines Geol., 190, p. 419-426.

Finch, R. H., 1928, Lassen report no. 14: The Volcano Letter, no. 161, p. 1.

Finch, R. H., 1933, Burnt lava flow in northern California: Zeitschr. Vulkanologie, v. 15, no. 3, p. 180-183.

Friedman, I., 1968, Hydration rind dating of volcanic glass: Science, v. 162, p. 813-814.

Green, T. H., Greene, D. H., and Ringwood, A. E., 1967, The origin of high-alumina basalts and their relationships to quartz tholeiites and alkali basalts: Earth and Planetary Sci. Letters, v. 2, p. 41-52.

Green, T. H., and Ringwood, A. E., 1968, Genesis of the calc-alkaline igneous rock suite: Contr. Mineralogy and Petrology, v. 18, p. 105-162.

Griffin, W. L., and Murthy, V. R., 1969, Distribution of K, Rb, Sr, and Ba in some minerals relevant to basalt genesis: Geochim. Cosmochim. Acta, v. 33, p. 1389-1414.

Hamilton, W., 1965, Geology and Petrogenesis of the Island Park caldera of rhyolite and basalt, eastern Idaho: Proc. Pap. U.S. Geol. Surv. 504-c, 37 p.

Hedge, C. E., and Walthall, F. G., 1963, Radiogenic strontium 87 as an index of geologic processes: Science, v. 140, p. 1214-1217.

Hedge, C. E., 1966, Variations in radiogenic strontium found in volcanic rocks: Jour. Geophys. Res., v. 71, no. 24, p. 6119-6120.

Hedge, C. E., and Knight, R. J., 1969, A study of lead and strontium isotopes in volcanic rocks from northern Honshu, Japan: Geochemical Jour., v. 2, p. 231-242.

Higgins, M. W., and Waters, A. C., 1967, Newberry Caldera, Oregon - A preliminary report: Ore Bin, v. 29, no. 3, p. 37-60.

Higgins, M. W., 1968, Geology of Newberry Caldera, central Oregon [Ph.D. dissert.]: Santa Barbara, California Univ., 320 p.

Higgins, M. W., and Waters, A. C., 1970, A re-evaluation of basalt-obsidian relations at East Lake Fissure, Newberry Caldera, Oregon: Geol. Soc. America Bull., v. 81, no. 9, p. 2835-2842.

Higgins, M. W., 1973, Petrology of Newberry Volcano, central Oregon: Geol. Soc. America Bull., v. 84, p. 455-488.

Higuchi, H., and Nagasawa, H., 1969, Trace element partition coefficients in volcanic rocks: Earth and Planetary Sci. Letters, v. 5, p. 47-51.

Irvine, T. N. and Baragar, W. R. A., 1971, A guide to the chemical classification of the common volcanic rocks: Can. Jour. Earth. Sci., v. 8, p. 523-548.

Ives, P. C., Levin, Betsy, Robinson, R. D., and Rubin, Meyer, 1964, U. S. Geological Survey radiocarbon dates VII: Am. Jour. Sci., Radiocarbon Supp., v. 6, p. 37-76.

Jenkins, R., and De Vries, J. L., 1966, Practical X-ray spectrometry: New York, Springer-Verlag, 181 p.

Kuno, H., 1960, High-alumina basalt: Jour. Petrol., v. 1, p. 121-145.

Kuno, H., 1966a, Lateral variation of basalt magma type across continental margins and island arcs: Bull. Volcanol., v. 29, p. 195-222.

Laidley, R. A., and McKay, D. S., 1971, Geochemical examination of obsidians from Newberry Caldera, Oregon: Contri. Mineralogy and Petrology, v. 30, p. 336-342.

Macdonald, G. A., 1966, Geology of the Cascade Range and Modoc Plateau: Bull. Calif. Div. Mines Geol., 190, p. 65-96.

MacGregor, I., 1969, The system MgO - SiO_2 - TiO_2 and its bearing on the distribution of TiO_2 in basalts: Am. Jour. Sci., v. 267, p. 342-363.

Nockolds, S. R., and Allen, R., 1953, The geochemistry of some igneous rock series: Geochim. Cosmochim. Acta, v. 4, p. 105-142.

Nockolds, S. R., The behavior of some elements during fractional crystallization of magma: Geochim. Cosmochim. Acta, v. 30, p. 267-278.

Osborn, E. F., and Roeder, P. L., 1960, Effect of oxygen pressure on crystallization in simplified basalt systems: International Geological Congress, XXI Session, Norden, Part XIII, Petrographic Provinces, Igneous and Metamorphic Rocks, p. 147-155.

Osborn, E. F., 1969, The complementariness of orogenic andesite and alpine peridotite: Geochim. Cosmochim. Acta, v. 33, p. 307-324.

Peacock, M. A., 1931a, The Modoc lava field, northern California: Geog. Rev., v. 21, no. 2, p. 259-275.

Peterman, Z. E., Carmichael, I. S. E., and Smith, A. L., 1970, Sr^{87}/Sr^{86} ratios of Quaternary lavas of the Cascade Range, northern California: Geol. Soc. America Bull., v. 81, p. 311-318.

Powell, J. L., and DeLong, S. E., 1966, Isotopic composition of strontium in volcanic rocks from Oahu: Science, v. 153, no. 3741, p. 1239-1242.

Powers, H. A., 1932, The lavas of the Modoc Lava Bed quadrange, California: Am. Mineralogist, v. 17, no. 7, p. 253-294.

Prinz, M., 1967, Geochemistry of basaltic rocks: trace elements: In: Hess, H. H., and Poldervaart, A. (eds.), Basalts - The Poldervaart treatise on rocks of basaltic composition: New York, J. Wiley and Sons, p. 271-324.

Pushkar, P., 1968, Strontium isotope ratios in volcanic rocks of three island arcs: Jour. Geophys. Res., v. 73, p. 2701-2714.

Roeder, P. L., and Osborn, E. F., 1966, Experimental data for the system $MgO - FeO - Fe_2O_3 - CaAl_2Si_2O_8$ and their petrologic implications: Jour. Sci., v. 264, p. 428-480.

Smith, A. L., and Carmichael, I. S. E., 1968, Quaternary lavas from the southern Cascades, western U.S.A.: Contr. Mineralogy and Petrology, v. 19, no. 3, p. 212-238.

Taylor, S. R., 1965, The application of trace element data to problems in petrology: Physics and Chemistry of the Earth, v. 16, p. 135-231.

Taylor, H. P., 1968, The oxygen isotope geochemistry of igneous rocks: Contr. Mineralogy and Petrology, v. 19, p. 1-71.

Tilley, C. E., 1950, Some aspects of magmatic evolution: Quart, Jour. Geol. Soc. London, v. 106, pt. 1, no. 421, p. 37-61.

Volborth, A., 1963, Total instrumental analysis of rocks: Nevada Bur. Mines Rept. 6, Part A, 72 p.

Wager, L. R., Vincent, E. A., and Smales, A. A., 1957, Sulphides in the Skaergaard intrusion, East Greenland: Econ. Geology, v. 52, p. 855-903.

Wager, L. R., and Brown, G. M., 1967, Layered igneous rocks: San Francisco, W. H. Freeman and Co., 588 p.

Walker, K. R., 1969, The Palisades Sill, New Jersey: A reinvestigation: Geol. Soc. America Spec. Paper III, 116 p.

Waters, A. C., 1962, Basalt magma types and their tectonic associations: Pacific Northwest of the United States. In: Macdonald, G. A., Juno, H. (eds.), The Crust of the Pacific Basin, Am. Geophys., Un., Geophys. Mono. 6, p. 158-170.

Williams, Howell, 1935, Newberry volcano of central Oregon: Geol. Soc. America Bull., v. 46, no. 2, p. 253-304.

Williams, Howell, 1949, Geology of the Macdoel quadrangle [California]: California Div. Mines Bull., no. 151, p. 7-60.

APPENDIX

Chemical Analyses

In the following tables a blank space indicates the element concentration for that sample was not determined. A hyphen (-) indicates the element concentration was below the limit of detection.

DEVIL'S HOMESTEAD FLOW

	H-1	H-2	H-3	H-4	H-5	H-6
SiO_2	50.52	51.69	50.09	51.54	52.40	51.04
TiO_2	0.97				0.98	
Al_2O_3	16.23				17.03	
Fe_2O_3	9.66				9.69	
MgO	5.19				5.46	
CaO	9.84				9.89	
Na_2O	3.02				2.82	
K_2O	0.71	0.66	0.67	0.67	0.73	0.78
Total	96.14				99.00	
Ba						
Co						
Cu	56				56	
Ni	90				119	
Rb	23				30	
Sr	217				214	
Zr	133				159	
Rb/Sr	0.11				0.14	
K/Rb	263.48				202.00	
K/Sr	27.93				28.32	

DEVIL'S HOMESTEAD FLOW

	H-7	H-8	H-9	H-10	H-11	H-12
SiO_2	51.04	51.65	50.89	51.88	51.92	50.89
TiO_2	0.99	1.04		1.00		
Al_2O_3	16.59	18.71		18.00		
Fe_2O_3	10.96	10.35		10.19		
MgO	5.60	6.36		6.50		
CaO	10.11	10.27		10.16		
Na_2O	2.95	2.89		3.04		
K_2O	0.66	0.67	0.69	0.71	0.69	0.53
Total	98.90	101.94		101.48		
Ba	95					
Co	51					
Cu	59	71		57		
Ni	100	99		98		
Rb	19	22		24		
Sr	213	216		211		
Zr	127	132		129		
Rb/Sr	0.09	0.10		0.11		
K/Rb	288.42	245.45		242.08		
K/Sr	25.73	25.00		27.54		

DEVIL'S HOMESTEAD FLOW

	H-13	H-14	H-15	H-16	H-17	H-18
SiO_2	51.69	51.56	52.07	50.07	52.25	51.71
TiO_2				1.00	1.01	0.99
Al_2O_3				17.28	19.06	17.86
Fe_2O_3				10.34	9.94	9.84
MgO				5.98	5.62	5.43
CaO				10.21	10.12	10.11
Na_2O				2.86	3.03	2.97
K_2O	0.64	0.71	0.70	0.58	0.79	0.74
Total				98.32	101.82	99.65
Ba				226	236	
Co				50	49	
Cu				64	61	64
Ni				103	105	108
Rb				19	30	27
Sr				209	222	215
Zr				134	139	130
Rb/Sr				0.09	0.14	0.13
K/Rb				257.89	213.00	227.41
K/Sr				23.44	28.78	28.56

BLACK CRATER FLOW

	H-20	H-21	H-22	H-23	H-24
SiO_2	52.44	50.30	50.54	49.69	49.26
TiO_2	0.82	0.83	0.83	0.84	0.83
Al_2O_3	16.75	18.03	18.98	19.42	19.63
Fe_2O_3	9.35	9.62	9.39	9.67	9.41
MgO	5.82	6.98	7.05	8.19	6.98
CaO	9.67	10.51	10.51	10.67	10.54
Na_2O	2.96	2.75	2.73	2.71	2.80
K_2O	0.82	0.32	0.31	0.23	0.35
Total	98.63	99.34	100.34	101.42	99.80
Ba		22		-	
Co		51		50	
Cu	50	57	61	56	55
Ni	145	130	132	151	125
Rb	32	10	12	4	12
Sr	260	237	238	241	238
Zr	101	105	105	93	107
Rb/Sr	0.12	0.04	0.05	0.02	0.05
K/Rb	215.31	266.00	214.17	477.50	242.50
K/Sr	26.50	11.22	10.80	7.93	12.23

ROSS CHIMNEYS FLOW

	H-30	H-31	H-32
SiO_2	47.76	49.08	49.32
TiO_2	0.80	0.82	0.84
Al_2O_3	20.46	20.18	18.98
Fe_2O_3	9.73	9.69	9.67
MgO	6.64	7.86	7.18
CaO	10.60	10.23	10.31
Na_2O	2.65	2.52	2.70
K_2O	0.15	0.08	0.17
Total	98.79	100.46	99.17
Ba	-	68	115
Co	52	54	48
Cu	57	65	61
Ni	121	137	138
Rb	-	4	5
Sr	243	240	238
Zr	97	95	100
Rb/Sr	-	0.02	0.02
K/Rb	-	165.00	282.00
K/Sr	5.14	2.75	5.92

SCHONCHIN FLOW

	H-40	H-41	H-42	H-43	H-44	H-45
SiO_2	54.70	55.52	55.85	54.60	54.44	55.54
TiO_2		1.31	1.23			
Al_2O_3		16.29	16.58			
Fe_2O_3		8.29	8.20			
MgO		4.01	3.93			
CaO		8.24	8.08			
Na_2O		3.78	3.71			
K_2O	1.55	1.77	1.87	1.75	1.59	1.70
Total		99.21	99.45			
Ba						
Co						
Cu		40	40			
Ni		30	37			
Rb		43	46			
Sr		636	608			
Zr		286	274			
Rb/Sr		0.07	0.08			
K/Rb		343.49	337.39			
K/Sr		23.22	25.53			

SCHONCHIN FLOW

	H-46	H-47	H-48	H-49	H-53	H-54
SiO_2	55.69	54.21	54.72	55.90	58.19	57.72
TiO_2	1.16	1.01	0.99		0.99	1.01
Al_2O_3	15.94	15.55	16.84		17.21	17.55
Fe_2O_3	8.12	8.11	8.05		7.55	7.69
MgO	3.68	3.66	3.88		3.70	3.87
CaO	8.06	8.06	8.10		7.75	7.76
Na_2O	3.66	3.75	3.68		3.73	3.72
K_2O	1.81	1.59	1.67	1.72	1.76	1.75
Total	98.12	95.94	97.93		100.88	101.07
Ba	598	558			610	
Co	26	16			25	
Cu	45	39	42		32	34
Ni	54	59	66		52	53
Rb	42	37	38		48	44
Sr	599	510	506		502	520
Zr	273	263	231		259	233
Rb/Sr	0.07	0.07	0.08		0.10	0.09
K/Rb	363.57	370.27	371.32		304.38	324.55
K/Sr	25.49	26.86	27.89		29.10	27.46

SCHONCHIN FLOW

	H-55	H-57
SiO_2	57.97	54.72
TiO_2	1.00	
Al_2O_3	17.76	
Fe_2O_3	7.67	
MgO	3.61	
CaO	7.81	
Na_2O	3.72	
K_2O	1.78	1.59
Total	101.32	
Ba		
Co		
Cu	41	
Ni	54	
Rb	44	
Sr	514	
Zr	228	
Rb/Sr	0.09	
K/Rb	330.23	
K/Sr	28.27	

THREE SISTERS FLOW

	H-60	H-61	H-63
SiO_2	54.60	54.03	54.51
TiO_2	0.81	0.83	0.81
Al_2O_3	19.14	18.24	19.36
Fe_2O_3	7.78	8.98	7.70
MgO	5.96	6.27	5.82
CaO	9.25	9.13	9.15
Na_2O	3.15	3.06	3.06
K_2O	1.01	1.03	0.91
Total	101.70	101.57	101.32
Ba		452	417
Co		37	40
Cu	43	50	55
Ni	86	112	117
Rb	36	39	32
Sr	284	250	259
Zr	144	139	133
Rb/Sr	0.13	0.16	0.12
K/Rb	228.33	214.87	230.94
K/Sr	28.94	33.52	28.53

CALLAHAN FLOW

	H-70	H-71	H-72	H-73	H-74	H-75
SiO_2	54.26	54.14	55.28	55.92	55.23	55.42
TiO_2	1.00					
Al_2O_3	17.50					
Fe_2O_3	8.88					
MgO	5.07					
CaO	9.72					
Na_2O	3.51					
K_2O	0.77	0.92	1.03	1.02	1.03	0.98
Total	100.71					
Ba						
Co						
Cu	48					
Ni	51					
Rb	24					
Sr	376					
Zr	149					
Rb/Sr	0.06					
K/Rb	262.92					
K/Sr	16.78					

CALLAHAN FLOW

	H-76	H-77	H-78	H-79	H-80	H-81
SiO_2	53.35	56.04	52.03	52.53	54.79	55.92
TiO_2			1.02	0.99		
Al_2O_3			18.37	18.67		
Fe_2O_3			9.84	9.78		
MgO			5.80	5.54		
CaO			10.02	9.91		
Na_2O			3.26	3.31		
K_2O	0.94	1.09	0.38	0.51	0.95	1.17
Total			100.72	101.24		
Ba			271			
Co			36			
Cu			49	47		
Ni			58	68		
Rb			-	13		
Sr			388	377		
Zr			143	151		
Rb/Sr				0.03		
K/Rb				319.23		
K/Sr			8.12	11.01		

CALLAHAN FLOW

	H-82	H-83	H-84	H-85	H-86	H-87
SiO_2	54.14	52.95	53.82	55.71	53.71	56.04
TiO_2	0.94			0.93	0.95	
Al_2O_3	17.82			17.88	17.19	
Fe_2O_3	8.97			8.54	9.08	
MgO	4.76			4.27	5.25	
CaO	9.23			8.71	9.33	
Na_2O	3.49			3.49	3.46	
K_2O	0.96	0.99	0.98	1.27	0.91	1.41
Total	100.31			100.80	99.88	
Ba	186			220		
Co	33			30		
Cu	44			43	42	
Ni	64			65	53	
Rb	30			42	30	
Sr	356			338	357	
Zr	168			174	163	
Rb/Sr	0.08			0.12	0.08	
K/Rb	263.00			274.14	251.67	
K/Sr	22.16			30.71	21.15	

CALLAHAN FLOW

	H-88	H-89	H-90	H-91	H-92	H-93
SiO_2	55.88	57.99	54.58	56.24	56.50	55.33
TiO_2		1.02		0.93		
Al_2O_3		18.09		18.12		
Fe_2O_3		8.33		8.88		
MgO		3.91		4.38		
CaO		8.20		8.58		
Na_2O		3.70		3.47		
K_2O	1.35	1.51	1.30	1.40	1.35	1.12
Total		102.75		102.00		
Ba		314				
Co		26				
Cu		37		41		
Ni		46		52		
Rb		56		51		
Sr		334		338		
Zr		192		177		
Rb/Sr		0.17		0.15		
K/Rb		216.25		221.37		
K/Sr		36.26		33.40		

CALLAHAN FLOW

	H-94	H-95	H-96	H-97	H-98	H-99
SiO_2	55.42	55.07	53.89	49.14	53.02	54.88
TiO_2		0.99				
Al_2O_3		17.46				
Fe_2O_3		8.68				
MgO		4.71				
CaO		8.97				
Na_2O		3.44				
K_2O	1.15	1.17	0.92	0.85	0.84	1.32
Total		100.49				
Ba						
Co						
Cu		43				
Ni		70				
Rb		40				
Sr		346				
Zr		166				
Rb/Sr		0.12				
K/Rb		240.75				
K/Sr		27.83				

CALLAHAN FLOW

	H-100	H-101	H-102	H-103	H-104	H-105
SiO_2	53.66	54.09	54.23	55.99	53.21	52.33
TiO_2					1.03	
Al_2O_3					18.27	
Fe_2O_3					9.20	
MgO					5.11	
CaO					9.52	
Na_2O					3.40	
K_2O	0.74	1.24	1.13	0.97	0.78	0.68
Total					100.52	
Ba						
Co						
Cu					46	
Ni					61	
Rb					20	
Sr					356	
Zr					161	
Rb/Sr					0.06	
K/Rb					319.50	
K/Sr					17.95	

CALLAHAN FLOW

	H-106
SiO_2	54.26
TiO_2	0.94
Al_2O_3	17.31
Fe_2O_3	8.60
MgO	4.45
CaO	9.14
Na_2O	3.50
K_2O	1.04
Total	99.24
Ba	
Co	
Cu	38
Ni	62
Rb	36
Sr	356
Zr	168
Rb/Sr	0.10
K/Rb	239.72
K/Sr	24.24

PAINT POT CRATER FLOW

	H-110	H-112	H-113	H-114
SiO_2	51.15	51.67	51.60	51.28
TiO_2	0.87	0.88	0.86	0.86
Al_2O_3	18.95	19.48	18.00	18.15
Fe_2O_3	8.77	8.85	8.85	8.81
MgO	6.62	6.22	6.43	6.46
CaO	9.79	10.01	9.73	9.81
Na_2O	3.30	3.23	3.25	3.16
K_2O	0.51	0.47	0.49	0.49
Total	99.96	100.81	99.21	99.02
Ba		290	318	
Co		36	37	
Cu	41	53	46	43
Ni	100	104	104	97
Rb	11	7	11	8
Sr	458	471	463	467
Zr	148	150	150	148
Rb/Sr	0.02	0.02	0.02	0.02
K/Rb	384.55	545.71	370.00	508.75
K/Sr	9.24	8.11	8.79	8.72

BURNT FLOW

	H-120	H-121	H-122	H-123	H-124	H-125
SiO_2	54.59	54.57	54.18	51.87	52.88	56.22
TiO_2	0.72		0.71	0.72	0.70	0.72
Al_2O_3	15.66		16.49	15.97	16.03	17.31
Fe_2O_3	7.49		7.43	7.64	7.56	7.50
MgO	5.75		5.28	5.11	4.76	5.21
CaO	8.90		8.87	8.97	8.92	8.77
Na_2O	3.13		3.16	3.11	3.16	3.13
K_2O	1.38	1.38	1.41	1.34	1.26	1.49
Total	97.62		97.53	94.73	95.27	100.35
Ba						
Co						
Cu	44		46	53	47	45
Ni	99		97	98	74	75
Rb	66		66	62	62	69
Sr	201		153	207	205	200
Zr	142		138	144	133	139
Rb/Sr	0.33		0.43	0.30	0.30	0.35
K/Rb	176.06		181.06	187.42	175.32	176.81
K/Sr	57.81		78.11	56.14	53.02	61.00

BURNT FLOW

	H-126	H-127
SiO_2	54.86	55.37
TiO_2	0.72	0.70
Al_2O_3	16.93	16.84
Fe_2O_3	7.58	7.40
MgO	5.08	5.13
CaO	9.02	8.82
Na_2O	3.16	3.18
K_2O	1.36	1.51
Total	98.71	98.95
Ba	387	203
Co	34	33
Cu	47	40
Ni	66	70
Rb	65	69
Sr	203	200
Zr	129	135
Rb/Sr	0.32	0.35
K/Rb	173.69	181.59
K/Sr	55.62	62.65

OLDER MODOC BASALT

	H-50	H-51	H-56	H-58	H-62	H-64
SiO_2	49.44	52.66	53.10	52.47	52.44	52.08
TiO_2	0.78	0.80	0.83			
Al_2O_3	19.45	17.64	19.51			
Fe_2O_3	9.62	8.69	8.53			
MgO	6.33	5.41	5.92			
CaO	10.59	9.54	9.73			
Na_2O	2.86	3.17	3.23			
K_2O	0.28	1.01	1.01	0.95	0.97	0.94
Total	99.35	98.92	101.86			
Ba	151	327				
Co	46	39				
Cu	50	45	43			
Ni	111	94	98			
Rb	-	41	30			
Sr	287	257	265			
Zr	93	131	129			
Rb/Sr		0.16	0.11			
K/Rb		204.39	271.00			
K/Sr	8.08	32.61	30.68			

OLDER MODOC BASALT

	H-130	H-131	H-136	H-137	H-138	H-139
SiO_2	50.93	50.88	52.28	53.64	51.24	53.71
TiO_2		0.87		0.86	0.84	
Al_2O_3		19.14		18.15	18.52	
Fe_2O_3		9.14		8.88	9.39	
MgO		6.45		6.06	6.59	
CaO		9.98		9.49	10.10	
Na_2O		2.96		3.19	2.93	
K_2O	0.79	0.73	0.99	1.06	0.66	0.90
Total		100.15		101.33	100.27	
Ba						
Co						
Cu		48		47	56	
Ni		118		97	127	
Rb		23		40	19	
Sr		269		256	269	
Zr		125		140	121	
Rb/Sr		0.09		0.16	0.07	
K/Rb		260.00		215.75	284.21	
K/Sr		22.23		33.71	20.07	

OLDER MODOC BASALT

	H-142	H-143	H-144	H-145	H-146	H-147
SiO_2	53.26	54.67	52.24	52.72	49.51	47.16
TiO_2	1.13		0.85			1.12
Al_2O_3	17.13		18.52			19.84
Fe_2O_3	8.83		8.60			11.77
MgO	4.20		5.59			5.94
CaO	8.54		9.82			10.57
Na_2O	3.79		3.20			3.18
K_2O	1.31	1.11	1.03	0.79	0.14	0.14
Total	98.19		99.85			99.72
Ba	376					129
Co	28					52
Cu	47		48			46
Ni	52		50			60
Rb	31		44			-
Sr	528		265			367
Zr	246		1			133
Rb/Sr	0.06		0.17			
K/Rb	356.13		194.32			
K/Sr	20.91		32.26			3.16

OLDER MODOC BASALT

	H-148	H-151	H-152	H-153	H-154	H-155
SiO_2	51.40	52.15	52.21	50.86	56.09	54.88
TiO_2						
Al_2O_3						
Fe_2O_3						
MgO						
CaO						
Na_2O						
K_2O	0.92	0.78	0.82	0.66	1.40	1.69
Total						
Ba						
Co						
Cu						
Ni						
Rb						
Sr						
Zr						
Rb/Sr						
K/Rb						
K/Sr						

OLDER MODOC BASALT

	H-156	H-157	H-158	H-159	H-160	H-161
SiO_2	52.24	48.08	50.42	49.12	49.49	52.65
TiO_2		1.10				
Al_2O_3		18.73				
Fe_2O_3		10.84				
MgO		6.63				
CaO		10.70				
Na_2O		2.94				
K_2O	0.46	0.17	0.32	0.50	0.91	1.24
Total		99.19				
Ba		366				
Co		52				
Cu		62				
Ni		146				
Rb		-				
Sr		366				
Zr		119				
Rb/Sr						
K/Rb						
K/Sr		3.85				

OLDER MODOC BASALT

	H-162	H-163	H-164	H-165
SiO_2	47.48	49.34	54.05	50.52
TiO_2	0.59	1.16	1.03	1.13
Al_2O_3	20.92	22.80	16.81	19.79
Fe_2O_3	10.16	9.70	8.91	9.18
MgO	7.05	6.47	5.08	6.49
CaO	10.98	10.58	8.99	10.49
Na_2O	3.01	2.33	3.52	3.12
K_2O	0.07	0.28	1.22	0.35
Total	100.26	102.66	99.61	101.07
Ba				
Co				
Cu	68	46	44	54
Ni				
Rb	1	-	34	-
Sr	197	569	350	431
Zr	61	155	175	139
Rb/Sr	0.01		0.10	
K/Rb	580.00		297.94	
K/Sr	2.94	3.94	28.94	6.54

LITTLE GLASS MOUNTAIN

	H-201	H-202	H-203	H-204	H-205	H-206
SiO_2	71.08	73.71	74.84	74.84	74.49	73.49
TiO_2				0.34		0.32
Al_2O_3				14.60		14.33
Fe_2O_3				1.98		1.97
MgO				0.19		0.21
CaO				1.13		1.08
Na_2O				4.33		4.22
K_2O	4.13	3.78	4.20	4.22	4.14	4.11
Total				101.63		99.73
Ba						880
Co						2.7
Cu				20	38	19
Ni						
Rb				163	160	157
Sr				95	94	95
Zr				195	191	193
Rb/Sr				1.72	1.70	1.65
K/Rb				208.28	214.75	214.65
K/Sr				357.37	365.53	354.74

MOUNT HOFFMAN - DOME

	H-221
SiO_2	66.32
TiO_2	0.41
Al_2O_3	13.29
Fe_2O_3	2.37
MgO	0.46
CaO	1.56
Na_2O	4.94
K_2O	3.58
Total	92.93
Ba	940
Co	4.2
Cu	15
Ni	
Rb	123
Sr	124
Zr	242
Rb/Sr	0.99
K/Rb	255.77
K/Sr	253.71

MEDICINE LAKE GLASS FLOW

	H-210	H-211	H-212	H-213	H-214
SiO_2	67.56	65.55	68.65	68.09	64.72
TiO_2	0.57		0.51	0.53	0.50
Al_2O_3	16.17		15.24	15.16	12.96
Fe_2O_3	4.01		3.47	3.66	3.67
MgO	1.35		0.96	1.18	0.92
CaO	4.13		3.41	3.71	3.24
Na_2O	4.01		4.03	3.96	3.81
K_2O	3.12	3.12	3.27	3.16	3.12
Total	100.92		99.54	99.45	92.94
Ba			735		
Co			8.2		
Cu	23		20	21	22
Ni					
Rb	128		132	131	140
Sr	278		248	258	243
Zr	195		192	193	183
Rb/Sr	0.46		0.53	0.51	0.58
K/Rb	197.81		205.61	200.23	185.00
K/Sr	91.08		109.44	101.67	106.58

HOFFMAN FLOW

	H-230	H-231	H-233	H-234	H-235	H-236
SiO_2	73.08	71.91	70.98	70.83	73.55	52.29
TiO_2		0.37	0.38	0.36	0.36	0.83
Al_2O_3		14.28	14.22	14.09	14.55	17.61
Fe_2O_3		2.45	2.64	2.49	2.42	9.37
MgO		0.46	0.60	0.52	0.46	7.42
CaO		1.88	2.13	1.84	1.73	10.45
Na_2O		4.22	4.22	4.13	4.28	2.72
K_2O	3.78	3.82	3.81	3.80	3.83	0.58
Total		99.39	98.98	98.06	101.18	101.27
Ba			738			
Co			5.9			
Cu		19	21	18	19	56
Ni						
Rb		153	155	155	153	18
Sr		146	144	142	141	223
Zr		189	194	185	184	112
Rb/Sr		1.05	1.08	1.09	1.09	0.08
K/Rb		207.25	204.00	204.58	202.35	258.33
K/Sr		214.19	219.58	223.31	219.57	20.85

HOFFMAN FLOW

	H-237	H-238
SiO_2	72.45	72.79
TiO_2		0.36
Al_2O_3		14.55
Fe_2O_3		2.40
MgO		0.41
CaO		1.72
Na_2O		4.32
K_2O	3.83	3.76
Total		100.31
Ba		830
Co		3.9
Cu		19
Ni		
Rb		152
Sr		149
Zr		182
Rb/Sr		1.02
K/Rb		201.52
K/Sr		205.57

GLASS MOUNTAIN COMPLEX - COMPOSITE FLOW
RHYOLITE OBSIDIAN SECTION

	H-250	H-251	H-252	H-253	H-254	H-255
SiO_2	74.32	74.29	73.52	73.91	73.14	71.98
TiO_2					0.33	0.31
Al_2O_3					14.11	13.95
Fe_2O_3					2.06	2.03
MgO					0.26	0.33
CaO					1.00	0.97
Na_2O					4.12	4.26
K_2O	4.13	4.21	4.08	4.14	4.19	4.21
Total					99.21	98.04
Ba					715	
Co					2.6	
Cu					18	16
Ni						
Rb					157	153
Sr					92	92
Zr					199	194
Rb/Sr					1.71	1.66
K/Rb					221.53	229.48
K/Sr					378.04	381.63

GLASS MOUNTAIN COMPLEX - COMPOSITE FLOW
RHYOLITE OBSIDIAN SECTION

	H-256	H-257	H-258	H-259	H-260	H-261
SiO_2	74.39	75.63	74.81	74.49	73.84	72.73
TiO_2	0.33	0.31			0.34	
Al_2O_3	14.94	14.17			14.74	
Fe_2O_3	2.11	1.94			2.09	
MgO	0.33	0.45			0.26	
CaO	1.03	0.89			1.03	
Na_2O	4.14	4.13			4.19	
K_2O	4.18	4.30	4.22	4.01	4.25	4.03
Total	101.45	101.82			100.74	
Ba		872			805	
Co		2.3			2.4	
Cu	15	18			23	
Ni						
Rb	157	157			154	
Sr	102	85			95	
Zr	192	192			191	
Rb/Sr	1.54	1.85			1.62	
K/Rb	220.96	219.94			224.22	
K/Sr	340.10	406.24			363.47	

GLASS MOUNTAIN COMPLEX - COMPOSITE FLOW
RHYOLITE OBSIDIAN SECTION

	H-262	H-263	H-264	H-265
SiO_2	69.77	73.55	74.58	74.65
TiO_2			0.34	
Al_2O_3			14.10	
Fe_2O_3			2.16	
MgO			0.29	
CaO			1.09	
Na_2O			4.27	
K_2O	3.83	4.04	4.13	4.17
Total			100.96	
Ba				
Co				
Cu			18	
Ni				
Rb			154	
Sr			101	
Zr			193	
Rb/Sr			1.53	
K/Rb			217.21	
K/Sr			331.19	

GLASS MOUNTAIN COMPLEX - DOME

	H-240	H-241	H-242	H-243	H-244
SiO_2	75.17	74.42	73.87	72.10	75.23
TiO_2	0.32	0.32	0.32	0.33	
Al_2O_3	13.95	14.09	14.03	14.30	
Fe_2O	2.04	2.05	1.99	2.08	
MgO	0.31	0.26	0.21	0.24	
CaO	1.01	0.96	1.00	0.98	
Na_2O	4.23	4.26	4.17	4.32	
K_2O	4.14	4.15	4.18	4.15	4.14
Total	101.17	100.51	99.77	98.50	
Ba	767		825		
Co	2.9		2.6		
Cu	13	18	16	16	
Ni					
Rb	154	157	159	157	
Sr	94	94	95	94	
Zr	189	190	197	195	
Rb/Sr	1.64	1.67	1.67	1.67	
K/Rb	217.21	215.16	215.60	219.43	
K/Sr	355.85	359.36	360.84	366.49	

GLASS MOUNTAIN COMPLEX - COMPOSITE FLOW
TRANSITION ZONE

	H-270	H-271	H-272	H-273	H-274
SiO_2	73.45	69.49	72.10	63.29	66.22
TiO_2	0.38	0.59	0.41	0.79	
Al_2O_3	14.57	15.49	14.05	15.56	
Fe_2O_3	2.47	3.96	2.26	4.99	
MgO	0.37	0.61	0.29	0.88	
CaO	1.35	2.42	1.21	3.68	
Na_2O	4.15	4.91	4.34	4.99	
K_2O	3.96	3.38	4.08	2.77	2.96
Total	100.70	100.85	98.74	96.95	
Ba					
Co					
Cu	17	19	18	27	
Ni					
Rb	145	118	153	94	
Sr	115	181	103	253	
Zr	197	233	192	230	
Rb/Sr	1.26	0.65	1.49	0.37	
K/Rb	222.07	232.12	221.31	249.04	
K/Sr	280.00	151.33	328.74	92.53	

GLASS MOUNTAIN COMPLEX - COMPOSITE FLOW
DACITE SECTION

	H-280	H-281	H-282	H-283	H-284	H-285
SiO_2	68.49	74.79	73.35	64.55	73.35	72.54
TiO_2	0.62	0.35		0.58	0.34	
Al_2O_3	15.31	14.82		15.39	14.62	
Fe_2O_3	3.55	2.16		4.03	2.07	
MgO	0.53	0.22		1.03	0.18	
CaO	2.28	1.12		3.47	1.08	
Na_2O	4.71	4.08		4.56	4.34	
K_2O	3.41	4.18	4.00	3.16	4.15	4.19
Total	98.90	101.72		96.77	100.13	
Ba	830	856		717	957	
Co	6.0	2.3		9.8	2.5	
Cu	27	21		24	18	
Ni						
Rb	122	156		122	159	
Sr	174	97		209	97	
Zr	232	192		208	189	
Rb/Sr	0.70	1.61		0.58	1.64	
K/Rb	231.97	215.52		219.10	213.52	
K/Sr	162.64	346.60		127.89	350.00	

GLASS MOUNTAIN COMPLEX - COMPOSITE FLOW
DACITE SECTION

	H-286	H-287	H-288	H-289	H-290	H-291
SiO_2	64.31	74.47	63.79	72.76	61.43	74.28
TiO_2	0.73		0.75	0.42	0.70	0.33
Al_2O_3	16.43		15.54	15.04	16.32	14.77
Fe_2O_3	5.09		5.89	2.45	5.31	2.06
MgO	1.31		1.82	0.37	2.09	0.29
CaO	4.27		4.61	1.42	5.42	1.01
Na_2O	4.85		4.70	4.22	4.22	4.14
K_2O	2.72	4.20	2.65	3.92	2.57	4.22
Total	99.71		99.75	100.10	98.06	101.10
Ba					574	874
Co					17.5	3.0
Cu	26		27	19	28	19
Ni						
Rb	103		99	161	100	157
Sr	261		273	118	287	96
Zr	224		222	205	197	190
Rb/Sr	0.40		0.36	1.36	0.35	1.64
K/Rb	216.80		222.22	202.11	214.00	217.26
K/Sr	85.56		80.59	275.76	74.60	355.31

GLASS MOUNTAIN COMPLEX - COMPOSITE FLOW
DACITE SECTION

	H-292	H-293	H-294	H-295	H-296
SiO_2	64.04	65.88	72.66	67.76	63.53
TiO_2		0.63			0.70
Al_2O_3		16.12			15.59
Fe_2O_3		4.54			5.17
MgO		1.50			1.90
CaO		4.03			5.13
Na_2O		4.25			4.75
K_2O	2.65	2.94	4.21	3.47	2.54
Total		99.89			99.31
Ba					
Co					
Cu		26			29
Ni					
Rb		126			100
Sr		244			284
Zr		213			204
Rb/Sr		0.52			0.35
K/Rb		191.03			210.80
K/Sr		98.65			74.23

This thesis is accepted on behalf of the faculty of the Institute by the following committee:

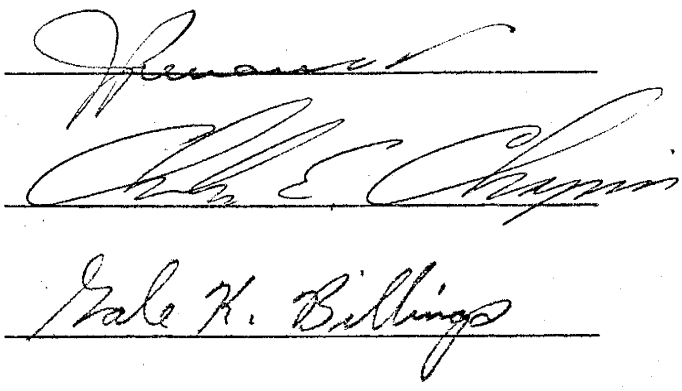

Date April 3, 1973